Time-Dependent Characterization of Viscoelastic Materials

Dissertation

by

Daniel Tscharnuter

prepared at the

Polymer Competence Center Leoben GmbH

and the

Institute of Materials Science and Testing of Plastics

submitted to the

Montanuniversität Leoben

Academic Advisor

Univ.-Prof. Dipl.-Ing. Dr. Gerald Pinter
Montanuniversität Leoben, Austria

Supervisor

Univ.-Prof. Dr. Zoltan Major
Johannes Kepler University Linz, Austria

Referees

Univ.-Prof. Dipl.-Ing. Dr. Gerald Pinter
Montanuniversität Leoben, Austria

Prof. Marta Rink
Politecnico di Milano, Italy

Leoben, October 2010

I declare in lieu of oath, that I wrote this dissertation and performed the associated research myself, using only the support indicated in the acknowledgements and literature cited.

Leoben, October 2010 Dipl.-Ing. Daniel Tscharnuter

Acknowledgements

This thesis has been accomplished at the Polymer Competence Center Leoben GmbH (PCCL) within the framework of the Kplus- and COMET-programs of the Austrian Ministry of Traffic, Innovation and Technology with contributions from Borealis Polyolefine GmbH. The PCCL is funded by the Austrian Government and the State Governments of Styria and Upper Austria. I thank these organisations for providing the means to conduct my research.

I am most grateful to Prof. Zoltan Major, at first for having considerable trust in my abilities, despite my lack of knowledge in polymers and mechanics at the time we first met, and in the long run for giving me a lot of freedom in the research work. The poster on our office door is testimony to his much appreciated unique personality and leadership.

I thank Prof. Reinhold W. Lang for the extensive reviewing of some of the included papers. Learning from his deep expertise in writing scientific papers was invaluable for the writing of this dissertation, and will remain so for my future work.

I wish to express my gratitude to Prof. Marta Rink and Prof. Gerald Pinter, for their interest in my work and for devoting time to review this dissertation.

To start working in a new field can be very demanding and often laborious without guidance by an experienced scientist. Therefore, I highly appreciate the advice and support given to me by my former colleague and friend Dr. Michael Jerabek. His expertise in experimental issues and knowledge of polymers, which he shared with me during many hours in the laboratory and by discussing countless questions, were elementary for this work.

I am grateful to Peter Moharitsch for his help in designing and for the excellent machining of devices for the interferometric test stand and of the compression specimens. I also thank David Mungenast, who performed numerous tests relating to the thermomechanical characterization, for his patient and careful experimental work.

I wish to thank my parents for their unconditional support during my studies.

Finally, and not least, I'm very grateful to my wife Astrid Rauschenbach for her patience with me while spending some long days and weekends in the laboratory and my occasional grumpy mood when the testing machines seemed to conspire against me, and for her encouragement in difficult times of work.

Abstract

The mechanical behavior of polymers depends on time, stress, strain and other influences such as temperature or moisture. Nonlinear behavior can be observed at strains well below 1%, but nevertheless linear viscoelastic behaviour is frequently assumed in the description of time-dependent mechanical properties. However, the nonlinear behavior is typically such that increased stress leads to an increased compliance, unless the deformation is large enough to introduce strong orientation. Hence, when linear viscoelasticity is assumed for e.g. the design of polymer products, the actual deformation at a given load situation may be much larger than anticipated by the linear viscoelastic predicition. In some cases, in addition to the viscoelastic deformation, a load history can cause irreversible deformation. As this deformation depends not only on the applied stress or strain, but on the entire load history, it is referred to as viscoplasticity. For comprehensive modeling of the mechanical behavior of a polymer and the simulation of polymer components, a thorough understanding of the viscoelasticity and viscoplasticity is required. The aim of this research is thus the investigation of experimental and theoretical methods for the characterization and modeling of nonlinear viscoelastic viscoplastic behavior.

Despite its limitations, the theory of linear viscoelasticity is useful for the characterization of time-dependent behavior at low strains or stresses, e.g. when the effect of temperature on the relaxation processes is investigated. The common practice in determining the Prony series parameters for e.g. the uniaxial relaxation modulus is to assume that instantaneous loading to a constant strain was performed. This greatly simplifies the solution of the constitutive equation of linear viscoelasticity but at the expense of a substantial amount of experimental data, which must be discarded to avoid transient effects of the finite loading rate. The relaxation modulus values are determined for each measured point and subsequently a Prony series is determined by fitting of calculated values. This is a very inefficient procedure and improved methods were developed for special loading situations such as constant strain rate loading. The specific assumptions on the loading were introduced in order to simplify the solving of the constitutive equation, but it is experimentally difficult to perform such idealized load histories. Therefore, a more general approach was chosen. A new method based on cubic splines was introduced. It provides an accurate model for the stress or strain and allows for an analytic solution of the constitutive equation in combination with a Prony series model for the viscoelastic material function. No data must be discarded due to simplifying assumptions and it was shown that therefore up to three additional decades of the measurement time can be used. The Prony series is directly determined by fitting the entire set of data to the solution of the constitutive equation, thus avoiding a calculation of point values of the viscoelastic material function. This approach proved especially useful in the determination of the Prony series for the time-dependent Poisson's ratio, for which a direct calculation assuming instantaneous loading is prone to large scatter.

The conducted tests showed that the applicability of linear viscoelasticity is limited to very low strains and stresses. Nonlinear viscoelastic effects were observed e.g. already at strains around 0.6% in stress relaxation. This shows the necessity of a nonlinear viscoelastic model but before a suitable model can be determined, the limits of reversible loading must be known. If the irreversible deformation is neglected, a nonlinear viscoelastic model that is determined by (partially) irreversible loadings can be expected to fail in general loading situations, e.g. repeated testing where viscoplastic strains accumulate. Hence, three experimental techniques were applied to gain insight into the viscoplastic deformation and the limit of reversible loading.

First, a thermomechanical analysis was performed. An experimental setup for very precise and accurate temperature measurements during mechanical testing was developed. The description of heat release or absorption due to elastic behavior follows from the thermodynamic theory. Heat released due to viscoelastic and viscoplastic effects leads to a deviation from the theoretical elastic behavior. The determination of the deformation heat can thus provide information on these processes. It was shown that for the interpretation of the experimental data, the temperature-dependence of the elastic properties must be considered but at the present state of research, an unambiguous distinction between the viscoelastic, viscoplastic and elastic contributions could not be achieved.

Second, a quantitative analysis of the stress whitening during uniaxial tensile testing was conducted. The experiment was designed to allow for the simultaneous measurement of true strain and stress whitening by means of digital image correlation. The stress whitening relates to cavitational processes in the polymer: Light is scattered by cavities, increasing the opacity of the material. The increase depends on the number and size of cavities and is manifested as increasing gray level values in the digital pictures. Hence, the onset of cavitation could be determined by evaluating the gray levels during tensile testing.

Third, strain recovery from uniaxial testing was measured to determine the viscoplastic strain component for various load levels. The viscoplastic strain is the irrecoverable strain that is observed after the completion of the recovery. In contrast to the stress whitening, the strain recovery is also sensitive to non-cavitational plastic deformation. By the latter two methods it was shown that irreversible deformation occurs below 4% strain in the uniaxial tensile tests. A more precise limit could not be given due to the limited strain resolution of the digital image correlation.

The strain recovery data provides a good basis for modeling. The strain-controlled loading at constant engineering strain rate is a complex load history, when the model is formulated with stress being the independent variable. The strain range covers strains close to yield point and thus nonlinear behavior is contained in the data. The stress-controlled recovery phase provides further information on the time-dependence. The determination of residual strain characterizes the evolution of plastic strain during constant strain rate loading. These data are used to define a uniaxial Schapery-type nonlinear viscoelastic viscoplastic model. The constitutive equation of this model is solved using an iterative scheme and the parameters are determined by fitting the solution to the data from the conducted strain recovery tests. It was possible to achieve a good prediction of the time-dependent behavior but it was also shown that the modeling of the viscoplastic strain component has a strong effect on the viscoelastic parameter identification.

Kurzfassung

Die mechanischen Eigenschaften von Kunststoffen hängen unter anderem von Zeit, Temperatur, Spannung und Dehnung ab. In einem kleinen Dehnungs- oder Lastbereich liegt lineares Verhalten vor und das mechanische Verhalten kann mit der Theorie der linearen Viskoelastizität beschrieben werden. Experimente zeigen, daß nichtlineares Verhalten bei thermoplastischen Kunststoffen bereits bei Dehnungen um $0,6\%$ auftreten kann. Wenn beispielsweise die Daten von Kriechversuchen bei verschiedenen Lasten im nichtlinearen Bereich linear viskoelastisch behandelt werden, findet man, daß die Kriechnachgiebigkeit mit steigender Last zunimmt. Bei der Verwendung linear viskoelastischer Gesetze in der Modellierung muss also damit gerechnet werden, daß die Deformation unterschätzt wird. Abhängig von dem Lastverlauf kann es zusätzlich zu nichtlinearem Verhalten auch zu irreversible Deformation kommen. Ähnlich wie die reversible Deformation hängt auch die irreversible Deformation (Viskoplastizität) neben verschiedenen Prüfbedingungen vom gesamten Lastverlauf ab. Eine genaue Modellierung des mechanischen Verhaltens setzt daher das Verständnis der Viskoelastizität und der Viskoplastizität voraus. Das Ziel dieser Arbeit ist daher die Entwicklung experimenteller und theoretischer Methoden zur Charakterisierung und Modellierung nichtlinear viskoelastisch-viskoplastischen Verhaltens.

Vermutlich aufgrund der Komplexität des nichtlinear viskoelastisch-viskoplastischen Verhaltens wird trotz der stark eingeschränkten Gültigkeit oft lineare Viskoelastizität zur Beschreibung des zeitabhängigen Verhaltens angenommen. Eine häufig verwendete Formulierung ist die sogenannte Prony-Reihe, eine endliche Summe von Exponentialfunktionen, die auch als linear viskoelastisches Modell in kommerzielle Simulationssoftware integriert ist. Die Parameter der Prony-Reihe werden häufig aus statischen Versuchen unter der Annahme instantaner Belastung bestimmt. Durch diese Annahme reduziert sich die Integralgleichung der linearen Viskoelastizität zu einer algebraischen Gleichung, wodurch die Auswertung stark vereinfacht wird. Um die Verfälschung des Ergebnisses eines Versuchs mit endlicher Beladungsdauer durch die Vereinfachung instantanen Ladens zu vermeiden, dürfen nur Daten verwendet werden, die nach dem Verstreichen der zehnfachen Beladungsdauer aufgenommen wurden. Angesichts der heutigen Messtechnik, die genaue Messungen je nach Versuchsart schon ab wenigen Zehntelsekunden ermöglicht, erscheint diese Praxis sehr ineffizient. Dies wurde schon vor mehr als drei Jahrzehnten erkannt und einfache Methoden zur Berücksichtigung spezieller Ladevorgänge wurden entwickelt. Mit besser werdenden Computern konnten verfeinerte Methoden entwickelt werden, mit denen eine beträchtliche Verbesserung der Auswertung erreicht werden kann. Diesen Methoden liegt eine spezifische Annahme über die Art des Versuchs, wie zum Beispiel Beladung mit konstanter Dehnrate auf eine dann konstant gehaltene Dehnung, zugrunde, für die die Integralgleichung einfach analytisch gelöst werden kann. In der Anwendung kann eine idealisierte Beladung je nach Regelkreis der Prüfmaschine nur teilweise erreicht werden und Abweichungen führen zu Folgefehlern in der Auswertung. Es wurde daher eine

Methode entwickelt, die auf allgemeine linear viskoelastische Lastverläufe anwendbar ist. Dabei wird ein allgemeiner Dehnungs- oder Spannungsverlauf durch kubische Splines abgebildet, für die ebenfalls eine analytische Lösung der Integralgleichung möglich ist. Ein Vorteil der allgemeinen Formulierung ist, daß alle zur Verfügung stehenden Datenpunkte verwendet werden können. Da das Abwarten der zehnfachen Beladungszeit entfällt, können im Vergleich zur einfachsten Methode zwei bis drei zusätzliche Dekaden der Messzeit ausgewertet werden. Die Parameter der Prony-Reihe werden durch ein *least squares*-Verfahren bestimmt, bei dem die Gesamtheit der Daten berücksichtigt wird. Gegenüber der Bestimmung von Parametern an punktweise berechneten Werten, wie sie bei der Annahme der instantanen Ladung erfolgt, bietet diese Methode eine größere Robustheit gegen Streuung in den Daten. Diese Eigenschaft erwies sich bei der Bestimmung der zeitabhängigen Poissonzahl als vorteilhaft.

Die durchgeführten Versuche zeigten, daß linear viskoelastisches Verhalten nur sehr eingeschränkt angenommen werden kann. Nichtlineares Verhalten wurde bei Polypropylen in Spannungsrelaxationsversuchen bereits bei Dehnungen um $0,6\%$ beobachtet. Es ist daher notwendig, auf ein nichtlinear viskoelastisches Modell zurückzugreifen. Für ein derartiges Modell ist die Anwendungsgrenze durch das Auftreten irreversibler Deformation gegeben. Um diese Grenze zu bestimmen, wurden verschiedene experimentelle Methoden angewendet.

Ein experimenteller Aufbau für thermomechanische Messungen mit einer Thermokamera wurde entwickelt. Durch eine differentielle Messtechnik wird eine sehr gute Reproduzierbarkeit bei hoher Genauigkeit erreicht. Die reversible Wärme, die während eines Versuch frei oder absorbiert wird, wird thermodynamisch durch die Thermoelastizität beschrieben. Abweichungen von der vorhergesagten elastischen Wärme entsteht durch viskoelastische und viskoplastische Dissipation. Das Ziel der thermomechanischen Analyse ist es, die letztgenannten Beiträge zur Wärme zu bestimmen und daraus Informationen über deren Auftreten während der Deformation zu gewinnen. Es konnte gezeigt werden, daß es hierfür notwendig ist, temperaturabhängiges mechanisches Verhalten in der Beschreibung der Thermoelastizität zu berücksichtigen. Eine eindeutige Bestimmung der viskoelastischen und viskoplastischen Beiträge zur Deformationswärme war dennoch nicht möglich.

Weiters wurde das Aufweißverhalten während eines Zugversuchs untersucht. Durch spezielle Probenvorbereitung konnte die Messung des Aufweißverhaltens gleichzeitig mit der Messung des Dehnungsfeldes erfolgen. Das Aufweißen des Materials ist durch das Entstehen von Hohlräumen im Material bedingt, an denen einfallendes Licht gestreut wird. Die Streuung bewirkt, daß das Material zunehmend weißer wird. Durch Quantifizierung des Aufweißens in digitalen Bildern konnte die Initiierung von Hohlräumen detektiert werden.

Im dritten Ansatz zur Untersuchung der Viskoplastizität wurde der Anteil plastischer Deformation durch Messung des Dehnungsrückgangs nach Entlastung bestimmt. Der Rückgang der Dehnung ist vollständig, solange die Deformation reversibel bleibt. Bei viskoplastischer Deformation erfolgt der Rückgang bis zur vorliegenden plastischen Dehnung. Im Gegensatz zur Messung des Aufweißens ist diese Methode auf jede Art der plastischen Deformation empfindlich. Mit beiden Methoden konnte gezeigt werden, daß irreversible Deformation bei uniaxialem Zug bereits unter 4% Dehnung auftritt. Die erreichbare Dehnungsauflösung von ca. 0.02% erlaubte keine genauere Angabe.

Die Daten dieser Messungen beinhalten neben der Information über die viskoplastische Dehnung

auch die nichtlinear viskoelastische Zeitabhängigkeit. Es wurde daher die Eignung dieser Versuchsart für die Bestimmung eines nichtlinear viskoelastisch viskoplastischen Schapery-Modells untersucht. Die Gleichung, die dieses Modell beschreibt, wurde mit einem iterativen Verfahren gelöst und die Parameter durch ein *least squares*-Verfahren bestimmt. Es konnte eine gute Beschreibung des gemessenen Verhaltens erreicht werden. Der Einfluß der Genauigkeit des viskoplastischen Modells auf das Ergebnis des *least squares*-Verfahren wurde diskutiert.

Contents

1 Scope, Content and Background

Polymer composites are widely used in numerous applications, e.g. automotive applications. The use of various filler materials enables a custom design of composite properties. The interaction between the filler and the polymer matrix has a strong influence on the deformation of the matrix and thus of the composite. In order to design a composite for a specific application, an understanding of these mechanisms is important and is therefore subject of current research (Jerabek, 2009; Móczó & Pukánszky, 2008; Renner *et al.*, 2005; Pukánszky, 2005). A large variety of filler materials with different mechanical properties and geometries is used, ranging from glass fibres to rubber inclusions. To reduce the expensive and time-consuming preparation and testing of several composite materials until the desired properties are met, computer simulations of material properties (Herbst, 2008; Sheng *et al.*, 2004; Zeng *et al.*, 2008; Goddard *et al.*, 2001; Marklund *et al.*, 2006; Nordin & Varna, 2006a) and polymer parts (Muliana & Haj-Ali, 2004a; Martin & Renault, 2009; Haj-Ali & Muliana, 2004; Muliana & Haj-Ali, 2006) are a valuable tool. The usefulness of such simulations depends not only on the proper description of the effect of fillers but also on the accurate modeling of the matrix material. The mechanical behavior of the polymer matrix depends on several parameters, including temperature, load history and strain rate. Simplified modeling can be performed by leaving some experimental paramters fixed, e.g. by isothermal testing using a specific load history such as monotonic uniaxial tension. Simulations with thus determined model parameters are invariably limited to problems that are similar to the test conditions applied in finding the model. For a correct prediction of polymer components under general loadings, the effect of e.g. strain rate and stress state must be considered in the model. Different types of models can be used: phenomenological models use mathematical expressions that represent observed mechanical behavior. Physical models use information on material properties and processes to derive a mathematical description (Drozdov & Gupta, 2003; Knauss & Emri, 1981). Other examples are mechanical models with (nonlinear) springs and dashpots, in series or parallel, from which the mechanical behavior is determined (Tschoegl, 1989; Klompen & Govaert, 1999). A very widely used model of this type is the linear viscoelastic Prony series model. In the thermodynamic approaches constitutive equations are inferred from thermodynamic potentials and functional representations of material properties are chosen phenomenologically. A widely used model of the latter type is the Schapery model (Schapery, 1969), where e.g. polynomials are chosen to represent the functions accounting for nonlinear viscoelastic behavior. In the literature these models are often built one-dimensionally from uniaxial data (Nordin & Varna, 2006b, 2005; Lai & Bakker, 1995b) and, for isotropic materials, extended to three dimensions by assuming a constant Poisson's ratio (Muliana & Haj-Ali, 2004b; Lévesque *et al.*, 2008). However, a time-dependent Poisson's ratio, typically (Tschoegl *et al.*, 2002) but not necessarily (Lakes & Wineman, 2006) monotonically increasing with time is observed in experiments. Despite this experimental observation, constant Poisson's ratio is frequently assumed

because of the difficulties in accurately measuring the small transverse strains and also to simplify the three-dimensional model equations. In fact, only few studies presenting data on time-dependent Poisson's ratio for polymeric materials have been published (Tschoegl *et al.*, 2002). In view of this unsatisfactory situation, the applicability of digital image correlation strain measurement to determine time-dependent Poisson's ratio of polypropylene was investigated for several temperatures and loading modes. A data reduction technique was developed that allows for a direct identification of the linear viscoelastic Prony series model parameters from the strain data, without any specific assumptions on the type of test, e.g. stress relaxation or creep. This technique uses least-squares fitting and has thus an inherent robustness against data scatter, which is especially useful when dealing with the determination of time-dependent Poisson's ratio. Additionally, due to the general formulation of the method, data from the loading ramp of creep or stress relaxation tests can be used for the Prony series parameter identification and thus the time range that can be covered by a single test is extended compared to traditional step-loading assumption evaluation. This was demonstrated for the uniaxial relaxation modulus and time-dependent Poisson's ratio for various load histories.

The uniaxial relaxation modulus and time-dependent Poisson's ratio are of theoretical and practical interest, because both material functions can be measured simultaneously on the same specimen. Theoretically, any of the four linear viscoelastic material functions - Poisson's ratio, uniaxial relaxation modulus, shear modulus and bulk modulus, can be calculated when two others are known. In commercial simulation software, such as Digimat, the bulk and shear moduli of the material must be provided, but it is difficult to determine the bulk modulus experimentally (Deng & Knauss, 1997), and thus only few directly measured bulk modulus data are available. Thus, it is desirable to find the bulk relaxation modulus by interconversion of other material functions. Interconversion of material functions is sensitive to errors caused by specimen-to-specimen or environmental and experimental variations (Tschoegl *et al.*, 2002), which implies for example that the use of the shear and the uniaxial relaxation modulus measured in separate tests is not acceptable. Hence, the uniaxial relaxation modulus and Poisson's ratio are an obvious choice for the calculation of the bulk modulus, but in practice, reliable interconversion is difficult because of the high accuracy and precision that is required, particularly for high values of Poisson's ratio. It has been estimated by Lu *et al.* (1997) that Poisson's ratio must be determined to an accuracy of up to 10^{-4} to obtain the bulk modulus within reasonable error bounds from the uniaxial relaxation modulus and Poisson's ratio, when the latter is close to 0.5. The requirements are less strict when Poisson's ratio is smaller but it is still experimentally challenging to measure and the lack of reliable data on time-dependent Poisson's ratio is an indication thereof. Nonetheless, the error on the time-dependence of the bulk modulus arising from the constant Poisson's ratio assumption is severe (Hilton, 2001) and research in time-dependent Poisson's ratio is justified.

Apart from the considerations above, the nonlinear reversible and irreversible deformation is of high importance in the prediction of mechanical behavior. For the investigated polypropylene nonlinear effects were already observed in creep at low loads of 3MPa, or in stress relaxation at low strains of 0.6%. Irreversible deformation is undesirable in applications or may be tolerable only up to certain levels. Like the reversible mechanical behavior, the irreversible behavior depends on the load history and is therefore termed viscoplasticity. The viscoplastic deformation and the limit of

reversible loading in uniaxial tension are studied using three different experimental techniques.

An experimental setup for very precise and accurate temperature measurements during mechanical testing was developed to conduct a thermomechanical analysis. This approach to examine the deformation from a thermodynamic point of view was intensively used by Oleinik and coworkers(Oleinik *et al.*, 1993; Shenogin *et al.*, 2002). They have investigated the energy storage and heat dissipation during the compressive deformation at low strain rates of various polymers using calorimetric techniques and formulated a deformation theory based on small-scale plastic shear transformations. In this approach the internal energy stored in the polymer upon deformation is calculated from the heat of deformation and the deformation work by the first law of thermodynamics. In order to determine the viscoelastic and viscoplastic contributions, the elastic parts must be accounted for. The elastic deformation work follows from Hooke's law and the elastic part of heat is given by the thermoelastic effect. The classic theory of thermoelasticity leads to a linear relation between heat and stress. However, in tensile experiments on polypropylene and polyethylene, Volodin & Slutsker (1994) observed a temperature decrease that is not consistent with the linear theory and explained this finding by considering the temperature-dependence of the mechanical properties. A thermoelastic theory for temperature-dependent elastic materials has already been developed by Wong *et al.* (1987) and Wong *et al.* (1988). However, in contrary to the findings on polypropylene and polyethylene, the linear theory was successfully used in in a number of publications (Shenogin *et al.*, 2002; Tregub *et al.*, 1994; Moreau *et al.*, 2005). The experimental results obtained with infrared imaging technique confirm the observation on polypropylene by Volodin and Slutsker. The thermodynamic theory does not make any specific assumptions on the material other than the temperature-dependent elasticity, hence similar behavior was expected for amorphous polymers. To rule out a coincidental effect of the semicrystalline structure of polypropylene, tests were also conducted with polycarbonate and polymethylmethacrylate. An experimental technique to determine one type of irreversible deformation was implemented by the analysis of the stress whitening of polypropylene during uniaxial tensile testing. Stress whitening describes the whitening of the material due to cavitational processes in the polymer: Light is scattered by cavities, increasing the opacity of the material. In the literature, the degree of whitening was examined dependent on the position on a tensile specimen to characterize localization effects (Dasari & Misra, 2004) or to analyze the scratch resistance of polymer surfaces (Kody & Martin, 1996). For the present research, the stress whitening was determined from digital pictures of the specimen taken during tensile testing for a simultaneous determination of whitening and true strain with digital image correlation. With this technique the onset of cavitational deformation was quantified for several test temperatures.

The third technique is the measurement of strain recovery. In strain recovery testing specimens are subjected to a specific load history and the recovery of strain after unloading is measured. The recovery may be complete, i.e. to the unstrained state, or residual strain may be present that does not recover or recovers only after very long times (Quinson *et al.*, 1996). Therefore, this residual strain can be regarded as plastic deformation and the strain recovery technique provides means to characterize this plastic deformation under several load histories (Fasce *et al.*, 2009) and to find yield criteria (Quinson *et al.*, 1997; Marano & Rink, 2001) or study deformation modes (Oleinik *et al.*, 1993). For this work, the strain recovery from uniaxial tension was measured with high

accuracy using the digital image correlation strain measurement technique. At room temperature, the reversible limit was found below a strain of 4%. The limit decreases with increasing temperature down to 2.2% at 80°C.

The observation that plastic deformation was already found at 4% strain shows that a nonlinear viscoelastic model for room temperature must be limited to this strain range. For the description of higher strains, a nonlinear viscoelastic viscoplastic model is needed. The strain recovery data provides good input for the definition of such a model, because it contains information on both viscoplasticity and viscoelasticity. For the modeling of these tests, a Schapery nonlinear viscoelastic model is combined with a viscoplastic model. This type of model has been successfully used for several materials, often to model creep behavior, e.g. by Lai & Bakker (1995a); Nordin & Varna (2006b). Instantaneous loading is assumed in many studies because the determination of the material functions is simple. This simplification can induce errors in the parameters (Sorvari *et al.*, 2006) but methods to solve the Schapery equation have already been developed e.g. for implementation in finite element method software by Henriksen (1984); Muliana & Haj-Ali (2004b); Lai & Bakker (1996) and Crochon *et al.* (2010), that can also be applied in the parameter identification without assumptions on the load history. In the present paper, the iterative solution for finite element implementation derived by Muliana & Haj-Ali (2004b) is used in an optimization algorithm to determine model parameters by fitting the data from the conducted strain recovery tests. Due to the current unavailability of multiaxial nonlinear viscoelastic viscoplastic data and due to the difficulties in three dimensional model definition referred to above, this research is restricted to isothermal uniaxial modeling.

2 Major Results

This section gives an overview of the major results of this dissertation. More detailed results are presented in the collection of papers.

2.1 Papers 1 & 2

In these papers, the application of a new evaluation technique for the determination of linear viscoelastic material functions of isotropic homogeneous materials from arbitrary strain histories within the linear viscoelastic domain is presented. The potential of this technique is demonstrated by the determination of the relaxation modulus of polypropylene from creep tests. The extension of the time range covered in the tests due to the use of data from the loading ramp allowed for a construction of a master curve encompassing roughly ten decades in time from four twenty minutes creep tests at four different temperatures. A traditional evaluation of the creep compliance requires 4 days of testing to cover the same time range. This is illustrated in figure 2.1, in which the creep modulus (inverse creep compliance) is compared to the relaxation modulus that was determined using the new method. The results thus obtained agree well with results from the relaxation tests, see figure 2.2.

An inherent robustness to data scatter is a beneficial property of the method. This is helpful for the determination of time-dependent Poisson's ratio, where the evaluation according to the ten-times rule leads to amplification of the data scatter (figure 2.3).

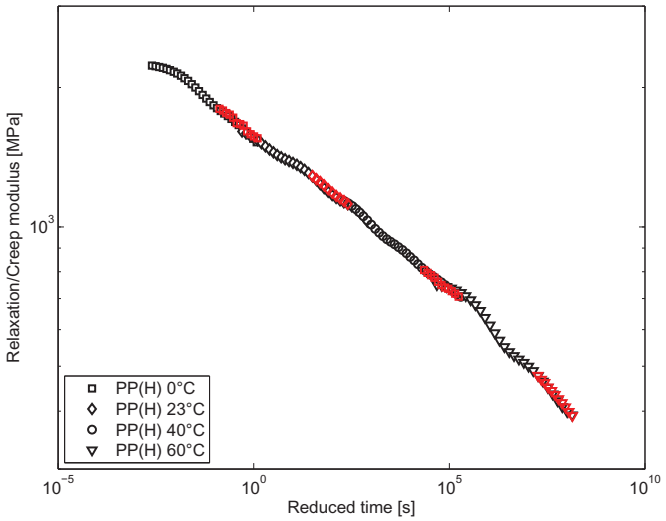

Figure 2.1: Relaxation modulus of PP(H) from creep tests. The red markers show the creep modulus evaluation using the ten-times rule. The master curve is referenced to 23°C.

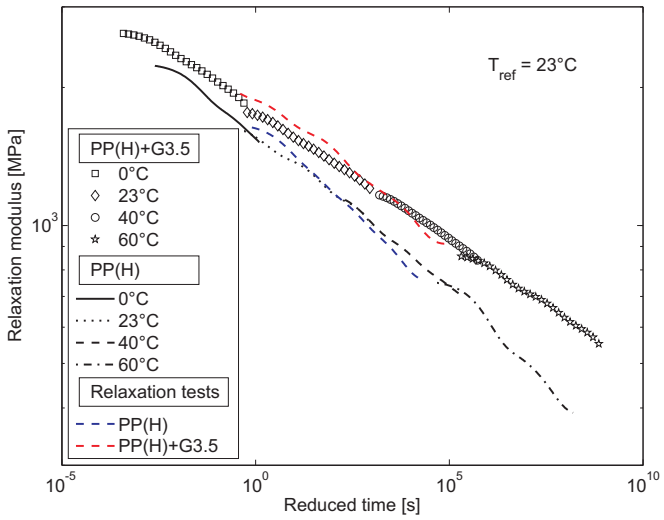

Figure 2.2: Comparison of the relaxation modulus results from tensile relaxation and creep tests for PP(H) and PP(H)+G3.5 for a reference temperature of 23°C.

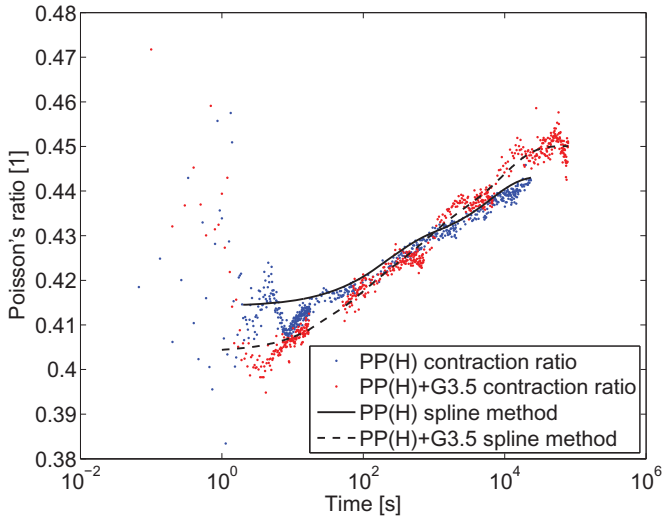

Figure 2.3: Poisson's ratio determined by spline method and contraction ratio of PP(H) and PP(H)+G3.5

2.2 Paper 3

A study of the thermoelastic effect and the heat evolution during uniaxial compression and tension of polypropylene, polycarbonate and polymethylmethacrylate has been presented. A carefully designed experimental setup enables high precision temperature measurements with an infrared camera. As the theoretical description of the thermoelastic effect assumes adiabatic conditions, the heat transfer due to convection in the temperature chamber and the heat flow in the specimen cross-section have been found by solving the heat equation. From this solution the heat generated per unit volume and unit time can be derived and compared to the thermoelastic heat. For a dissipating material, the measured heat release must exceed the heat predicted by the thermoelastic theory. To determine the reversible heat and the dissipated heat, the reversible thermoelastic prediction was

subtracted from the measured heat. It was possible to show that the revised thermoelastic theory for temperature-dependent elastic materials must be used to obtain heat dissipation data (figure 2.4). However, the calculated thermoelastic effect according to this theory appears to be too pronounced when compared to the deformation work. It was found that with the present thermoelastic theory, the dissipated heat exceeds the deformation work (figure 2.5). Further refinement of the theory, e.g. considering stress-dependent physical properties, may resolve this problem.

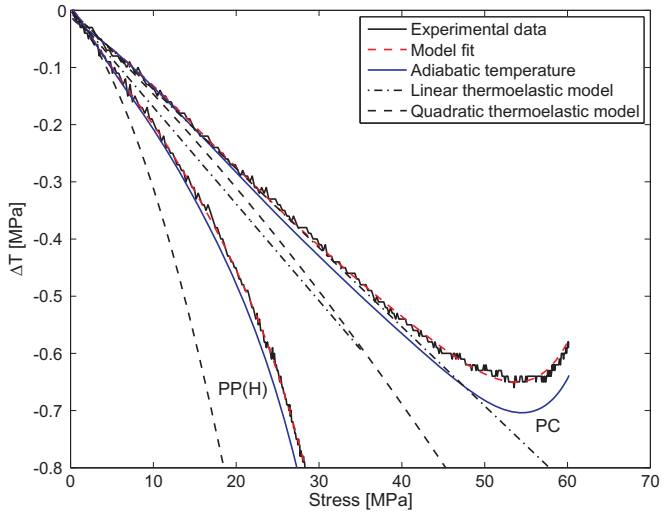

Figure 2.4: Experimental data from uniaxial tensile tests, calculated adiabatic temperature and thermoelastic curves for PC and PP(H).

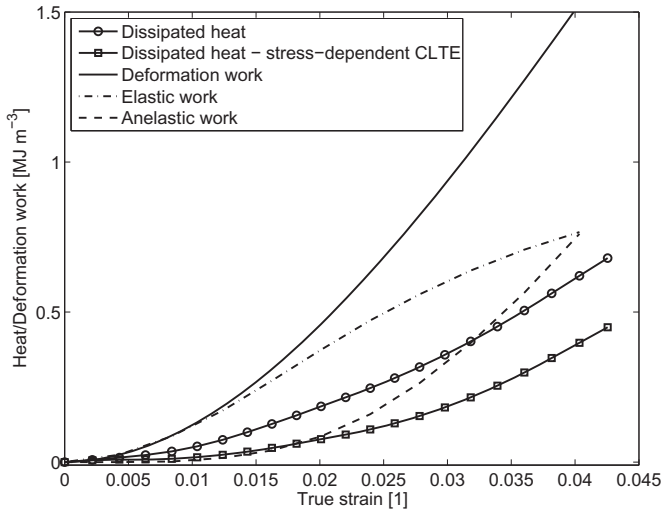

Figure 2.5: Dissipated heat and total, elastic and anelastic deformation work of PC in uniaxial tension. One heat curve (square markers) was calculated assuming an arbitrarily stress-dependent CLTE.

2.3 Paper 4

Recovery tests of polypropylene from engineering strains between 0.5% and 8% at temperatures of 23°C, 40°C, 60°C and 80°C have been performed. Once a steady strain state was achieved, the strain was averaged over about one decade of testing time to define the residual plastic strain. In figure 2.6, the residual strain is depicted over the peak true strain together with the true stress-true strain curve. Plastic deformation was observed below 4% strain. Repeated recovery tests have been carried out from 4%, 6% and 8% nominal strain. In these tests a specimen has been subjected to a second recovery test after having completed the first test. The true stress-true strain curves of the two loadings indicate a loss of mechanical strength. This decrease is small at 4% peak strain and more pronounced at 6% and 8% strain. At the nominal strain of 8% the maximum true strain measured on the inhomogeneously deformed specimen was 9.7% after the first and 11.1% after the second loading. An increase of 0.8% in plastic strain after the second loading was detected.

A physical aging effect has been observed while testing at 60°C and 80°C. After a certain recovery time shrinkage of the specimen occured. The effect was most distinct during recovery from lower strains. The shrinkage had set in before a fully steady recovery state was achieved. The residual strain has therefore been approximated by the strain achieved before the appearance of aging in the recovery curves. The error in this approximation is small because the major part of the recovery has already been completed before the aging effect appeared. Polynomials have been fitted to the data to determine the onset of plastic deformation as the strain at which the plastic strain exceeds the arbitrarily chosen value of 0.05%. Thus it was found that the limit of reversible loading under the present experimental conditions is 3.9% at 23°C and decreases to 2.2% at 80°C.

The plastic deformation can be classified as cavitational deformation and shear yielding. In this case, cavitation includes the formation of voids and craze-like structures. Cavitation is indicated by stress whitening of the semitransparent material: Light scattering on voids creates an opaque appearence. The degree of opacity depends on the density of voids, hence it increases with tension. In the measurement of stress whitening the degree of voiding is characterized by the gray level of digital images of a specimen. This technique provides additional information on the plastic

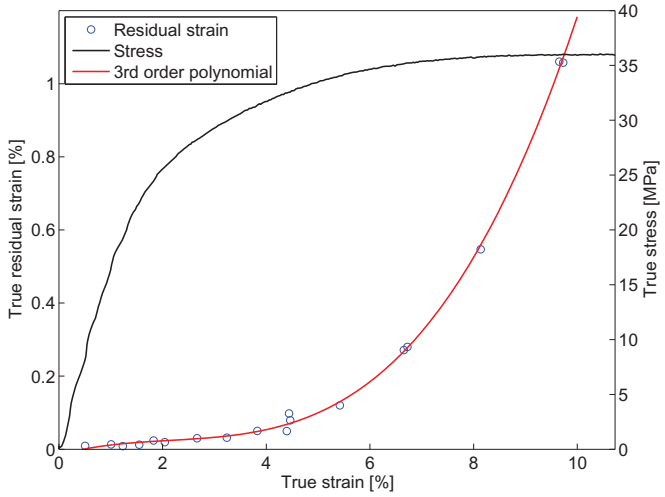

Figure 2.6: Residual strain and true stress-true strain curve of polypropylene for tests at 23°C.

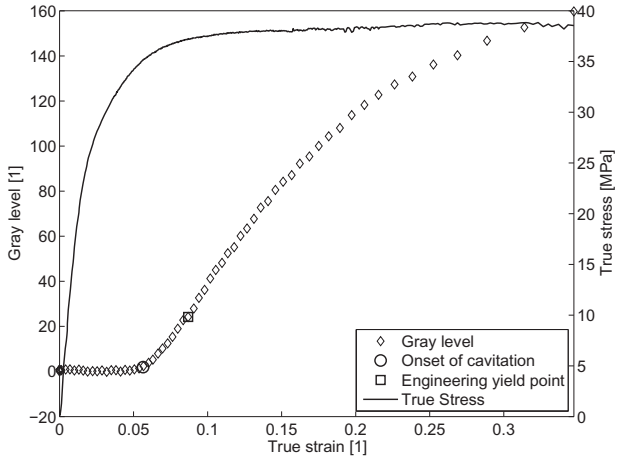

Figure 2.7: True stress-true strain curve and the gray level vs. true strain for polypropylene at room temperature and a strain rate of $8.7 \cdot 10^{-3}$. The strain at the onset of cavitation (circle) and the engineering yield strain (square) are indicated. For clarity of the plots markers are only shown for a subset of the data of each test.

deformation measured in strain recovery because it can be inferred when cavities of sufficient size for light scattering are formed.

Tensile tests have been conducted at temperatures ranging from $-20°$C to $80°$C and true stress and true strain were determined. From the pictures taken by the digital image correlation strain measurement system the gray level in the zone of maximum deformation was determined. Figure 2.7 shows the true stress-true strain curve and the gray level vs. true strain from a test conducted at room temperature and a strain rate of $8.7 \cdot 10^{-3}$ s^{-1}. The gray level starts to increase rather sharply when a certain strain level is achievend, which is arbitrarily defined as the strain at the largest curvature of the gray level curve, which is approximately 5% strain for the room temperature test. In comparison, the yield strain (strain at maximum engineering stress) is 8.7%. In the tests at higher temperatures it was found that the cavitational strain increases more heavily with temperature than the engineering yield strain.

2.4 Paper 5

The strain recovery data includes information on the nonlinear plasticity and time-dependence of polypropylene. In terms of stress the data cannot be described by a simple mathematical expression because the initial loading has been done at constant engineering strain rate. Hence, the parameter identification procedure was implemented for general load histories. The considered uniaxial model is a Schapery-type nonlinear viscoelastic viscoplastic model for the strain. The parameters describing the viscoplasticity were determined by fitting the viscoplastic component of the model strain to the residual strains observed in strain recovery. The viscoelastic part of the model was then solved with an iterative scheme and nonlinear optimization was used to find the nonlinear stress-functions and the Prony series compliance parameters. The optimization was performed over the collection of strain recovery tests. The formulation is general and data from other types of tests can be included. The result of the parameter identification is shown for representative tests in

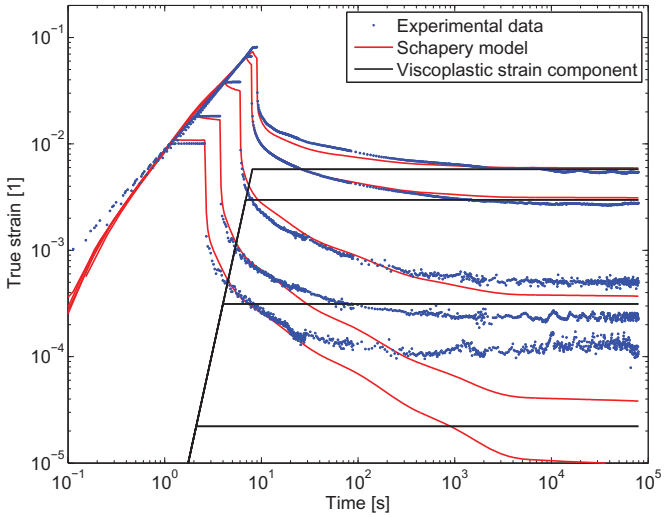

Figure 2.8: Strain recovery data and Schapery model result for recovery tests of polypropylene conducted with peak true strains of 8.1%, 6.7%, 3.8%, 1.8% and 1.0%.

figure 2.8. Good agreement has been achieved for the initial loading and the initial recovery, however the agreement at the larger times was limited by the accuracy of the viscoplastic model. By manipulation of the Prony series to account for the discrepancy between the viscoplastic model and the measured plastic strains in the intermediate strain range, an improvement of the optimization result was obtained.

3 Conclusion and Outlook

In this dissertation the time-dependent reversible and irreversible mechanical behavior of polypropylene was investigated. Experimental setups and theoretical methods have been developed to measure and model the nonlinear viscoelastic viscoplastic behavior.

First, a semi-analytic method for the determination of linear viscoelastic Prony series models for any linear viscoelastic material function of an isotropic, homogeneous material has been derived. It was demonstrated that with a careful experimental setup data reduction can be performed on data down to a few tenths of seconds of testing time. Limitations are given by the initial instabilities of the testing machine and the achievable stress and strain resolution. Compared to traditional data reduction it was shown that approximately two additional decades of the testing time can be covered, by proper treatment of the linear viscoelastic constitutive equation without any kind of extrapolation. The developed method also proved very useful in the determination of time-dependent Poisson's ratio because it has improved robustness to data scatter. The parameter identification for Prony series models can be readily accomplished to define linear viscoelastic models for simulations with commercial simulation software. Applications apart from of this dissertation included the modeling and simulation of polypropylene composites, forwhich the polypropylene investigated in this dissertation serves as matrix, and the linear viscoelastic modeling of thermoplastic polyurethanes.

In order to further enhance the knowledge about the mechanical behavior of polypropylene, the nonlinear viscoelasticity and viscoplasticity has been studied. In one approach, the deformation heat during uniaxial compression and tension of polypropylene has been measured using infrared imaging and were then compared to the thermoelastic heat. The latter was calculated from the thermodynamic theory of temperature-dependent elastic materials. An experimental setup for high precision temperature measurements has been developed and a heat transfer model has been introduced to account for the convection in the temperature chamber. It was shown that the consideration of the temperature-dependence of the mechanical properties is required in order to obtain meaningful heat dissipation data. However, an inconsistency between the deformation heat and work has been observed, which indicates that further refinement of the thermoelastic model is necessary. The origin of this discrepancy is not yet clear. Further research should concentrate on the effect of the stress-dependence of thermal and physical properties, e.g. coefficient of thermal expansion, density or thermal conductivity, and on aspects of the definition of the elastic mechanical parameters. After this problem is solved, the gathered thermal data can be used to distinguish the elastic from the viscoelastic and viscoplastic deformation heat to provide information on the deformation mechanisms.

Another approach to characterize the viscoplastic deformation is the measurement of strain recovery and stress whitening. The stress whitening has been quantified by digital imaging of the specimen with a digital image correlation system. This allows for a simultaneous measurement of

the strain field and the stress whitening. The initiation of cavitation was determined from the gray level vs. true strain curves. Cavitation has been detected before the engineering yield strain was reached, except for the test temperature of 80°C. With increasing temperature the crystalline phase becomes weaker, which influences the competition between cavitation and plastic shear deformation. With a rise in temperature shear yielding becomes more dominant. On the other hand, it has been found that the residual strain for a given maximum load increases with temperature. Hence, cavitation is reduced by higher temperatures but the load range admissible for reservible behavior becomes smaller because of increased shear yielding. Strain recovery from various tensile strain levels also showed that plastic deformation occurs well before the yield point and the onset of cavitation at all investigated temperatures between 23°C and 80°C. The measurement of strain recovery proved to be a valuable tool for the characterization of the deformation behavior.

Finally, the strain recovery data were used to identify the parameters of a Schapery-type nonlinear viscoelastic viscoplastic model. The parameters for a simple viscoplastic model were determined by fitting the model to the residual strains observed in strain recovery. The viscoelastic part of the model was solved using an iterative scheme and nonlinear optimization was applied to determine the nonlinearizing functions and the Prony series compliance parameters from the collection of strain recovery tests. Good agreement has been obtained for the loading ramp and the initial recovery, but it also became apparent that the accuracy of the viscoplastic component has a strong influence on the identification of the viscoelastic parameters. Some error has been detected in the application of the determined model to stress relaxation data and it was found that different models which offer equally good representations of the strain recovery data can exhibit very different behaviors in stress relaxation.

It has thus been concluded that future work should include testing at a variety of different load histories to obtain further data on the viscoplasticity and to gain more data for the parameter identification of the viscoelastic model. For this purpose a more elaborate viscoplastic model, which can describe e.g. the effect of stress state, loading rate or creep time, is required. Even when only uniaxial tests are used a large number of experiments must be conducted. Potential tests include stress relaxation for a number of testing times at various strains and monotonic loading at different strain and stress rates as well as creep recovery for different loads and creep times. For future work a specialized creep test stand set up while writing this thesis has been adapted for carrying out creep and relaxation recovery tests. Finally, the model must be formulated in three dimensions for implementation in a finite element method software. In the literature, the three dimensional model is constructed from the uniaxial model by assuming a constant Poisson's ratio, which is clearly a very rough simplification for most thermoplastics. With a constant Poisson's ratio the bulk compliance is proportional to the creep compliance. In contrast, the scarce experimental data on bulk relaxation shows that there is significantly less relaxation than in the shear or uniaxial relaxation moduli. Hence, future will focus on the identification of parameters of a generally formulated three dimensional model. The two main tasks will be the numerical implementation of the model for parameter optimization and finite element method simulations, as well as multiaxial testing for a proper treatment of the stress state dependence of the nonlinearizing functions, which account for the stress dependence of the mechanical behavior.

References

Crochon, T., Schönherr, T., Li, C., & Lévesque, M. 2010. On finite-element implementation strategies of Schapery-type constitutive theories. *Mechanics of Time-Dependent Materials*, 1–29.

Dasari, A., & Misra, R.D.K. 2004. The role of micrometric wollastonite particles on stress whitening behavior of polypropylene composites. *Acta Materialia*, **52**, 1683–1697.

Deng, T.H., & Knauss, W.G. 1997. The Temperature and Frequency Dependence of the Bulk Compliance of Poly(Vinyl Acetate). A Re-Examination. *Mechanics of Time-Dependent Materials*, **1**, 33–49.

Drozdov, A. D., & Gupta, R. K. 2003. Non-linear viscoelasticity and viscoplasticity of isotactic polypropylene. *International Journal of Engineering Science*, **41**(20), 2335 – 2361.

Fasce, Laura A., Pettarin, Valeria, Marano, Claudia, Rink, Marta, & Frontini, Patricia M. 2009. Biaxial Yielding of Polypropylene/Elastomeric Polyolefin Blends: Effect of Elastomer Content and Thermal Annealing. *Polymer Engineering and Science*, **48**(7), 1414–1423.

Goddard, William A., Cagin, Tahir, Blanco, Mario, Vaidehi, Nagarajan, Dasgupta, Siddharth, Floriano, Wely, Belmares, Michael, Kua, Jeremy, Zamanakos, Georgios, Kashihara, Seichi, Iotov, Mihail, & Gao, Guanghua. 2001. Strategies for multiscale modeling and simulation of organic materials: polymers and biopolymers. *Computational and Theoretical Polymer Science*, **11**(5), 329 – 343.

Haj-Ali, Rami M., & Muliana, Anastasia H. 2004. A multi-scale constitutive formulation for the nonlinear viscoelastic analysis of laminated composite materials and structures. *International Journal of Solids and Structures*, **41**(13), 3461 – 3490.

Henriksen, Mogens. 1984. Nonlinear Viscoelastic Stress Analysis - A Finite Element Approach. *Computers & Structures*, **18**(1), 133–139.

Herbst, Harald. 2008. Micro-mechanical modelling of heterogeneous polypropylene compounds. *Dissertation, University of Leoben*.

Hilton, Harry H. 2001. Implications and Constraints of Time-Independent Poisson Ratios in Linear Isotropic and Anisotropic Viscoelasticity. *Journal of Elasticity*, **63**(3), 221–251.

Jerabek, Michael. 2009. Advanced Characterization of the Tensile and Compressive Behavior of PP and PP Composites. *Dissertation, University of Leoben*.

Klompen, E.T.J., & Govaert, L.E. 1999. Nonlinear Viscoelastic Behaviour of Thermorheologically Complex Materials. *Mechanics of Time-Dependent Materials*, **3**, 49–69.

Knauss, W.G., & Emri, I.J. 1981. Non-linear Viscoelasticity based on Free-Volume Considerations. *Computers and Structures*, **13**, 123–128.

Kody, R.S., & Martin, D.C. 1996. Quantitative characterization of surface deformation in polymer composites using digital image analysis. *Polymer Engineering and Science*, **36**(2), 298–304.

Lai, J., & Bakker, A. 1995a. Analysis of the non-linear creep of high-density polyethylene. *Polymer*, **36**(1), 93–99.

Lai, J., & Bakker, A. 1995b. An Integral Constitutive Equation for Nonlinear Plasto-Viscoelastic Behavior of High-Density Polyethylene. *Polymer*, **35**(17), 1339–1347.

Lai, J., & Bakker, A. 1996. 3D schapery representation for non-linear viscoelasticitiy and finite element implementation. *Computational Mechanics*, **18**, 182–191.

Lakes, R.S., & Wineman, A. 2006. On Poisson's Ratio in Linear Viscoelastic Solids. *Journal of Elasticity*, **85**(1), 45–63.

Lu, H., Zhang, X., & Knauss, W.G. 1997. Uniaxial, Shear and Poisson Relaxation and Their Conversion to Bulk Relaxation: Studies on Poly(Methyl Methacrylate). *Polymer Engineering and Science*, **37**(6), 1053–1063.

Lévesque, M., Derrien, K., Baptiste, D., & Gilchrist, M.D. 2008. On the development and parameter identification of Schapery-type constitutive theories. *Mechanics of Time-Dependent Materials*, **12**(2), 95–127.

Marano, Claudia, & Rink, Marta. 2001. Shear yielding threshold and viscoelasticity in an amorphous glassy polymer: a study on a styrene-acrylonitrile polymer. *Polymer*, **42**, 2113–2119.

Marklund, E., Varna, J., & Wallström, L. 2006. Nonlinear viscoelasticity and viscoplasticity of flax/polypropylene composites. *Journal of Engineering Materials and Technology, Transactions of the ASME*, **128**(4), 527–536.

Martin, C., & Renault, T. 2009. On the Modeling of the Static and Dynamic Behavior of a Beam Molded in STAMAX (Long Glass Fiber PP). *Digimat User Meeting.*

Móczó, J., & Pukánszky, B. 2008. Polymer micro and nanocomposites: Structure, interactions, properties. *Journal of Industrial and Engineering Chemistry*, **14**(5), 535–563.

Moreau, S., Chrysochoos, A., Muracciole, J.-M., & Wattrisse, B. 2005. Analysis of thermoelastic effects accompanying the deformation of PMMA and PC polymers. *Comptes Rendus - Mecanique*, **333**(8), 648–653.

Muliana, Anastasia H., & Haj-Ali, Rami M. 2004a. Nested nonlinear viscoelastic and micromechanical models for the analysis of pultruded composite materials and structures. *Mechanics of Materials*, **36**(11), 1087 – 1110.

Muliana, Anastasia H., & Haj-Ali, Rami M. 2004b. Numerical finite element formulation of the Schapery non-linear viscoelastic material model. *International Journal for Numerical Methods in Engineering*, **59**(1), 25–45.

Muliana, Anastasia H., & Haj-Ali, Rami M. 2006. Analysis for creep behavior and collapse of thick-section composite structures. *Composite Structures*, **73**(3), 331 – 341.

Nordin, L.-O., & Varna, J. 2006a. Nonlinear viscoplastic and nonlinear viscoelastic material model for paper fiber composites in compression. *Composites Part A: Applied Science and Manufacturing*, **37**(2), 344–355.

Nordin, Lars-Olof, & Varna, Janis. 2005. Methodology for Parameter Identification in Nonlinear Viscoelastic Material Model. *Mechanics of Time-Dependent Materials*, **9**(4), 57–78.

Nordin, Lars-Olof, & Varna, Janis. 2006b. Nonlinear viscoplastic and nonlinear viscoelastic material model for paper fiber composites in compression. *Composites: Part A*, **37**, 344–355.

Oleinik, E.F., Salamatina, O.B., Rudnev, S.N., & Shenogin, S.V. 1993. A New Approach to Treating Plastic Strain in Glassy Polymers. *Polymer Science*, **35**(11), 1532–1558.

Pukánszky, B. 2005. Interfaces and interphases in multicomponent materials: Past, present, future. *European Polymer Journal*, **41**(4), 645–662.

Quinson, R., Perez, J., Rink, M., & Pavan, A. 1996. Components of non-elastic deformation in amorphous glassy polymers. *Journal of Materials Science*, **31**, 4387–4394.

Quinson, R., Perez, J., Rink, M., & Pavan, A. 1997. Yield criteria for amorphous glassy polymers. *Journal of Materials Science*, **31**, 1371–1379.

Renner, K., Yang, M.S., Móczó, J., Choi, H.J., & Pukánszky, B. 2005. Analysis of the debonding process in polypropylene model composites. *European Polymer Journal*, **41**(11), 2520–2529.

Schapery, R.A. 1969. On the Characterization of Nonlinear Viscoelastic Materials. *Polymer Engineering and Science*, **9**(4), 295–310.

Sheng, N., Boyce, M. C., Parks, D. M., Rutledge, G. C., Abes, J. I., & Cohen, R. E. 2004. Multiscale micromechanical modeling of polymer/clay nanocomposites and the effective clay particle. *Polymer*, **45**(2), 487 – 506.

Shenogin, S. V., Höhne, G. W. H., & Oleinik, E. F. 2002. Thermodynamics of the pre-yield deformation behavior of glassy polymers: measurements with new deformation calorimeter. *Thermochimica Acta*, **391**(1-2), 13 – 23.

Sorvari, Joonas, Malinen, Matti, & Hämäläinen, Jari. 2006. Finite ramp time correction method for nonlinear viscoelastic material model. *International Journal of Non-Linear Mechanics*, **41**, 1050–1056.

Tregub, A., Privalko, V.P., Kilian, H.G., & Marom, G. 1994. The thermoelastic behaviour of semicrystalline and of glassy poly(ether-ether-ketone). *Applied Composite Materials*, **1**(2), 167–176.

Tschoegl, N.W. 1989. *The Phenomenological Theory of Linear Viscoelastic Behavior: An Introduction*. Springer.

Tschoegl, N.W., Knauss, W., & Emri, I. 2002. Poisson's ratio in linear viscoelasticity - A critical review. *Mechanics of Time-Dependent Materials*, **6**(1), 3–51.

Volodin, V.P., & Slutsker, A.I. 1994. Specific features of the thermoelastic effect in polymers. *Thermochimicia Acta*, **247**, 121–128.

Wong, A.K., Jones, R., & Sparrow, J.G. 1987. Thermoelastic constant or thermoelastic parameter? *J. Phys. Chem. Solids*, **48**(8), 749–753.

Wong, A.K., Sparrow, J.G., & Dunn, S.A. 1988. On the revised theory of the thermoelastic effect. *J. Phys. Chem. Solids*, **49**(4), 395–400.

Zeng, Q.H., Yu, A.B., & Lu, G.Q. 2008. Multiscale modeling and simulation of polymer nanocomposites. *Progress in Polymer Science*, **33**(2), 191 – 269.

Collection of Papers

On the Determination of the Relaxation Modulus of PP Compounds from Arbitrary Strain Histories

Daniel Tscharnuter · Michael Jerabek · Zoltan Major · Reinhold W. Lang

Abstract Advanced evaluation methods for the determination of linear viscoelastic material functions have been developed already forty years ago, but it is still common practice to use the so-called ten-times rule. The rule is that a sufficiently long time needs to pass after a constant load or strain is applied so that the material response is close to the response of step excitation. A substantial amount of experimental data in the short-term range has to be discarded to obtain valid results. Renewed attention has been given to improving this situation during the last few years.

In this paper, the application of modern evaluation techniques to the determination of the relaxation modulus of isotropic homogeneous linear viscoelastic materials is presented. A new method that is applicable to general strain histories is introduced and applied to different loading types.

Keywords viscoelastic behavior, ramp loading, relaxation test, creep test, relaxation modulus

1 Introduction

Within the framework of linear viscoelasticity, the relaxation modulus is theoretically simply determined from the stress that occurs in response to a step strain. As it is impossible to apply a step strain in experiments, one has to deal with the finite loading time. One may do so by either using only data that has been measured a suitable time after the end of the loading ramp and compute the relaxation modulus as if a step strain had been applied, $E(t) = \sigma(t)/\varepsilon_0$. This approach, the so-called ten-times rule, is simple but it implies the loss of a substantial amount of data. Lee & Knauss (2000) and Zapas & Craft (1965) developed methods to reduce this loss by explicitly taking into account the loading procedure. Recently, a new method that allows the calculation of the relaxation modulus at arbitrary times with an error that is comparable to the Zapas-Craft approach on the time scale that is accessible to both methods has been proposed by Sorvari & Malinen (2006). Another approach for linear ramp loading tests is due to Knauss & Zhao (2007), who used an analytic solution of the Boltzmann superposition integral and nonlinear optimization to determine the material function.

In this work, a general optimization approach for arbitrary strain histories is presented. The investigated materials are a polypropylene homopolymer and glass bead filled polypropylene. The new method to extend the covered time range is applied to uniaxial compression and tensile relaxation tests as well as to tensile creep tests.

The problems considered in this paper deal with the determination of the uniaxial relaxation modulus. Due to the symmetry of the linear viscoelastic equations, the same procedures can be applied to the compliance formulation or to the other viscoelastic material functions with the appropriate substitution of stress, strain and material function for a specific case. The application of the method to determine time-dependent Poisson's ratio is presented elsewhere (Tscharnuter *et al.* (2010)).

D. Tscharnuter · M. Jerabek
Polymer Competence Center Leoben GmbH, Roseggerstrasse 12, 8700 Leoben, Austria
E-mail: tscharnuter@pccl.at
Present address: M. Jerabek, Borealis Polyolefine GmbH, St. Peter Strasse 25, 4021 Linz, Austria

Z. Major
Institute of Materials Science and Testing of Plastics, Franz-Josef-Strasse 18, 8700 Leoben, Austria
Present address: Institute of Polymer Product Engineering, Johannes Kepler University Linz, Altenbergerstrasse 69, 4021 Linz, Austria

R.W. Lang
Institute of Materials Science and Testing of Plastics, Franz-Josef-Strasse 18, 8700 Leoben, Austria
Present address: Institute of Polymeric Materials and Testing, Johannes Kepler University Linz, Altenbergerstrasse 69, 4021 Linz, Austria

2 Ramp loading in linear viscoelasticity

The traditional approach to determine the relaxation modulus is to perform a relaxation test, where a constant strain is maintained for a prolonged period of time. It is assumed that the loading is instantaneous. The strain history is then $\varepsilon(t) = \varepsilon_0 \Theta(t)$, where Θ is the step function. In this special case, the superposition integral that relates stress and strain,

$$\sigma(t) = \int_{0^-}^{t} E(t-\tau)\frac{d\varepsilon(\tau)}{d\tau}d\tau \tag{1}$$

reduces to the simple algebraic equation

$$E(t) = \frac{\sigma(t)}{\varepsilon_0} \tag{2}$$

However, loading is never done infinitely fast. In order for equation (2) to yield valid results, only data from a sufficient time after the initial loading must be used for further analysis. It was found that ten times the loading time is long enough, and evaluation using this technique is therefore called the ten-times rule. For a loading time of e.g. 10 seconds, this simple analysis thus requires discarding data up to 100 seconds. If it is possible to use data from down to the first tenths of seconds of the test with a more elaborate evaluation technique, two to three decades of time can be gained from a single test in comparison to the ten-times rule time range. This in turn allows for a large reduction of the experimental time and number of tests that need to be performed to cover a given time range with a master curve.

Recently the consideration of the ramp loading for improved data analysis has received attentionby the aforementionend work of Sorvari & Malinen (2006) and Knauss & Zhao (2007). In both works it was assumed that the relaxation strain level is reached by a constant strain rate loading,

$$\varepsilon(t) = \begin{cases} \dot{\varepsilon}_0 t & t < t_1 \\ \varepsilon_0 & t \geq t_1 \end{cases} \tag{3}$$

where $\varepsilon_0 = \dot{\varepsilon}_0 t_1$, with the loading time t_1 and the strain rate during the loading $\dot{\varepsilon}_0$. More general loading ramps are expressed as

$$\varepsilon(t) = \begin{cases} f(t) & t < t_1 \\ \varepsilon_0 & t \geq t_1 \end{cases} \tag{4}$$

where $f(t)$ is e.g. a polynomial and $f(t_1) = \varepsilon_0$.

In order to assess the error that can arise from neglecting the ramp loading and assuming instantaneous loading (step strain), a linear viscoelastic material with a relaxation modulus defined by the Prony series

$$E(t) = E_\infty + \sum_i E_i \exp(-t/\tau_i) \tag{5}$$

is considered. E_i denotes the relaxation strength associated with the relaxation time τ_i. It is assumed that this material is loaded with a linear ramp strain history as given in equation (3). The stress for times $t \geq t_1$ is calculated using equations (5) and (3) in equation (1). The integration is straight forward and yields

$$\sigma(t) = \varepsilon_0 E_\infty + \sum_i \dot{\varepsilon}_0 E_i \tau_i \left(\exp(t_1/\tau_i) - 1\right)\exp(-t/\tau_i) \tag{6}$$

This is the stress that would be measured when a material described by equation (5) is loaded as prescribed by equation (3). To determine the modulus from this stress assuming step loading, the stress is divided by the constant strain (equation (2)). In terms of the Prony series model the obtained modulus is

$$E_{\text{step}}(t) = E_\infty + \sum_i \underbrace{E_i \frac{\tau_i}{t_1}\left(\exp(t_1/\tau_i) - 1\right)}_{\tilde{E}_i} \exp(-t/\tau_i) \tag{7}$$

By comparing this result with the true modulus defined in equation (5), it follows that the relative error in each term of the Prony series depends on the ratio of the loading time and the relaxation time. Thus, the magnitude of the error depends on the material's relaxation spectrum. A series expansion of the exponential term in the relative error yields

$$\Delta_i := \frac{\tilde{E}_i - E_i}{E_i} = \frac{\tau_i}{t_1}\left(\exp(t_1/\tau_i) - 1\right) - 1 = \sum_{n=1}^{\infty} \frac{1}{(n+1)!} \frac{t_1^n}{\tau_i^n} \tag{8}$$

Clearly the error approaches zero as the relaxation time approaches infinity. Hence long-term relaxations do not contribute to the error made by assuming step loading. The error is larger for short-term relaxation, e.g. the error is $e-1$ or approximately 72% when the relaxation time equals the loading time. This error is weighted by the decaying exponential term, $\exp(-t/\tau_i)$. After ten times the loading time the weight is only $\exp(-10) \approx 5 \cdot 10^{-5}$. Hence, the ten-times rule result is accurate unless the material exhibits strong short-term relaxation.

3 Pointwise evaluation methods

Assuming step loading, the relaxation modulus is calculated from each available data point independently of the remaining data points. Therefore, the ten-times rule can be termed a pointwise method. The earliest more sophisticated pointwise method is due to Zapas & Craft (1965). For a linear ramp loading, it was shown that the relaxation modulus can be approximately calculated by

$$E(t) = \frac{\sigma(t + t_1/2)}{\varepsilon_0} \quad \text{for } t \geq t_1/2 \tag{9}$$

Another technique was developed by Lee & Knauss (2000). It is not pointwise in the same sense as the ten-times rule or the Zapas-Craft method because it is a recursive procedure. The iteration can be formulated to proceed forward in times as

$$E(t) = E(t - t_1) + \frac{1}{2\dot{\varepsilon}_0} \frac{\mathrm{d}\sigma(t)}{\mathrm{d}t} \quad \text{for } t \geq t_1 \tag{10}$$

or backwards in time as

$$E(t - t_1) = E(t) - \frac{1}{2\dot{\varepsilon}_0} \frac{\mathrm{d}\sigma(t)}{\mathrm{d}t} \quad \text{for } t \geq t_1 \tag{11}$$

Both methods where comprehensively examined by Flory & McKenna (2004). The latest approach is due to Sorvari & Malinen (2006), who showed that the relaxation modulus can be estimated by

$$E(t) = \frac{\sigma(t + t_1)}{\varepsilon_0} - \frac{\dot{\sigma}(t + t_1)}{2\dot{\varepsilon}_0} \tag{12}$$

when the stress is the response to a strain history as stated in equation (3). The method is easily extended to general loading ramps, i.e. polynomials. For the strain history given in equation (4) the superposition integral is

$$\sigma(t) = \int_0^t E(t - \xi) f'(\xi) d\xi \tag{13}$$

By using the mean value theorem this is equal to

$$f'(\zeta)\int_0^t E(t-\xi)d\xi \tag{14}$$

for a specific value of $\zeta \in (0,t_1)$. This equation is of the same form as the constant strain rate equation given by Sorvari and Malinen with $f'(\zeta)$ in place of $\dot{\varepsilon}_0$. The adapted ramp correction formula is

$$E(t) = \frac{\sigma(t+t_1)}{f'(\zeta)t_1} - \frac{\dot{\sigma}(t+t_1)}{2f'(\zeta)} \tag{15}$$

To complete the formula, the appropriate value of ζ must be determined. By the ten-times rule equation (7) must coincide with equation (15) a sufficiently long time after the end of the loading ramp. Therefore, ζ is the value that minimizes the sum of squared residuals

$$\sum_i \left(\frac{\sigma(t_i+t_1)}{f'(\zeta)t_1} - \frac{\dot{\sigma}(t_i+t_1)}{2f'(\zeta)} - \frac{\sigma(t_i)}{\varepsilon_0} \right)^2 \tag{16}$$

on $(0,t_1)$, where the sum extends over all $t_i \gg t_1$.

This evaluation method requires the stress and its time derivative at times $t+t_1$, which generally do not coincide with the times of the available data points. Additionally, numerical differentiation tends to amplify the data scatter. For practical use of this method, a smoothing spline is therefore applied to the stress for the evaluation of equation (15). The polynomial coefficients of the spline are determined by minimizing the sum of squared residuals with an additional smoothing term,

$$(1-\lambda)\sum_i (\sigma_{x,i} - \sigma_x^{(i)}(t_i))^2 + \lambda \int w(t) \left| \frac{\partial^2 \sigma_x^{(i)}(t)}{\partial t^2} \right| dt \tag{17}$$

where $\sigma_x^{(i)}$ denotes the spline on the interval $[t_i, t_{i+1}]$, $\sigma_{x,i}$ is the measured stress at time t_i and $w(t)$ is a weight function for the smoothing term. The integral of the absolute value of the spline's second derivative serves as a measure of its roughness. The larger λ is chosen, the more rough solutions are penalized. Hence, the spline representations are very convenient for addressing data scatter, interpolation, and taking derivatives.

4 Optimization methods

Unlike the fast but approximate pointwise methods, optimization based approaches using exact analytic solutions have no inherent error but require more computational effort. In a recent work, Knauss & Zhao (2007) showed that a nonlinear optimization algorithm is capable of fitting equation (6) to experimental data to determine the Prony series parameters for the relaxation modulus. Their investigations showed that ideally three to four additional decades in time can be evaluated compared to the ten-times rule. However, a less restrictive strain model that is easier to achieve experimentally is desirable. A smoothing spline representation is assumed for the strain history, which is written as

$$\varepsilon_x(t) = \sum_i (a_i(t-t_i)^3 + b_i(t-t_i)^2 + c_i(t-t_i) + d_i)\Theta(t_i < t < t_{i+1}) \tag{18}$$

Here a_i, b_i, c_i, d_i and t_i are the spline coefficients and nodes. Hence, no specific assumptions on the strain history are made.

To obtain the corresponding model for the stress, equation (1) must be solved. Substituting a Prony series for the relaxation modulus, the stress is expressed as

$$\sigma(t) = \sum_{i=1}^{N_i-1} E_\infty\left(\varepsilon_x^{(i)}(t_{i+1}) - \varepsilon_x^{(i)}(t_i)\right) + \sum_{i=1}^{N_i-1}\sum_j E_j \int_{t_i}^{t_{i+1}} \exp\left(-\frac{t-\xi}{\tau_j}\right)\frac{\partial \varepsilon_x^{(i)}(\xi)}{\partial \xi} d\xi$$
$$+ E_\infty\left(\varepsilon_x^{(N_i)}(t_{N_i}) - \varepsilon_x^{(N_i)}(t)\right) + \sum_j E_j \int_{t_{N_i}}^{t} \exp\left(-\frac{t-\xi}{\tau_j}\right)\frac{\partial \varepsilon_x^{(N_i)}(\xi)}{\partial \xi} d\xi \tag{19}$$

N_i is the index of the interval for which $t_i < t \leq t_{i+1}$ and $\varepsilon_x^{(i)}$ denotes the spline on the interval $[t_i, t_{i+1}]$. A piecewise constant function is chosen for $w(t)$. Nonuniform weighting is needed when ε_x changes quickly, specifically the transition from loading to relaxation or creep, because otherwise the transition is exceedingly altered by the smoothing.

The solution of these integrals, which is given in the appendix, provides a model for the stress arising from an arbitrary strain history. The Prony series parameters are determined by the set of parameters which gives the minimum quadratic error (sum of squared residuals; SSR) between the model and the measured stress. The most widely used optimization routines are deterministic gradient based algorithms, as used by Knauss & Zhao (2007) for the case of a constant strain rate loading relaxation test. In case of a problem with multiple minima, gradient methods yield a minimum close to the initial guess for the parameters. In general this is not the global minimum[1] or at least a sufficiently close one. As the number of minima is unknown, trying different initial values until a good fit is found is not a very efficient approach, especially when dealing with a computationally demanding problem. An algorithm capable of leaving local minima is thus useful in dealing with this kind of problem.

Two optimization methods based on the idea of the stochastic optimization method Simulated Annealing were investigated. Only a brief overview of Simulated Annealing (SA) is given; further details are provided elsewhere (Kirkpatrick *et al.* (1983)).

In Simulated Annealing, a sequence of points in the parameter space is generated that leads (close) to the global minimum. At any given point, the following point (trial point) in the vicinity of the current point is suggested at random. If the trial point provides a smaller quadratic error, it is accepted and the search for the minimum proceeds by suggesting the next random trial point. If, however, the trial point gives a larger quadratic error, it is decided at random whether or not the worse suggestion is still accepted. Thus, contrary to gradient methods, the search path through the parameter space does not only lead 'downhill'. It is possible to make 'uphill' moves during the search for the minimum, which allows the method to leave local minima. The probability of accepting a worse value depends on a temperature parameter. In the initial phase, this artifical temperature is high, implying that most suggestions are accepted. This allows the search to proceed through the entire parameter space. Hence, the result does not depend on the initial guess. Over the course of the minimization, the temperature is gradually decreased, so that suggestions that are not close to the global minimum are less and less likely accepted. Thus, the accessible region of the parameter space becomes smaller and ultimately shrinks to a small region close to the global minimum.

For the present application the optimization algorithm must also account for the monotonicity of the material function, which can be ensured by bound constraints on the relaxation strengths. Relaxation times are also subject to bound constraint to enforce positivity.

In classical SA the trial points are generated using a Gaussian distribution. As the probability density function of the Gaussian distribution is nonzero on $\mathbb{R}$, there will be trial points that violate the constraints and therefore the method is unsuitable for constrained problems. Approaches to solve constrained problems with Simulated Annealing methods exist (Hedar & Fukushima (2006) or Pedamallu & Ozdamar (2008)), but these are fairly complex algorithms that are not easily implemented. Other approaches transform the constrained problem to an unconstrained problem by adding penalty terms for constraint violations to the SSR. This allows the search to proceed through infeasible domains in the parameter space as long as the temperature is sufficiently high, thus ensuring that all feasible domains can be reached from the initial point. In pracice, these methods have their own pitfalls, e.g. in the choice of magnitude of the penalty, see Pedamallu & Ozdamar (2008) and the references therein.

The quickest option to incorporate bound constraints is to reset all trial point coordinates that exceed the constraints to their respective boundary values. This is not a very efficient approach in the early stages of the optimization because trial points with coordinates on the bounds occur frequently and do not contribute to any progress towards the sought minimum. Nevertheless, this option has been tested using the Fast Simulated Annealing (FSA; Szu & Hartley (1987)) and it was found capable of achieving the desired fits. However, the large number of required SSR evaluations lead to an unsatisfactory computational performance. Therefore, the Simplex Simulated Annealing (SSA; Press & Teukolsky (1991)) algorithm was investigated. A simplex is a polytope of $N+1$ points in the N-dimensional parameter space,

[1] Or one of the global minima.

i.e. a triangle in a 2-dimensional space. The downhill simplex method by Nelder & Mead (1965) finds local minima by deforming a simplex according to a specific set of rules. Press & Teukolsky (1991) modified this method by adding random perturbations to the points of the simplex. The C code for the basic SSA is available in Press *et al.* (1992) or on the Numerical Recipes website, http://www.nr.com. Cardoso *et al.* (1996) used the same reset-method as described above to allow for constraints, but they report that this lead to degenerate simplexes[2] in the problems investigated, causing failure of the algorithm. However, for the present problem it was found that a minor modification of the algorithm eliminates the problem of degenerate simplexes. Degeneration is a consequence of too many bound violations. Assume for instance that all coordinates in at least two points of the simplex violate the bound constraints by certain amounts. Then these two points would be reset to an identical point in the parameter space. Since a large number of randomly fluctuating points is generated during the optimization, this is likely to occur and one occurence is sufficient for algorithm failure. Hence, bound violations were not reset to the value of the constraint, but to the constraint value plus or minus a small random number. Parameters that violate the bound constraints are thus assigned random values close to the bounds instead of the precise value, making degeneration very unlikely. This modified algorithm was succesfully tested and good results were obtained with fewer SSR evaluations than needed with FSA. Hence, the SSA modified to obey bound constraints was chosen as the optimization algorithm for the spline-based method.

5 Experimental

5.1 Materials

The materials investigated are a polypropylene homopolymer (PP(H)), and polypropylene filled with 3.5% percent volume of glass beads (PP(H)+G3.5). The materials and injection molded specimens according to ISO 3176 type B were manufactured by Borealis Polyolefine GmbH (Linz, A). Further details as to these materials are described elsewhere (Jerabek *et al.* (2010c, 2009)).

5.2 Tensile relaxation tests

Tensile relaxation tests were performed with a screw-driven electro-mechanical universal test system (type Zwick Z250, Zwick-Roell; Ulm, Germany) equipped with a temperature chamber to maintain the temperature inside the chamber at $23 \pm 0.5\,^{\circ}\mathrm{C}$. Over the 22 hours test duration, the standard deviation of the temperature was smaller than 0.1 K in all tests. To simultaneously ensure an accurate strain control independet of the room temperature variations, a linear variable differential transducer (LVDT) linked to the control unit of the test system was mounted on the specimen grips inside the temperature chamber to serve as the displacement sensor. In this manner, the specimen and the LVDT experienced the same narrow temperature control.

A full-field strain measurement technique was applied using the digital image correlation (DIC) system ARAMIS (GOM mbH, Germany). Various aspects and details of this technique are described elsewhere (Jerabek *et al.* (2010b)).

5.3 Compression relaxation tests

The compression relaxation tests were done on an Instron 5500 electro-mechanical universal testing machine. Cylindrical specimens were used. The displacement was measured using a LVDT and the strain was calculated from the displacement. The entire setup is decribed in detail by Jerabek *et al.* (2010c).

5.4 Tensile creep tests

The Instron 5500 electro-mechanical universal testing machine was also used for the creep tests. To remain within the limits of linear viscoelasticity, the load was chosen as 2 MPa with a loading rate of 0.2 MPa/s. The tests were carried out at temperatures of 0 °C, 23 °C, 40 °C and 60 °C. Because of resolution issues with the DIC system strain gauges were used to measure the axial strain. This will be discussed in more detail in a following section.

[2] A degenerate simplex has two or more identical points.

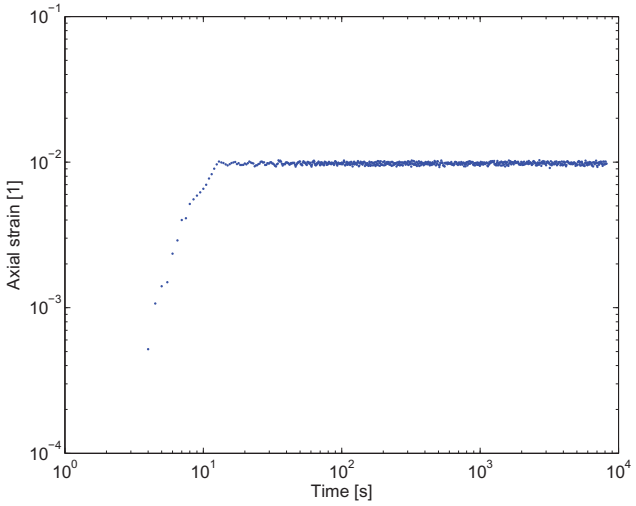

Fig. 1: Axial strain in a compression relaxation test of PP(H) at $-19°C$

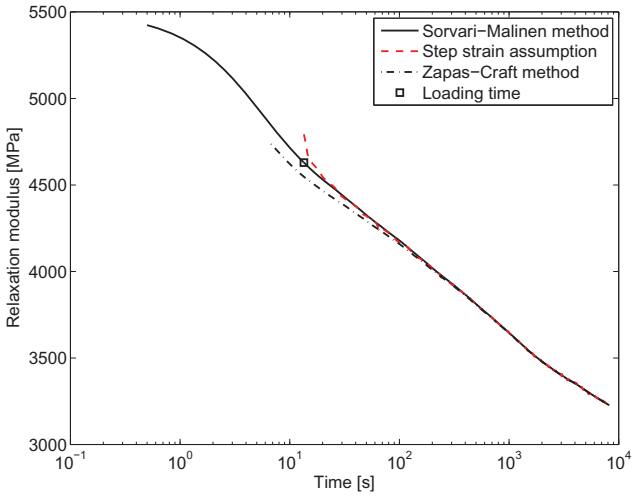

Fig. 2: Relaxation modulus data for PP(H) in uniaxial compression at $-19°C$ comparing the Sorvari-Malinen method and the Zapas-Craft method.

6 Results

6.1 Polypropylene in uniaxial compression relaxation with linear ramp loading

The cylindrical specimens were tested at various temperatures as described previously. Each test was evaluated using the Sorvari-Malinen method and the spline method and a master curve was constructed from the results. With the former method, good results were obtained when a smoothing spline was applied to deal with the uncertainty in the strain data (figure 1). For comparison, the results obtained with the Zapas-Craft method and the step strain assumption are depicted in figure 2. In these tests, the Zapas-Craft method does not yield significant improvement compared to the step strain assumption. With the Sorvari-Malinen method, the relaxation modulus could be determined back to 0.5s, which adds more than a decade of covered time compared to the step strain result.

As these tests were performed prior to the development of the spline method, not enough data were recorded during the loading for the nonlinear optimization. Therefore, the spline method was restricted to evaluating data after the initial loading. On the common time range, both methods yielded quasi identical results. The resulting master curves of the Sorvari-Malinen and the spline method are given in figure 3.

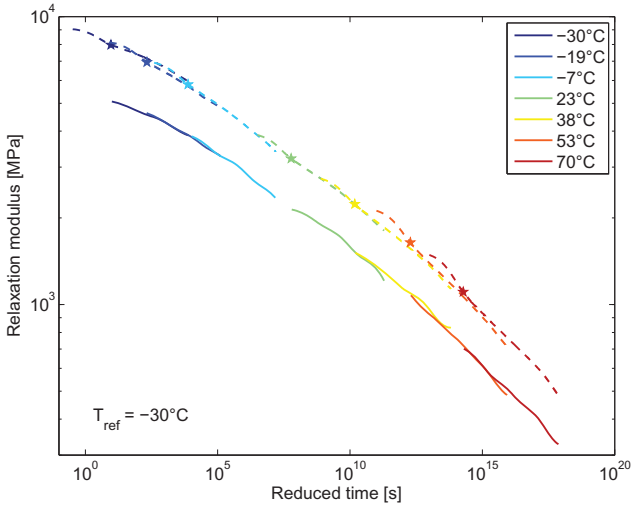

Fig. 3: Relaxation modulus master curve for PP(H) for a reference temperature of $-30\,^{\circ}$C calculated using the Sorvari-Malinen method (dashed lines) and the spline method (solid lines). The stars indicates the end of the loading ramps. The dashed lines have been vertically shifted to distinguish the two near identical results.

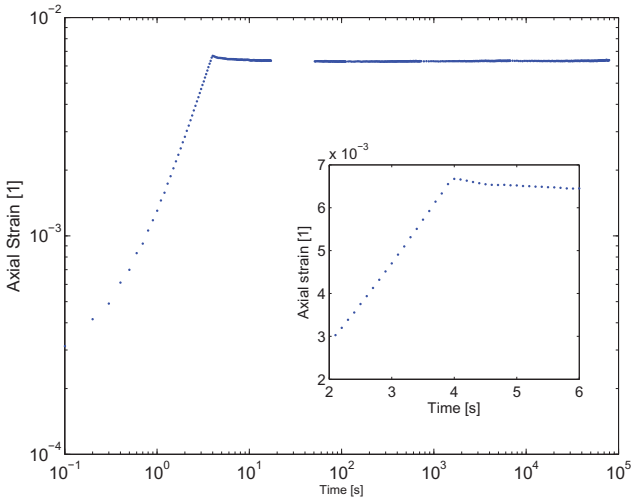

Fig. 4: Axial strain of PP(H)+G3.5 at $23\,^{\circ}C$ in a relaxation test with polynomial ramp loading. The detail figure shows the non-ideal transition from loading to relaxation.

6.2 Polypropylene in uniaxial tensile relaxation with nonlinear ramp loading

Tensile relaxation tests with a nonlinear loading ramp were performed. The axial strain during loading and relaxation is shown in figure 4. This loading can be nicely modelled using a polynomial. A fourth degree polynomial was used in this case with the generalized Sorvari-Malinen method (section 3) to determine the relaxation modulus.

The P-control of the Zwick testing machine initially causes a slight overshoot of the target strain before the desired value is gradually approached. Altering the P value changes this behavior but also results in unsatisfactory performance in the earlierst stages of the test. Thus, the overshoot cannot be eliminated and limits the applicability of the generalized Sorvari-Malinen method, which assumes constant strain for $t > t_1$.

The same data were also evaluated using the spline method, which explicitly considers the measured strain, including any non-ideal behavior, when matching the predicted stress to the measured stress (figure 5). Thus, this method is not limited by the testing machine's precision in the transition. The limits of applicability are defined by the achievable temporal resolution as a sufficient number of data points is required, by the strain and stress resolution because data must be taken at low stress and strain, and by the initial instability of the testing machine up to the first tenths of seconds.

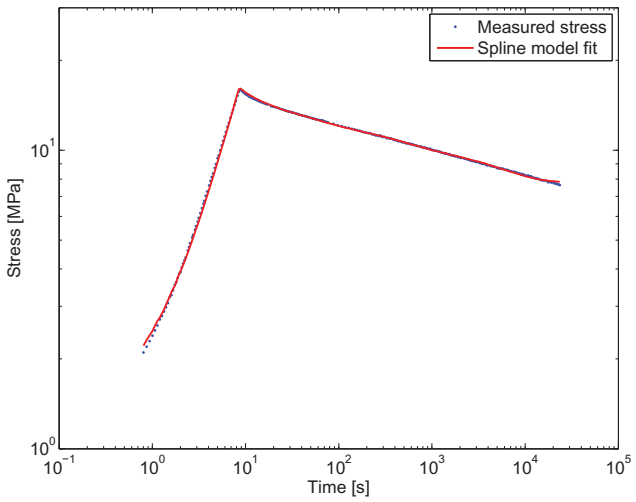

Fig. 5: Stress of PP(H) in a relaxation test and the spline model fit based on the modulus shown in figure 6.

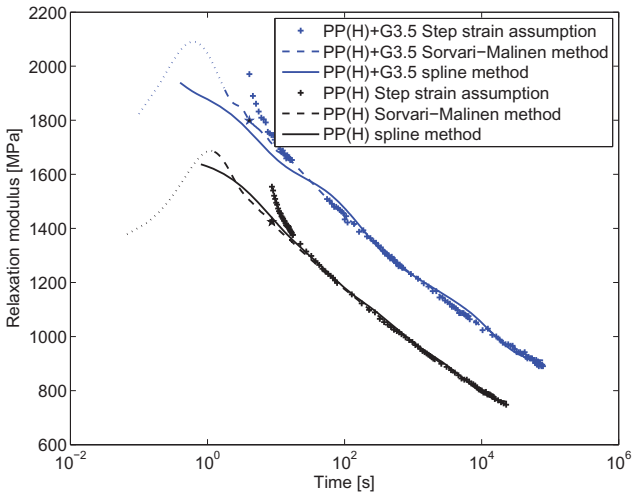

Fig. 6: Relaxation modulus of PP(H) and PP(H)+G3.5 from relaxation tests. The dotted part of the results of the Sorvari-Malinen method is unreliable due to the non-ideal transition.

The results achieved with both methods for PP(H) and PP(H)+G3.5 are presented in figure 6. It was found that the deviation from the constant strain assumption leads to oscillations in the results for the generalized Sorvari-Malinen method. The spline method yielded smoother curves on a larger time range. The minor waviness of the curves is an artifact of the Prony series modelling.

6.3 Determination of the relaxation modulus by creep tests

Since no assumptions on the shape of the strain history are made, any kind of test can be evaluated to determine the relaxation modulus, including the performed creep tests. The strain in these tests was measured using strain gauges. The main reason for not using the DIC system was the low strain encountered in such tests. All tests were supposed to be performed within the range of linear viscoelasticity, in this case simply defined by a stress-independent creep compliance or relaxation modulus. For PP(H) in creep, this limit was found to be between 2 and 3 MPa. On the other hand, in relaxation, the limit was above 0.6%, where the peak stress is about 13 MPa. However, strain gauges locally increase the stiffness of the specimens to a certain degree that depends on the mechanical properties of the specimens and the strain gauge materials (typically copper and polyimide). Therefore, the relaxation modulus may have been shifted to higher values. An altered relaxation behavior due to the polyimide support is possible. Nevertheless, the strain gauge data are worthwhile to examine because of the good strain resolution and the high sampling rate, which allows

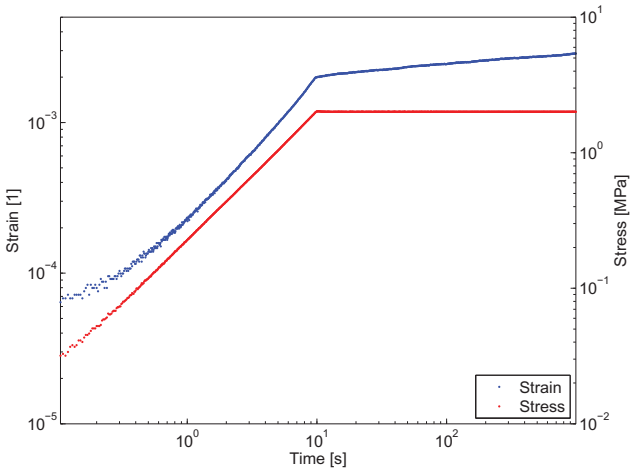

Fig. 7: Axial stress and strain of PP(H)+G3.5 in creep at room temperature.

for the investigation of the testing machine's performance at short times and the number of data points needed for the optimization. For all fits, a logarithmically spaced subset of the recorded data was used and several optimizations were done. 100 data points per decade worked fine in all examined tests, but a lower number of e.g. 20 points per decade proved sufficient as well. To a certain degree, the necessary number of data points depends on the shape of the strain curve. Care must be taken in the transition from loading to creep. When there are too few data points, the spline may start to oszillate and then no longer accurately models the strain. As mentioned before, proper weighting is also needed for the spline in transition regions.

The strain and stress history up to 100 s of a creep test are shown in figure 7. The double logarithmic plot reveals that there is some initial instability. Due to this uncertainty in the data a lower time limit was introduced in the fitting. All (logarithmically sampled for weighting) short time strain data was used in the spline calculation, but for the optimization only stress data from times above the time limit was used. The lower time limit varied between 0.2 s and 1 s. This depends on the characteristics of the initial instability and varies from test to test. A linear fit to the stress could possibly eliminate scatter in the stress data and reduce the time limit, but as an influence of the amount of smoothing in the scattered strain is still to be expected, this was not examined. With these time limits, master curves spanning 3 to 3.5 decades in time can be determined from a 1000 s test. The master curves for PP(H) and PP(H)+G3.5 are printed in figure 8. These master curves span roughly ten decades in time and are constructed from four 20 minutes creep tests at different temperatures.

The relaxation modulus curves as determined from creep and relaxation tests are compared in figure 8. The standard relaxation test showed the higher modulus and delayed relaxation of the glass bead filled material compared to the neat material. The same behavior was found in the strain gauge tests and the agreement between the creep and relaxation results is good. This indicates that the strain gauges exerted only a minor influence in these tests. Note that the agreement between the results from different strain histories may vary because of effects that are not captured by the viscoelastic model, e.g. the strain-rate or stress-state dependence (Jerabek *et al.* (2010a)) of the material.

7 Conclusion

The aim of this work was to improve the time range that can be used for viscoelastic model parameter determination from uniaxial tests. The method presented by Sorvari & Malinen (2006) was successfully used to calculate the relaxation modulus of neat and glass bead filled polypropylene in compressive and tensile relaxation tests. With the introduction of the spline model for the axial strain and a stochastic nonlinear optimization routine a framework for a general linear viscoelastic parameter determination for isotropic materials was developed. This spline method was used to determine the relaxation modulus from the aforementioned tests, and good results were obtained with both the spline method and the Sorvari-Malinen method.

Due to its generality, the spline method furthermore allowed the determination of the relaxation modulus from creep tests. The thus obtained result showed good agreement with the other results. The extension of the time range covered in a single tests allowed for a construction of a relaxation modulus master curve spanning roughly ten decades in time from four 20-minutes creep tests at four different temperatures. A traditional ten-times rule evaluation of the creep compliance requires 4 days of testing to cover the same time range.

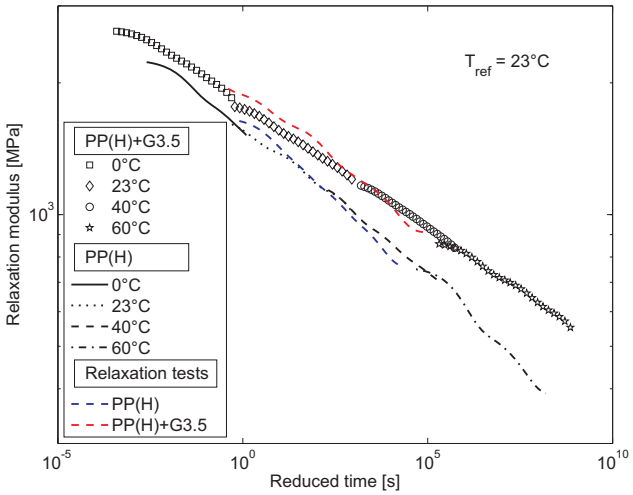

Fig. 8: Comparison of the relaxation modulus results from tensile relaxation and creep tests for PP(H) and PP(H)+G3.5 for a reference temperature of 23°C.

The experimental care and accuracy of the measured stress and strain determine the amount of data that can be gained in comparison to a simple step strain assumption evaluation. For typical tests with a loading time of a few seconds we found that data from a few tenths of a second onward could be used. Thus, between two and three decades of additional information could be gained. The advantage with regard to either shorter experimental time or increased overlap in master curves is obvious.

A Appendix

Using the spline model, the stress is described by the following equation (equation (19))

$$\sigma(t) = \sum_{i=1}^{N_i-1} E_\infty \left(\varepsilon_x^{(i)}(t_{i+1}) - \varepsilon_x^{(i)}(t_i)\right) + \sum_{i=1}^{N_i-1}\sum_j E_j \underbrace{\int_{t_i}^{t_{i+1}} \exp\left(-\frac{t-\xi}{\tau_j}\right) \frac{\partial \varepsilon_x^{(i)}(\xi)}{\partial \xi} d\xi}_{A}$$
$$+ E_\infty \left(\varepsilon_x^{(N_i)}(t_{N_i}) - \varepsilon_x^{(N_i)}(t)\right) + \sum_j E_j \int_{t_{N_i}}^{t} \exp\left(-\frac{t-\xi}{\tau_j}\right) \frac{\partial \varepsilon_x^{(N_i)}(\xi)}{\partial \xi} d\xi \tag{20}$$

For a complete solution, the integral A needs to be solved. With the notation that has been introduced for the spline the strain term is

$$\frac{\partial \varepsilon_x^{(i)}(\xi)}{\partial \xi} = 3a_i(\xi - t_i)^2 + 2b_i(\xi - t_i) + c_i \tag{21}$$

This integral can be solved by partial integration. The solution is

$$\begin{aligned} A = & -\tau_j \exp\left(-\frac{t}{\tau_j}\right)\left((6\tau_j^2 a_i - 2\tau_j b_i + c_i)\exp\left(\frac{t_i}{\tau_j}\right)\right. \\ & + \left(-3a_i t_i^2 + 2b_i t_i - c_i + 2\tau_j b_i - 6\tau_j t_i a_i - 6\tau_j^2 a_i\right. \\ & \left.\left. -2b_i t_{i+1} + 6a_i t_{i+1} t_i + 6\tau_j a_i t_{i+1} - 3a_i t_{i+1}^2\right)\exp\left(\frac{t_{i+1}}{\tau_j}\right)\right) \end{aligned} \tag{22}$$

References

Cardoso, M.F., Salcedo, R.L., & de Azevedo, S. Feyo. 1996. The simplex-simulated annealing approach to continuous non-linear optimization. *Computers and chemical engineering*, **20**(9), 1065–1080.

Flory, A., & McKenna, G.B. 2004. Finite step rate corrections in stress relaxation experiments: A comparison of two methods. *Mechanics of time-dependent materials*, **8**, 17–37.

Hedar, A.-R., & Fukushima, M. 2006. Derivative-free filter simulated annealing method for constrained continuous global optimization. *Journal of global optimization*, **35**(4), 521–549.

Jerabek, Michael, Major, Zoltan, Renner, Károly, Móczó, János, Pukánszky, Béla, & Lang, Reinhold W. 2009. Filler/matrix-debonding and micro-mechanisms of deformation in particulate filled pp composites under tension. *submitted to polymer*.

Jerabek, Michael, Tscharnuter, Daniel, Major, Zoltan, Ravi-Chandar, Krishnaswamy, & Lang, Reinhold W. 2010a. Relaxation behavior of neat and particulate filled polypropylene in uniaxial and multiaxial compression. *Mechanics of time-dependent materials*, **14**(1), 47–68.

Jerabek, Michael, Major, Zoltan, & Lang, Reinhold W. 2010b. Strain determination of polymeric materials using digital image correlation. *Polymer testing*, **29**(3), 407–416.

Jerabek, Michael, Major, Zoltan, & Lang, Reinhold W. 2010c. Uniaxial compression testing of polymeric materials. *Polymer testing*, **29**(3), 302–309.

Kirkpatrick, S., Gelatt, C.D., & Vecchi, M.P. 1983. Optimization by simulated annealing. *Science*, **220**(4598), 671–680.

Knauss, W.G., & Zhao, J. 2007. Improved relaxation time coverage in ramp-strain histories. *Mechanics of time-dependent materials*, **11**(3-4), 199–216.

Lee, S., & Knauss, W.G. 2000. A note on the determination of relaxation and creep data from ramp tests. *Mechanics of time-dependent materials*, **4**, 1–7.

Nelder, J.A., & Mead, R. 1965. A simplex method for function minimization. *Computer journal*, **7**, 308.

Pedamallu, C.S., & Ozdamar, L. 2008. Investigating a hybrid simulated annealing and local search algorithm for constrained optimization. *European journal of operational research*, **185**(3), 1230–1245.

Press, W.H., & Teukolsky, S.A. 1991. Simulated annealing optimization over continous spaces. *Computers in physics*, **5**(4), 426.

Press, W.H., Flannery, B.P., Teukolsky, S.A., & Vetterling, W.T. 1992. *Numerical recipes in c: The art of scientific computing*. Cambridge University Press.

Sorvari, J., & Malinen, M. 2006. Determination of the relaxation modulus of a linearly viscoelastic material. *Mechanics of time-dependent materials*, **10**, 125–133.

Szu, H., & Hartley, R. 1987. Fast simulated annealing. *Physics letters a*, **122**(3 & 4), 157–162.

Tscharnuter, Daniel, Jerabek, Michael, Major, Zoltan, & Lang, Reinhold W. 2010. Time-dependent poisson's ratio of polypropylene compounds for various strain histories. *submitted to mechanics of time-dependent materials*.

Zapas, L.J., & Craft, T. 1965. Correlation of large longitudinal deformations with different strain histories. *J. res. nat. bur. stds.*, **69A**(6), 541–546.

Time-Dependent Poisson's Ratio of Polypropylene Compounds for Various Strain Histories

Daniel Tscharnuter · Michael Jerabek · Zoltan Major · Reinhold W. Lang

Abstract Due to the viscoelastic behavior of polymers mechanical properties are strongly affected by the loading history. To obtain the time-dependent Poisson's ratio without further data manipulation, stress relaxation tests have to be carried out. Only few results for viscoelastic materials have been published to date, but the theory of Poisson's ratio in the framework of linear viscoelasticity has received some attention with respect to loading histories other than relaxation, i.e. creep and constant rate of strain tests.

The main objective of this work is to compare the potential of different testing methods to determine Poisson's ratio. Transverse and axial strain have been measured in relaxation tests, creep experiments and displacement rate controlled tensile tests. Relaxation tests are evaluated accounting for the finite loading time and the results are compared with those of tensile creep and displacement rate controlled tensile tests. An optimization based method to determine linear viscoelastic material functions developed previously is applied to calculate Poisson's ratio.

Keywords Poisson's ratio · linear viscoelasticity · lateral contraction · time dependence

1 Introduction

As one of the four basic material functions - Poisson's ratio, uniaxial relaxation modulus, shear modulus and bulk modulus - Poisson's ratio is important for the description of stress and strain states of linear viscoelastic materials. Similar to the case of an isotropic elastic material, any two material functions can be used to calculate the remaining two material functions of an isotropic linear viscoelastic material. This is referred to as interconversion of material functions. Hence, two material functions are sufficient for a complete description of the mechanical behavior. In theory, the choice of two material functions is arbitrary, but in practice there are limitations that must be considered. First, it is difficult to determine the bulk modulus experimentally (Deng & Knauss (1997)), and thus only few directly measured bulk modulus data are available. Second, the measurement of a pair of viscoelastic material functions must be performed simultaneously on the same specimen to avoid excessive errors caused by specimen-to-specimen or environmental variations which are magnified in the subsequent interconversion analysis (Tschoegl *et al.* (2002)). This excludes for example the use of the shear and the uniaxial relaxation modulus measured in separate tests. The simultaneous measurement of two material functions is possible in a confined compression setup (Qvale & Ravi-Chandar (2004), Jerabek *et al.* (2010b)) or a uniaxial tensile or compression setup when the axial and lateral strain are measured (Jerabek *et al.* (2010c)). The former yields the bulk and the

D. Tscharnuter · M. Jerabek
Polymer Competence Center Leoben GmbH, Roseggerstrasse 12, 8700 Leoben, Austria
E-mail: tscharnuter@pccl.at
Present address: M. Jerabek, Borealis Polyolefine GmbH, St. Peter Strasse 25, 4021 Linz, Austria

Z. Major
Institute of Materials Science and Testing of Plastics, Franz-Josef-Strasse 18, 8700 Leoben, Austria
Present address: Institute of Polymer Product Engineering, Johannes Kepler University Linz, Altenbergerstrasse 69, 4021 Linz, Austria

R.W. Lang
Institute of Materials Science and Testing of Plastics, Franz-Josef-Strasse 18, 8700 Leoben, Austria
Present address: Institute of Polymeric Materials and Testing, Johannes Kepler University Linz, Altenbergerstrasse 69, 4021 Linz, Austria

shear relaxation moduli, the latter provides the uniaxial relaxation modulus and Poisson's ratio. Contrary to the elaborate confined compression test, uniaxial stress relaxation is a standard method to characterize viscoelastic materials that can be assumed to be widely used. Theoretically, the bulk behavior could also be inferred from the uniaxial relaxation modulus and Poisson's ratio, but in practice, accurate interconversion is difficult because of the high precision that is required, particularly for high values of Poisson's ratio. It has been estimated by Lu *et al.* (1997) that Poisson's ratio must be determined to a precision of up to 10^{-4} to obtain the bulk modulus within reasonable error bounds from the uniaxial relaxation modulus and Poisson's ratio, when the latter is close to 0.5. The accuracy requirement is less strict when Poisson's ratio is smaller, nonetheless it is experimentally challenging to measure and the lack of reliable data on time-dependent Poisson's ratio is an indication thereof. On the other hand, time-dependent Poisson's ratio is clearly needed for a complete characterization of the viscoelastic deformation behavior. Under simple uniaxial load, Poisson's ratio governs the evolution of the lateral strain. In multiaxial stress or strain states, Poisson's ratio affects the stress and strain field. For example, even when the macroscopic load is uniaxial, in particle filled materials or in multicomponent parts, multiaxial stresses occur on a local scale in the vicinity of the particles or in interface near regions when the Poisson's ratios of the material constituents do not match. Thus, for advanced finite element calculations time-dependent Poisson's ratio functions are essential for accurate simulation results which cannot be achieved by assuming a constant bulk modulus (Knauss & Emri (1981)) or a constant Poisson's ratio (Hilton (2001)).

There are various definitions of Poisson's ratio for viscoelastic materials, which are comprehensively discussed by Hilton (2001). The present paper is restricted to the definition that uses the axial and transverse strain in the time domain. By substituting the time-dependent strains into the equation for the elastic Poisson's ratio, the time-dependent ratio is defined es

$$\nu(t) = -\frac{\epsilon_y(t)}{\epsilon_x(t)} \tag{1}$$

It has been shown that this definition is only a valid viscoelastic analogue of Poisson's ratio in accordance with the correspondence principle in the special case of a constant axial strain, $\epsilon_x(t) = \epsilon_0 \Theta(t)$ where Θ is the step function (van der Varst & Kortsmit (1992)). This is the only proper definition of the viscoelastic Poisson's ratio. It corresponds to strains measured in an ideal stress relaxation test. For other time-dependent strain histories, the time-dependent ratio in equation (1) is referred to as contraction ratio to distinguish it from the constant axial strain case.

The relaxation definition can be immediately generalized to arbitrary strain histories by expressing any strain history as a superposition of infinitesimal steps (Tschoegl *et al.* (2002)). Thus, a constitutive relation similar to the Boltzmann superposition integral for the relaxation modulus or creep compliance can be formulated for Poisson's ratio:

$$-\epsilon_y(t) = \int_{0^-}^{t} \nu(t-\tau)\frac{\partial \epsilon(\tau)}{\partial \tau} d\tau \tag{2}$$

This equation is the basis for advanced evaluation techniques that consider more complex strain histories than step strains. The standard approach is to assume step strain loading in a relaxation test as this provides the simplest determination of viscoelastic material functions, however at the cost of data from times below ten times the loading time. This "ten-times rule" ensures that inaccuracies related to transient effects are avoided. It applies to all step loading assumptions, whether it is a tensile test to determine the relaxation modulus or a creep test to determine the creep compliance. Considering the superposition integral definition, it equally applies to Poisson's ratio. More sophisticated techniques are needed to take the finite loading period into account. Apart from scientific aspects related to the increased precision of the method of data reduction, making the ten-times rule obsolete, a proper procedure for utilizing data from the short-term transient regime to determine Poisson's ratio values in this time range is also desirable to reduce the required number of experiments to generate a reliable master curve. This is particularly true for experiments to be conducted at low temperatures (i.e. significantly below 0°C) which correspond to the short-term regime of master curves at ambient and above reference temperatures.

The scarcity of experimental data on time-dependent Poisson's ratio is largely due to difficulties in achieving the necessary strain resolution. In their review published in 2002, Tschoegl *et al.* concluded that the *only more or less acceptable determination* of Poisson's ratio was the one by Lu *et al.* (1997). In a more recent work, O'Brien *et al.* (2007) determined $\nu(t)$ of epoxy resins from creep tests with very good accuracy using Moiré interferometry.

In this work we explore the applicability of Digital Image Correlation (DIC) to simultaneously measure the axial and transverse strain of polypropylene specimens for various strain histories is explored. For this purpose, an analytical procedure described in a previous paper (Tscharnuter *et al.* (2010)) for determining the relaxation modulus is applied here for the time-dependent Poisson's ratio. In applying this method, it will be shown that the effective time for data reduction covered by a relaxation test can be extended by more than a decade compared to the conventional ten-times rule. Furthermore, the method allows for the determination of Poisson's ratio from strain histories that are not accessible when using the ten-times rule. Finally, results on Poisson's ratio from confined compression tests are presented, where an interconversion technique was used to derive Poisson values from bulk and shear relaxation moduli.

2 Experimental

2.1 Materials

The materials investigated include a polypropylene homopolymer (PP(H)), a glass bead filled polypropylene (PP(H)+G3.5), and talc filled polypropylene (PP(H)+T3.5). The numbers in the material designation indicate the filler content in terms of percent volume. The materials and injection molded specimens according to ISO 3176 type B were manufactured by Borealis Polyolefine GmbH (Linz, A). Further details as to these materials are described elsewhere (Jerabek *et al.* (2010d,a)).

2.2 Tensile relaxation tests

Using the materials PP(H) and PP(H)+G3.5, tensile relaxation tests were performed with a screw-driven electro-mechanical universal test system (type Zwick Z250; Zwick-Roell, Ulm, Germany) equipped with a temperature chamber to maintain the temperature inside the chamber at $23\pm0.5^{\circ}$C. A precise and narrow temperature control over the entire test time of up to 22 hours is of extraordinary importance for high precision measurements of Poisson's ratio. Over the 22 hours test duration, the standard deviation of the temperature was smaller than 0.1K in all tests. To simultaneously ensure an accurate strain control independet of the room temperature variations, a linear variable differential transducer (LVDT) linked to the control unit of the test system was mounted on the specimen grips inside the temperature chamber to serve as the displacement sensor. In this manner, the specimen tested and the LVDT experienced the same narrow temperature control.

The rather stringent requirement of a stable test temperature is exemplified by the following consideration. The coefficient of linear thermal expansion of PP(H)+G3.5 is of the order of $10^{-4}\mathrm{K}^{-1}$. Hence, a temperature change of 0.5K causes a thermal strain of $5\cdot10^{-5}$, which is only one order of magnitude smaller than the expected transverse strain, thus causing an additional measurement error amounting to about 10%.

2.3 Tensile creep tests

Creep tests in tension were carried out with neat PP(H) at 23°C with a self-constructed dead-weight test system (Steinberger *et al.* (2006)). The predefined creep load was applied in a moderate manner via a hand-driven crank shaft table (loading time ca. 5 to 10 s). As this test system was not equipped with a load cell, the precise loading history during the loading phase is not known. Hence, in this particular case, strain was also not measured in the initial loading phase, so that the methodology for data reduction in this stage of ramp loading could not be applied. Creep tests at 40°C and 50°C were done using the setup described above for relaxation testing with the testing machine operating in force controlled mode.

2.4 Displacement controlled monotonic tensile tests

Displacement controlled tensile tests up to ultimate failure were performed with an electro-mechanical universal testing machine (type Instron 5500, Instron, High Wycombe, UK). The tests were conducted with PP(H) at temperatures of -30°C, -10°C, 23°C, 50°C and 80°C and at various displacement rates ranging from 0.0001 to 1 mm/s. The data reduction scheme to deduce Poisson's ratio values was confined to the small strain linear viscoelastic region of the tensile curves.

2.5 Full-field strain measurement

In all of the above tests, a full-field strain measurement technique was applied using the digital image correlation (DIC) system ARAMIS (GOM mbH, Germany). While various aspects and details of this technique are described elsewhere (Jerabek *et al.* (2010c)), those relevant for an accurate determination of Poisson's ratio values are briefly summarized here. First, as the two cameras of the DIC system required for 3D displacement measurements cannot be positioned inside the temperature chamber, a special frame attached to the test system frame was used to mount the two cameras in a fixed and well-defined position relative to the specimen in front of the glass window chamber door but outside the temperature chamber. For the specific camera positions, the calibration algorithm assumes straight light paths. However, due to the refraction of the glass window, this assumption is inaccurate, leading to slightly erroneous strain calculations and a significant increase in data scatter. Moreover, below ambient temperatures, the resolution of the DIC system is further decreased by nitrogen fog inside the temperature chamber. Finally, a further source of enhanced data scatter are vibrations caused by the fan inside the temperature chamber that are transmitted to the two cameras via the rigid mounting frame.

For the creep tests on the dead-weight test system a CCIR camera with a resolution of 768x572 pixels that is installed in the test system was used for the full-field strain measurement. Due to the lower specifications in comparison to the cameras used with the ARAMIS system, a lower strain sensitivity is to be expected.

3 Results

3.1 Poisson's ratio from relaxation experiments

As pointed out above, stress relaxation measurements allow for a direct determination of time-dependent Poisson's ratio values, $\nu(t)$ being defined as

$$\nu(t) = \frac{-\epsilon_y(t)}{\epsilon_0} \tag{3}$$

Because of the simplicity of this equation, such ideal step loading assumptions are commonly used in the determination of viscoelastic material functions. However, the finite loading time of practical relaxation experiments instead of the ideal instantaneous loading (step strain assumption) does not allow for the direct use of the initial experimental data in combination with the above equation (ten-times rule for applicability of equation (3)). To properly account also for the data generated during ramp loading and within the ten-times period, more advanced data reduction techniques are needed. Such techniques have been proposed by Sorvari & Malinen (2006) and Knauss & Zhao (2007) for the determination of the relaxation modulus, and were also applied recently for relaxation modulus determination by the authors (Tscharnuter *et al.* (2010)).

Based on equation (2) and using the approach described for linear ramp loading (constant strain rate) by Sorvari & Malinen (2006) modified for more arbitrary ramp loading that is modelled by a function $f(t)$ (Tscharnuter *et al.* (2010)), Poisson's ratio can be defined in a good approximation by

$$\nu(t) \approx -\frac{\epsilon_y(t+t_1)}{f'(\zeta)t_1} + \frac{\dot{\epsilon}_y(t+t_1)}{2f'(\zeta)} \tag{4}$$

with t_1 being the loading time and $\zeta \in (0, t_1)$. For the special case of linear ramp loading, equation (4) may be rewritten in a more simplified form as

$$\nu(t) \approx -\frac{\epsilon_y(t+t_1)}{\epsilon_0} + \frac{\dot{\epsilon}_y(t+t_1)}{2\dot{\epsilon_0}} \tag{5}$$

In terms of conducting relaxation experiments, polynomial loading is easier to achieve than linear loading, so that equation (4) is to be applied for data reduction. On the one hand, the interpolation of measured transverse strain data is required for the shifted times $t + t_1$, on the other, a rather precise determination of the time derivative of the transverse strain is needed. For this purpose smoothing splines (piecewise polynomials) were used, because they allow for a custom degree of smoothing and provide interpolation by evaluating the splines

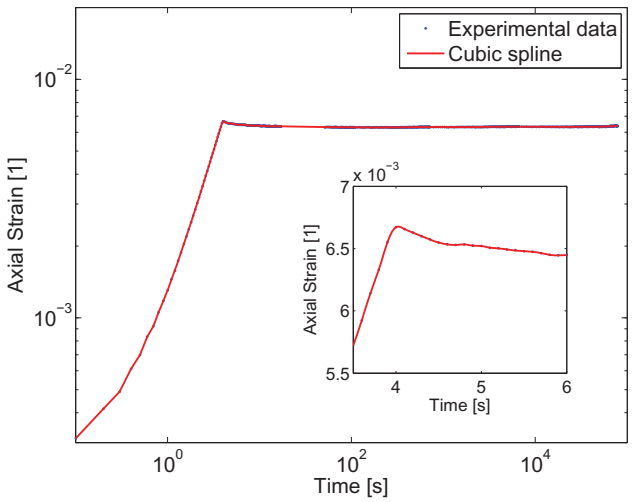

Fig. 1 Measured axial strain and a cubic spline interpolation of the strain for PP(H)+G3.5. The detail shows the transition from loading to relaxation

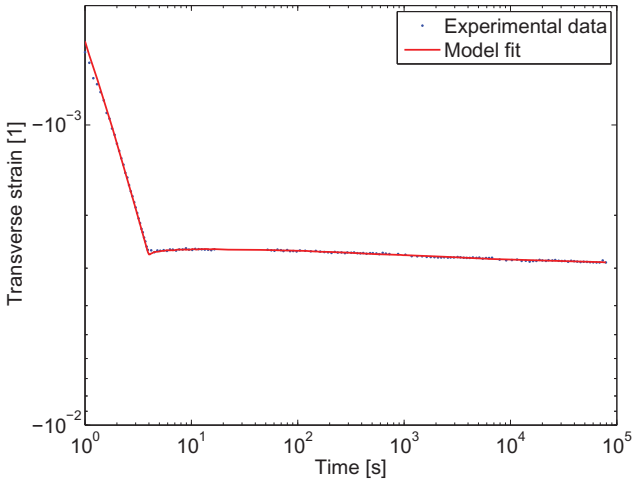

Fig. 2 Measured transverse strain and the least-squares fit for PP(H)+G3.5

at any desired point in time. This procedure of smoothing via splines also alleviates the problem of small strain oscillations during the initial loading phase until the predefined stable axial strain value ϵ_0 is reached.

A further problem, illustrated in figure (1) for PP(H)+G3.5, is related to the strain overshoot that still takes roughly 20 s to disappear, even for optimized strain control conditions. The strain history in this regime violates the assumption of the evaluation method considerably and thus may lead to erroneous results when applying the Sorvari-Malinen approach, particularly as the time approaches the ramp loading time t_1. To resolve the problem of strain overshooting (figure 1) associated with the test machine strain control system, a methodology described previously by us elsewhere was applied (Tscharnuter *et al.* (2010)). When utilizing this methodology, which is based on a least-squares optimization, compared to a point-by-point method, the least-squares optimization offers the advantage of simultaneously considering all available data, some exhibiting positive and others negative errors. This results in an inherent robustness against local errors and simultaneously provides results closer to the real values.

The basic idea of the optimization method is to solve the integral equation (2) using model functions for the axial strain and Poisson's ratio. The solution of the integral is then fit to the measured transverse strain to determine the model parameters. For Poisson's ratio a standard Prony series model was used, with the choice of an appropriate axial strain model defining the type of test that can be examined. For example, for relaxation modulus analysis, Knauss & Zhao (2007) used a linear loading followed by a constant strain in the form

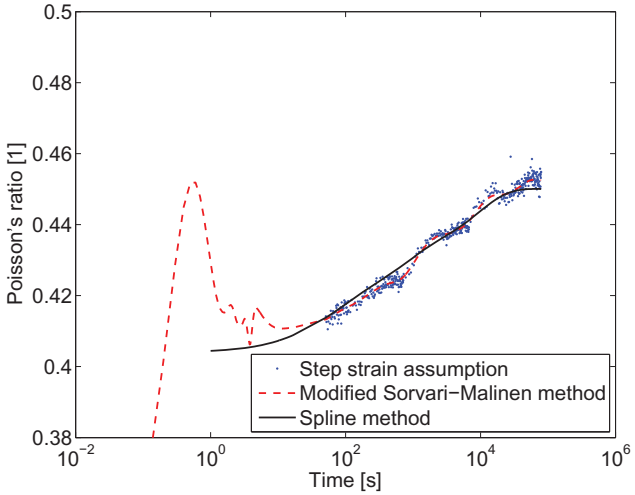

Fig. 3 Poisson's ratio of PP(H)+G3.5 as determined using step strain assumption, the modified Sorvari-Malinen method and the spline method

$$\epsilon(t) = \begin{cases} \dot{\epsilon}_0 t & t < t_1 \\ \epsilon_0 \equiv \dot{\epsilon}_0\, t_1 & t \geq t_1 \end{cases} \tag{6}$$

Such a model imposes very strict conditions on the loading history, so that care must be taken in the design of the experiment to achieve a strain that matches the model. These requirements may be relaxed by a more general strain model, referred to as spline method, in which the axial strain is modelled by a smoothing cubic spline as (Tscharnuter *et al.* (2010))

$$\epsilon_x(t) = \sum_i (a_i(t-t_i)^3 + b_i(t-t_i)^2 + c_i(t-t_i) + d_i)\Theta(t_i < t < t_{i+1}) \tag{7}$$

As the spline allows for a description of a slow transition from loading to both relaxation or creep, this method may be applied not only to relaxation tests but also to creep tests. And yet, this general formulation is no substitute for properly conducting the experiment, and accurate loading ramps and stress-strain measurements are still essential for a precise material function determination.

The smoothing spline that was used to model the axial strain is also shown in figure (1), illustrating that the spline precisely follows the transition from loading to stress relaxation at constant strain. This knowledge of the precise analytical history of the axial strain allows for a much improved interpretation of the accompanying transverse strain, which itself was modelled by the procedure described above (Prony series along with the cubic spline), see figure 2. Figure 3 depicts Poisson's ratio as a function of time comparing three methodologies for Poisson's ratio determination, the conventional point-by-point analysis along with the ten-times rule for step strain assumption, the modified Sorvari-Malinen method, and the spline method. While the spline method results are in excellent agreement with the results of the other two methods, it leads to a much reduced data scatter and simultaneously extends the range of valid Poisson's ratio data by up to two decades towards shorter times. In other words, the spline method indeed allows for a sufficiently accurate determination of Poisson's ratio values also in the loading period.

Analagous relaxation tests as described above for glass bead filled PP were performed with neat PP(H) and the results for both materials are compared in figure 4. In this case, the raw data were directly used to determine the contraction ratio as defined in equation (1), also including data from the loading period. As can be seen the data scatter is rather substantial and becomes excessive at short times during the loading phase including the transition regime. The spline method again offers a more precise description of the Poisson's ratio of these materials, extending into the short time range. As one would expect considering a simple rule of mixture, the glass bead filled PP exhibits lower values for Poisson's ratio at shorter times. At around 200 s a crossover of the curves occurs, with ν values of the glass bead material surpassing those of neat PP(H). While this change in ranking versus relaxation time is somewhat unexpected, the inhomogeneous strain distribution on a local scale in the polymer matrix of PP(H)+G3.5 along with strain magnification and perhaps even partial debonding may

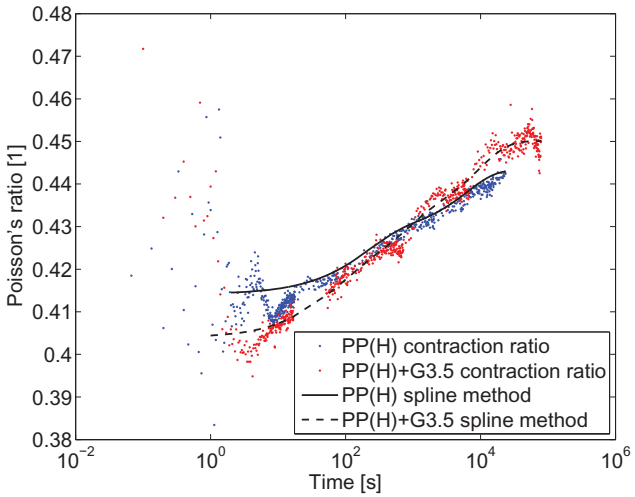

Fig. 4 Poisson's ratio determined by spline method and contraction ratio of PP(H) and PP(H)+G3.5

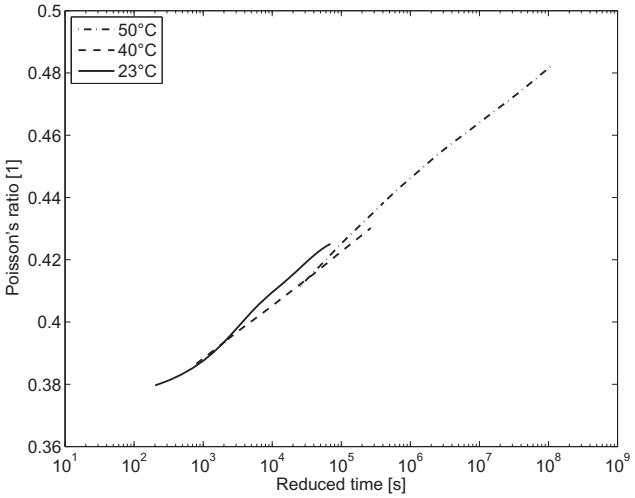

Fig. 5 Poisson's ratio master curve of PP(H) from creep experiments at 23°C, 40°C and 50°C. The master curve is referenced to 23°C

play a role in explaining this phenomenon. However, further investigations are needed to validate and explain this type of time-dependent behavior when comparing the two materials.

3.2 Poisson's ratio from creep experiments

As described above, applying the spline model to the axial strain also allows for a proper determination of Poisson's ratio from creep tests. Since no strain data were recorded during the dead-weight creep load application, the strain during the load application was approximated by interpolating the cubic spline between the first strain measurement point and a strain of zero at time zero.

A master curve of Poisson's ratio was constructed from the creep tests at 23°C, 40°C and 50°C (figure 5). The shift factors applied were obtained from previous studies on relaxation modulus master curves generated from tensile creep tests (Tscharnuter *et al.* (2010)), confined compression shear relaxation tests (Jerabek *et al.* (2010b)), and uniaxial compression relaxation tests (Jerabek *et al.* (2010d)), for which good agreement was observed in terms of the shift parameters (as to the determination and selection of the shift factors see also the discussion in the next section).

From the tests performed on the dead-weight test system, rather low values of Poisson's ratio were obtained. The applied creep load of 2MPa is small compared to the 12MPa peak stress of the relaxation test, therefore at 23°C the lateral strain does not exceed −0.2%. The low creep stress level was however necessary to remain within

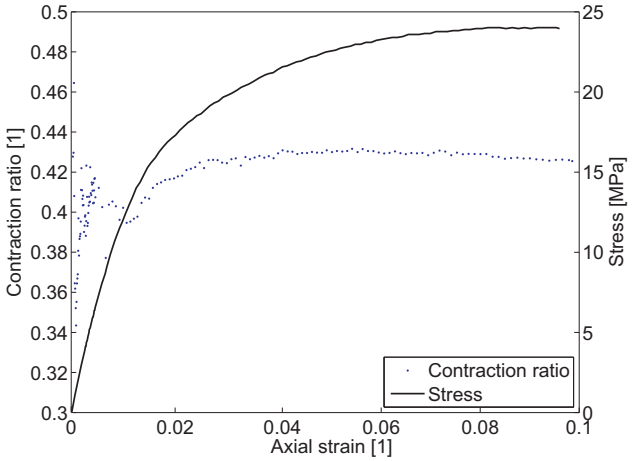

Fig. 6 Tensile stress and contraction ratio of PP(H) as a function of axial strain for PP(H)

the linear viscoelastic regime. Due to the fact that the corresponding creep strains are significantly smaller than in the relaxation experiments, small strain errors could account for the difference to the relaxation test result. To investigate this situation, creep experiments were also performed using the tensile testing machine under force control with a loading rate of 0.2 MPa/s up to the creep stress level of 2 MPa. The tests were conducted at temperatures of 40°C and 50°C to achieve somewhat higher strains. It is evident from the master curve shown figure 5 that the results from 40°C and 50° agree reasonably well with the room temperature data.

Further creep experiments were performed with biaxial strain gauges applied to the specimens. For reasons described by Arzouminidis & Liechti (2003), these could not provide the necessary strain accuracy in the transverse direction due to reinforcing effects associated with the stiffness of the copper wires and had to be discarded.

3.3 Poisson's ratio from displacement controlled monotonic tensile experiments

In addition to the problems in the strain measurement arising from the use of the temperature chamber, in displacement controlled monotonic tensile tests another problem exists related to the short duration over which the specimen is being deformed within the limits of linear viscoelasticity. In figure 6, tensile stress and contraction ratio (ratio of lateral and axial strain) are shown for a tensile test at room temperature for a loading rate of 0.01 mm/s. While there is some data scatter initially, the contraction ratio then increases from a level of about 0.35 to about 0.42 as the stress level approaches the yield stress and the contraction ratio reaches a plateau. In agreement with Jerabek *et al.* (2010a), the difference in the experimentally determined Poisson's ratio and the value of 0.5 for constant volume deformation is believed to be related to mechanisms of volume dilatation such as micro-crazing and possibly micro-cracking in the yield and post-yield regime.

In any case, the data in the nonlinear viscoelastic regime are not amendable to linear viscoelasticity theory and thus are of no further relevance here. However, considering that the initial data scatter may cover a strain regime from about 0.2% to 0.5%, or even 1% at the highest and lowest temperatures, it becomes apparent that the window of valid measurements before reaching the limit of linear viscoelasticity at about 1% to 2% can be very narrow. Consequently, Poisson's ratio measurements from tensile tests at various temperatures are only of rather limited use for the deduction of time temperature shift factors and the construction of master curves. It should be mentioned, however, that these restrictions do not apply in the same manner to the relaxation modulus determination from tensile tests, as forces can be measured to a higher accuracy compared to transverse strains. Hence, the shift factors for Poisson's ratio were deduced from the same tensile tests via the determination of relaxation modulus values. Using these shift factors, the Poisson's ratio master curve shown in figure 7 was constructed. The different curvature of individual data sets within the master curve reflects the inaccuracies with regard to temperature chamber effects and the limited window of valid data in the linear viscoelastic regime alluded to above. Also, regarding the shifting procedure, it is recognized that shift factors obtained from various viscoelastic functions may not necessarily be identical. For example, experiments performed by Deng & Knauss (1997) and Sane & Knauss (2001) indicate differences in the time-temperature shift for bulk and shear modulus data of PVAc. Conversely, O'Brien *et al.* (2007) found for epoxy resins that shift factors determined from creep compliance data lead to a smooth Poisson's ratio master curve. Similarly, Ma & Ravi-Chandar (2000) applied the same shift factors for shear and bulk moduli and obtained smooth master curves for PMMA and PC.

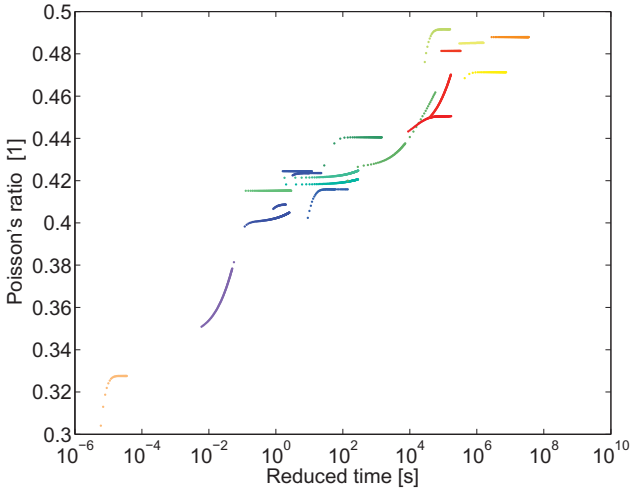

Fig. 7 Poisson's ratio master curve for PP(H) from displacement controlled tensile tests at temperatures ranging from −30°C to 80°C and loading rates from 1 to 0.0001 mm/s. The reference temperature is 23°C

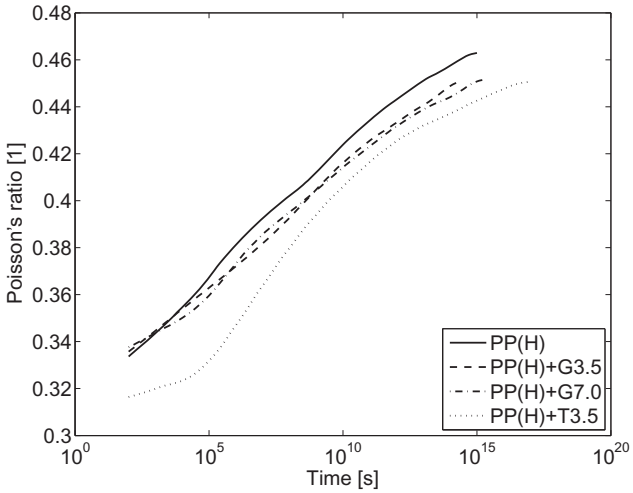

Fig. 8 Poisson's ratio master curves for PP(H), PP(H)+G3.5, PP(H)+G7.0 and PP(H)+T3.5 obtained from confined compression relaxation tests for a reference temperature of −30°C

3.4 Poisson's ratio from confined compression relaxation experiments

Confined compression relaxation experiments were performed for PP(H) and PP(H) glass and talc compounds at nine temperatures ranging from −30°C to 65°C. Based on the bulk and shear relaxation modulus data, master curves were constructed. Applying Prony series to the bulk and shear moduli master curves, master curves for Poisson's ratio were determined for the various materials and are depicted in figure 8 for a reference temperature of −30°C. Details as to the measurement and interconversion procedure are provided elsewhere (Jerabek *et al.* (2010b)).

As expected, by adding hard filler particles of a smaller Poisson's ratio than the one of PP(H), Poisson's ratio values of the particle compounds are lower than those of neat PP(H). At the short-term end of the time scale corresponding to low temperature measurements, experimental difficulties associated with the formation of ice were encountered, leading perhaps to some inaccuracy of the data, which, however, cannot be quantified.

4 Comparison of various Poisson's ratio master curves

An overview and a comparison of the Poisson's ratio master curves determined in this investigation for various loading situations is depicted in figure 9. Apart from effects related to measurement inaccuracies, some differences in the curves may be expected based on effects related to differences in the hydrostatic stress contribution for the

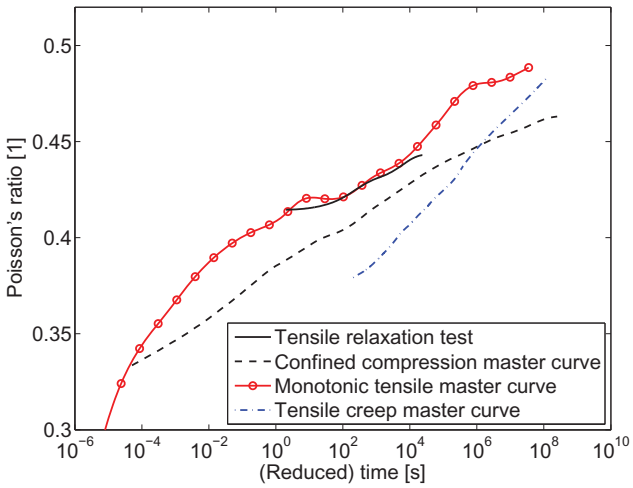

Fig. 9 Overview of Poisson's ratio of PP(H) obtained from various strain histories. The master curves are referenced to 23°C. The displacement controlled tensile test results were combined to a smoothed curve for this overview

various loading modes. As the hydrostatic stress contribution is clearly the highest for the confined compression tests, this may explain why the Poisson's ratio master curve for this loading mode is somewhat below the other curves. Moreover, as indicated above, the short-term section of the tensile creep master curve may be due to some measurement inaccuracy of the strain measurement device used in these tests. The discrepancy between the relaxation and creep test result can be explained by an error in the transverse strain of 0.01%. Nevertheless, considering such effects, there is a reasonable agreement between the master curve data obtained from various tests.

5 Conclusion

The application of Digital Image Correlation (DIC) as full-field strain measurement technique for the determination of Poisson's ratio from various strain histories was investigated. Tensile relaxation tests were performed with neat and glass bead filled polypropylene, and Poisson's ratio was determined including the loading ramp in the data analysis by applying a recently developed optimization method. Compared to the tradition ten-times rule evaluation, Poisson's ratio can be determined accurately over an extended time range using this procedure.

Furthermore, Poisson's ratio values were determined for neat polypropylene from creep tests. As the limits of linear viscoelasticity, where the ratio of strain and stress are independent of the stress level, were found to be lower in creep loading compared to relaxation loading, creep experiments must be performed at smaller strain levels. For these conditions, it turned out that the DIC setup was not precise enough to reliably determine Poisson's ratio.

In addition, displacement controlled tensile tests at various temperatures and loading rates were performed to determine Poisson's ratio for neat PP. The time range for recording valid data for Poisson's ratio determination was found to be rather limited as it was restricted by high data scatter at very small strain levels and by entering the regime of nonlinear viscoelasticity at higher strains. Thus, although the Poisson's ratio master curve from monotonic tensile tests closely resembles the master curves obtained from other tests, it does exhibit a higher data scatter. Lower loading rates were found to be advantageous as there is more time for the testing machine to stabilize and as there is a larger time range before nonlinear effects occur.

Poisson's ratio master curves for various materials (neat PP, glass bead and talc filled PP) were also determined by interconversion of bulk and shear modulus master curves obtained from confined compression relaxation tests. The interconversion yielded reasonable results for all materials considered, also revealing the influence of hard particle fillers in terms of a reduction in Poisson's ratio.

Acknowledgement

This research was performed at the Polymer Competence Center Leoben GmbH (PCCL, Austria) within the framework of the Kplus-program of the Austrian Ministry of Traffic, Innovation and Technology with contributions

by the University of Leoben (Institute of Materials Science and Testing of Plastics) and Borealis Polyolefine GmbH. The PCCL is funded by the Austrian Government and the States Governments of Styria and Upper Austria.

References

Arzouminidis, G.A., & Liechti, K.M. 2003. Linear viscoelastic property measurement and its significance for some nonlinear viscoelasticity models. *Mechanics of time-dependent materials*, **7**(3-4), 209–250.

Deng, T.H., & Knauss, W.G. 1997. The temperature and frequency dependence of the bulk compliance of poly(vinyl acetate). a re-examination. *Mechanics of time-dependent materials*, **1**, 33–49.

Hilton, Harry H. 2001. Implications and constraints of time-independent poisson ratios in linear isotropic and anisotropic viscoelasticity. *Journal of elasticity*, **63**(3), 221–251.

Jerabek, Michael, Major, Zoltan, Renner, Károly, Móczó, János, Pukánszky, Béla, & Lang, Reinhold W. 2010a. Filler/matrix-debonding and micro-mechanisms of deformation in particulate filled pp composites under tension. *Polymer*, **51**(9), 2040–2048.

Jerabek, Michael, Tscharnuter, Daniel, Major, Zoltan, Ravi-Chandar, Krishnaswamy, & Lang, Reinhold W. 2010b. Relaxation behavior of neat and particulate filled polypropylene in uniaxial and multiaxial compression. *Mechanics of time-dependent materials*, **14**(1), 47–68.

Jerabek, Michael, Major, Zoltan, & Lang, Reinhold W. 2010c. Strain determination of polymeric materials using digital image correlation. *Polymer testing*, **29**(3), 407–416.

Jerabek, Michael, Major, Zoltan, & Lang, Reinhold W. 2010d. Uniaxial compression testing of polymeric materials. *Polymer testing*, **29**(3), 302–309.

Knauss, W.G., & Emri, I.J. 1981. Non-linear viscoelasticity based on free-volume considerations. *Computers and structures*, **13**, 123–128.

Knauss, W.G., & Zhao, J. 2007. Improved relaxation time coverage in ramp-strain histories. *Mechanics of time-dependent materials*, **11**(3-4), 199–216.

Lu, H., Zhang, X., & Knauss, W.G. 1997. Uniaxial, shear and poisson relaxation and their conversion to bulk relaxation: Studies on poly(methyl methacrylate). *Polymer engineering and science*, **37**(6), 1053–1063.

Ma, Z., & Ravi-Chandar, K. 2000. Confined compression: A stable homogeneous deformation for constitutive characterization. *Experimental mechanics*, **40**(1), 38–45.

O'Brien, D.J., Sottos, N.R., & White, S.R. 2007. Cure-dependent viscoelastic poisson's ratio of epoxy. *Experimental mechanics*, **47**(2), 237–249.

Qvale, D., & Ravi-Chandar, K. 2004. Viscoelastic characterization of polymers under multiaxial compression. *Mechanics of time-dependent materials*, **8**(3), 193–214.

Sane, S.B., & Knauss, W.G. 2001. On interconversion of various material functions of pmma. *Mechanics of time-dependent materials*, **5**, 325–343.

Sorvari, J., & Malinen, M. 2006. Determination of the relaxation modulus of a linearly viscoelastic material. *Mechanics of time-dependent materials*, **10**, 125–133.

Steinberger, Robin, Vezer, Szilard, Major, Zoltan, & Lang, Reinhold W. 2006. Testing system for the creep characterization of polymers. *Proceedings of the 2006 sem annual conference and exposition on experimental and applied mechanics 2006*, **4**, 1767–1772.

Tscharnuter, Daniel, Jerabek, Michael, Major, Zoltan, & Lang, Reinhold W. 2010. On the determination of the relaxation modulus of pp compounds from arbitrary strain histories. *Mechanics of time-dependent materials*, 1–14.

Tschoegl, N.W., Knauss, W., & Emri, I. 2002. Poisson's ratio in linear viscoelasticity - a critical review. *Mechanics of time-dependent materials*, **6**(1), 3–51.

van der Varst, P.G.Th., & Kortsmit, W.G. 1992. Notes on the lateral contraction of linear isotropic visco-elastic materials. *Archive of applied mechanics*, **62**(5), 338–346.

The thermoelastic effect of polymers

D. Tscharnuter[a,*], M. Jerabek[b], D. Mungenast[a], Z. Major[c], G. Pinter[d]

[a] *Polymer Competence Center Leoben GmbH, Roseggerstrasse 12, 8700 Leoben, Austria*
[b] *Borealis Polyolefine GmbH, St. Peter Strasse 25, 4021 Linz, Austria*
[c] *Institute of Polymer Product Engineering, Johannes Kepler University Linz, Altenbergerstrasse 69, 4021 Linz, Austria*
[d] *Institute of Materials Science and Testing of Plastics, Franz-Josef-Strasse 18, 8700 Leoben, Austria*

Abstract

An experimental technique using an infrared camera for surface temperature measurements during mechanical testing was developed. A differential measurement between the tested specimen and a dummy specimen in a well-controlled temperature chamber provided excellent reproducability and temperature resolution. It was thus possible to conduct an investigation of the deformation heat during tensile and compressive testing of polypropylene, polycarbonate and poly(methyl-methacrylate). The materials were tested at a constant engineering strain rate of $8.7 \cdot 10^{-3}$ s^{-1} at 23°C. A heat conduction model was used to determine the deformation heat under consideration of convection on the specimen surface. Mechanical and physical parameters were measured to determine the reversible thermoelastic contribution to the deformation heat. It was shown that the effect of the temperature-dependence of the mechanical properties on the thermoelastic response must be considered to obtain consistent heat dissipation data.

Keywords: thermoelastic effect, polymer, temperature-dependent

1. Introduction

The deformation mechanisms of amorphous and semicrystalline polymers have been investigated in numerous studies using combinations of several techniques, such as deformation calorimetry [1, 2], syncrotron radiation X-ray scattering[3, 4] and electron microscopy [5, 6]. Other approaches with more readily available equipment are based on the evaluation of volume strain [7] or strain recovery [8–10]. These works provide a better understanding of the deformation mechanisms and structure-property-relations of polymers, which can lead to the development of improved tailor-made materials. For engineering materials, knowledge of the stages of deformation is also important for the definition of design limits for components, for neat polymers as well as for composites.

In several comprehensive studies, Oleinik and co-workers [1, 11] have investigated the energy storage and heat dissipation during the compressive deformation at low strain

*Corresponding author
Email address: tscharnuter@pccl.at (D. Tscharnuter)

rates of various polymers using calorimetric techniques and formulated a deformation theory based on small-scale plastic shear transformations. While this work is far too exhaustive for a brief summary, the basic idea of the calorimetric measurements is that the internal energy ΔU stored in the polymer upon deformation can be calculated, when the heat Q and the work of deformation W are known, according to the first law of thermodynamics

$$\Delta U = W + Q \tag{1}$$

In order to determine the viscoelastic and viscoplastic contributions to ΔU, the elastic parts must be subtracted. The elastic part of W is calculated using Hooke's law and the elastic part of Q is given by the thermoelastic effect or Thomson heat[1]. The classic equation for the thermoelastic effect is derived by thermodynamical considerations [12] and reads in terms of temperature

$$\Delta T = -\frac{T\alpha}{\rho c_p}\sigma \tag{2}$$

Here, ρ is the density, c_p the specific heat at constant stress, σ the axial stress, and α the coefficient of linear thermal expansion (CLTE). According to this equation, the thermoelastic effect leads to a temperature decrease in tension (positive stress) and an increase in compression (negative stress) proportional to the applied stress, provided α is positive, which is generally the case for the discussed polymeric materials. However, in tensile experiments on polypropylene and polyethylene conducted under adiabitic conditions in a vacuum chamber, Volodin and Slutsker [12] observed a temperature decrease larger than the decrease predicted according to equation (2) and explained this by considering the temperature-dependence of the mechanical properties. This effect of temperature-dependent mechanical properties has also been recognized in studies dealing with thermoelastic stress analysis [13], and Wong et al. [14, 15] derived a general thermodynamic expression for temperature-dependent materials. In contrast to the findings of Volodin and Slutsker, the classical equation (2) was successfully used in calorimetric studies to calculate the thermoelastic effect [1, 16, 17]. However, it was found insufficient to explain the thermal behavior observed in the tests conducted in this study. Hence, the aim of this work is to present the results of temperature measurements on amorphous and semi-crystalline polymers in uniaxial tension and compression and to show the importance of the effect of temperature-dependent mechanical properties on the thermoelastic behavior.

2. The thermoelastic effect

In thermoelastic stress analysis (TSA), specimes are subjected to a cyclic load under adiabatic conditions. Due to the thermoelastic effect, the temperature varies with stress,

[1] After William Thomson, 1st Baron Kelvin (Lord Kelvin), who first derived the equation for the effect.

Table 1: Notation

T	Temperature	ϵ_{ij}	Strain tensor
T_0	Reference (initial) temperature	σ_{ij}	Stress tensor
ΔT	$T - T_0$	ρ	Density
c_v	Specific heat at constant volume	q	Heat per unit mass
c_p	Specific heat at constant pressure	λ	Thermal conductivity
a	Thermal diffusivity	E	Young's Modulus
h	Heat transfer coefficient	Nu	Nusselt number
v	Air velocity in the temperature chamber	Pr	Prandtl number
ν	Kinematic viscosity of air	Re	Reynolds number
α	Coefficient of linear thermal expansion (CLTE)	μ	Poisson's ratio

which is used to determine the stress field by measuring the temperature field. An influence of the mean stress on the thermal response and the existence of the second harmonic of the applied frequency were recognized in TSA experiments [18], which lead to the development of an improved thermodynamic theory [14, 15]. A detailed review of this theory is given in reference [13], only the essentials are provided here.

From the first and second laws of thermodynamics, it follows that

$$\mathrm{d}T = \frac{T}{\rho c_v}\frac{\partial \sigma_{ij}}{\partial T}\mathrm{d}\epsilon_{ij} + \frac{\delta q}{c_v} \tag{3}$$

For an isotropic homogeneous material with temperature dependent mechanical properties, this leads to

$$c_v\rho\frac{\mathrm{d}T}{T} - \rho\frac{\delta q}{T} = -\left[\alpha + \left(\frac{\mu}{E^2}\frac{\partial E}{\partial T} - \frac{1}{E}\frac{\partial \mu}{\partial T}\right)\sigma_{kk}\right]\mathrm{d}\sigma_{kk} + \left(\frac{1+\mu}{E^2}\frac{\partial E}{\partial T} - \frac{1}{E}\frac{\partial \mu}{\partial T}\right)\sigma_{ii}\mathrm{d}\sigma_{ii} \tag{4}$$

For uniaxial stress under adiabatic conditions ($\delta q = 0$), integration of equation (4) yields

$$c_v\rho\left(\ln T - \ln T_0\right) = -\alpha\sigma + \frac{1}{2}\frac{\partial E}{\partial T}\frac{\sigma^2}{E^2} \tag{5}$$

or for small temperature changes

$$c_v\rho\Delta T = -\alpha T_0\sigma + \frac{T_0}{2}\frac{\partial E}{\partial T}\frac{\sigma^2}{E^2} \tag{6}$$

The left-hand side of this equation gives the heat released or absorbed per unit volume. By considering temperature-dependent mechanical properties, an additional quadratic contribution of the stress to the thermoelastic temperature is obtained.

3. Experimental

3.1. Materials

The materials investigated are a model polypropylene homopolymer (PP(H); Borealis Polyolefine GmbH), polycarbonate (PC; Makrolon 2405, Bayer) and poly(methylmethacrylate) (PMMA; Plexiglas 7N, degussa). The PP(H) injection molded specimens according to ISO 3167 type B were manufactured by Borealis Polyolefine GmbH (Linz, A). The injection molded specimens according to ISO 3176 type A of PC and PMMA were produced at the Institute of Plastics Processing, University of Leoben, Austria.

Due to a shortness of PP(H) specimens during the development of the testing and evaluation procedure, spare poly(butylene-terephthalate) (PBT; Ultradur 4500, BASF) specimens were used for initial testing and verification.

3.2. Tensile tests

Monotonic tensile tests were performed on a screw-driven electro-mechanical universal test system (type Zwick Z250; Zwick-Roell, Ulm, Germany) with a constant engineering strain rate of $8.7 \cdot 10^{-3}$ s^{-1}. The system is equipped with a temperature chamber to maintain the desired test temperature of 23°C. A precise temperature control over the entire test time is important, hence a careful tuning of the temperature controller is necessary.

Full-field strain was measured using the digital image correlation (DIC) system ARAMIS from GOM mbH, Germany. To measure the strain with optimal accuracy and precision, the specimen must be well illuminated to achieve a good image quality. We found that the cold lights used still affect the surface temperature of the specimen. Therefore, it was decided to measure the strain and temperature fields in separate tests. A series of tensile tests showed that the stress-strain curves of the various tests agree very well up to high strains. Small differences between tests arise only sometimes after yielding due to the individual nature of the necking.

To determine the rate of change of Young's modulus with temperature, dE/dT, for the thermoelastic model, several tensile tests at low strains (ISO 527 strain range) were performed at various temperatures. Three measurements were conducted at each temperature. To account for the strain-rate dependence of the mechanical properties, the modulus measurements were performed at the same strain rate used in the tensile tests describe above. dE/dT was calculated from a third degree polynomial fit.

True longitudinal strain $\epsilon_{t,l}$ and transverse strain $\epsilon_{t,t}$ are calculated from the engineering strains by

$$\epsilon_{t,l} = \ln(\epsilon_{n,l} + 1) \tag{7}$$

and

$$\epsilon_{t,t} = \ln(\epsilon_{n,t} + 1) \tag{8}$$

The one-point values of Poisson's ratio were determined by the longitudinal and transverse strains in the longitudinal strain range of 0.05% to 0.25%. The true stress is defined as

$$\sigma_t = \frac{F}{A_0} \frac{1}{(1+\epsilon_{n,t})^2} \tag{9}$$

where F is the force and A_0 the cross-sectional area of the unstrained specimens.

3.3. Compression tests

Monotonic uniaxial compression tests with a constant engineering strain rate of $8.7 \cdot 10^{-3}$ s^{-1} were performed on an Instron 5500 electro-mechanical universal testing machine. The displacement was measured using a LVDT and the strain was calculated from the displacement. The entire setup is decribed in detail elsewhere[19]. The 8x4x10 mm^3 specimens were machined from the injection molded tensile specimens. This specimens have two distinct advantages. First, the material is identical to the material used in the tensile tests. Second, on rectangular cross-sections the angle-dependence of the emissivity does not need to be considered.

Young's modulus is larger in compression than in tension, e.g. by around 10% for PP(H) [19], so dE/dT in compression likely differs from the tensile result by a similar amount. Because of the difficulties involed in compression modulus testing [19, 20], E(T) and dE/dT from the tensile tests are also used for the analysis of the compression tests, bearing in mind that as a consequence the quadratic term of equation (6) may be off by about 10%.

As the transverse strain is not measured during the compression tests, the true stress is approximated assuming a constant Poisson's ratio in equation (9).

3.4. Material parameters

The thermoelastic analysis requires several parameters to predict the thermoelastic temperature change. The density, specific heat and thermal conductivity were determined by hydrostatic weighing, DSC (DSC 831; Mettler-Toledo, Switzerland) and the transient plane source method (HotDisk TPS 2500; HotDisk AB, Sweden), respectively. Note that c_v and c_p are related by [13]

$$c_p - c_v = \frac{3\alpha^2 E T_0}{\rho(1-2\mu)} \tag{10}$$

The CLTE was measured using an interferometry set-up (ESPI; GoM mbH, Germany) similar to the set-up described in reference [21].

3.5. Temperature field measurement

The specimen temperature was monitored using a JADE III MWIR camera by Cedip Infrared Systems (now FLIR). The camera is equipped with a 320x240 pixel InSb detector with a noise equivalent temperature difference of 20 mK at room temperature. As the glass windows of the temperature chamber are not transparent at the infrared wavelengths, the window of the chamber was replaced by a properly sized block of extruded polystyrene foam. A hole matching the dimensions of the lens was cut into the foam to accomodate the camera, effectively placing the lens inside the chamber. All specimens were coated with graphite spray to achieve a defined and uniform emissivity. The emissivity was determined by simultaneously measuring the temperature with the infrared

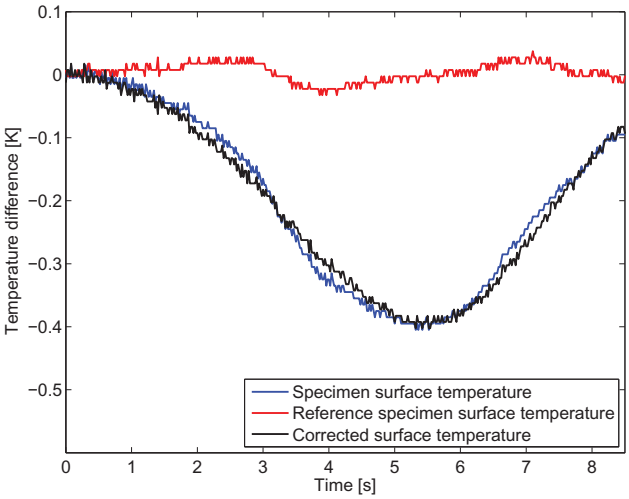

Figure 1: Specimen, reference specimen and venting/heating corrected temperature of PP(H) at 0°C.

camera and a resistance thermometer. The emissivity was 0.85. As spray coating by hand does not provide a reproducable coating thickness, the influence of graphite layer thickness on the emissivity was investigated by comparing different thicknesses obtained by various spraying times. No influence of the coating thickness was found. Additionally, the emissivity of a specimen was measured before and after stretching beyond the yield point. It was found that the emissivity does not depend on the strain in this deformation region. At larger strains, the spray coating is thinned and the temperature value becomes increasingly unreliable.

As the temperature changes due to the thermoelastic effect up to yield are in the range of 1 K, care must be taken to ensure the stability of the ambient temperature. The temperature chamber controls the temperature by a combination of heating via heating coils and cooling by venting with cold nitrogen gas. Hence, the specimen is subject to periodic cooling and heating. The surface temperature drops during the venting phase and subsequently increases until the next venting occurs. The choice of proper control parameters ensures that neither heating nor venting is performed excessively and keeps the temperature difference before and after nitrogen venting small. Nevertheless, these periodic environmental changes have to be accounted for to obtain correct temperature measurements. This is achieved by simultaneous monitoring of a reference specimen that is mounted on the unmoving specimen grip next to the tested specimen and not subjected to any loading. The surface temperature of the reference specimen allows for the correction of the effects of heating and venting on the specimen temperature by taking the difference to the reference temperature. This is a reasonable procedure because the bulk temperature is not affected by the short-term fluctations due to *smearing* of the irregularities by heat conduction. The periodic nitrogen venting effect, occuring 3 s and 7 s after the start of a tensile test at 0°C is shown in figure 1 along with the measured surface temperature and the corrected surface temperature.

The thermal data is available in the image coordinate system or pixel coordinates.

As the specimen is stretched during a tensile test, the point on the specimen that is registered in a certain pixel changes during the test. Thus, a statistical evaluation on any subset of the pixels does not correspond to the statistic of a specific region on the specimen. Depending on the test temperature and material, a specimen may or may not form a necking zone at high strains. A necking zone is generally hotter than other regions of the specimen. As these regions are the primary zones of deformation, temperature data is gathered from these zones. If the displacement is not accounted for, the necking region moves through the pixel subset that is selected for temperature evaluation. In this case, the slope of the temperature curve is altered because colder pixels enter the evaluation region. To address this problem, a motion tracking algorithm was used to account for the displacement of the specimen. An aluminum coated adhesive tape was placed on the moving specimen grip. This reflective surface is clearly visible in the IR image and was used to determine the displacement in terms of pixels. This avoids the need to calculate the pixel displacement from the actual displacement and the optical parameters of the camera setup. As motion tracking works best when the tracked object has distinct features, the tape was applied in a crumpled manner. The tracking was done using the Lucas-Kanade algorithm [22]. A brief description of the general approach is given. The first image of the thermal measurement, which corresponds to the unstrained state of the specimen, is denoted by $I_1(\mathbf{x})$, where $\mathbf{x} = (x, y)$ is the pixel position in the coordinate system of this image. In this image, a rectangular subset of pixels containing the adhesive tape was selected. This subset is denoted as the template $T(\mathbf{x})$. In the subsequent image, $I_2(\mathbf{x})$, the template position differs from the previous image because of the displacement of the grip. This motion is expressed by the mapping $\mathbf{W(x,p)}$, where $\mathbf{p}$ are the parameters of the transformation. Since the grips are rigid and do not rotate, it is sufficient to consider the translations

$$\mathbf{W(x,p)} = (x + p_x, y + p_y) \tag{11}$$

The translation vector $\mathbf{p}$ is found by minimizung the quadratic error between the translated image and the template,

$$\sum_{\mathbf{x}} \left[I_2(\mathbf{W(p,x)}) - T(\mathbf{x}) \right]^2 \tag{12}$$

where the sum extends over all pixels of the template. Once the pixel displacement has been determined for each frame of the measurement, the images are scaled using linear interpolation. The camera was rotated to align the load axis with the 320 pixel x-axis. Then p_x is the measure of the axial displacement and p_y indicates the precision of the alignment of the camera and the testing machine axis. The scaling is performed to maintain an equal distance between the grips and thus equal length of the specimen throughout the test. The scaled images as depicted in figure 2 are then used for a statistical temperature evaluation. The temperature is determined by the mean value of an approximately 3 mm wide rectangular area centered on the area of interest on the specimen. The averaging reduces the overall noise and allows for a better temperature

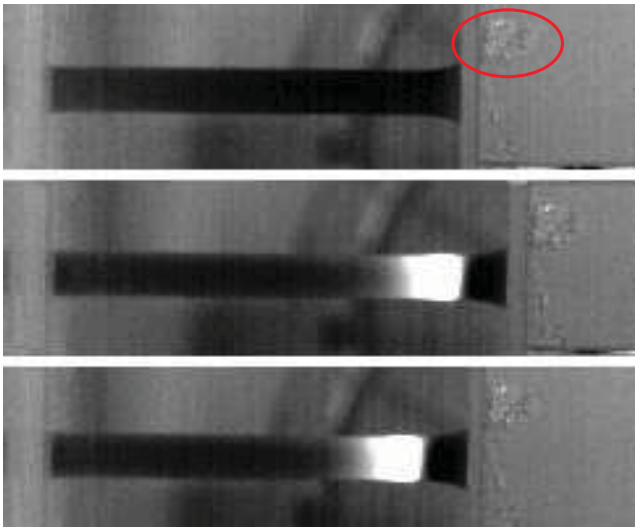

Figure 2: Displacement correction in thermal images. Top: Unstrained specimen. Middle: Strained specimen showing a hot necking zone (white). Bottom: Strained specimen image corrected for the displacement. The reflective tape is highlighted by the ellipse in the top image.

resolution than the 20 mK noise in each pixel suggests. By all the measures described, an excellent reproducability and temperature resolution is achieved. An example for polypropylene is shown in figure 3.

4. The heat transfer problem

The spatial and temporal evolution of the temperature field $u(x, y, t)$ in the 10x4 mm^2 cross-section of the specimen is governed by the heat equation

$$\frac{\partial u(x,y,t)}{\partial t} = a\left(\frac{\partial^2 u(x,y,t)}{\partial x^2} + \frac{\partial^2 u(x,y,t)}{\partial y^2}\right) + \frac{1}{c_p}\dot{q}(t) \tag{13}$$

Here it is assumed that the heat sources q are homogeneously distributed in the cross-section. This is an approximation especially in the case of semicrystalline polymers, where the morphology depends on the processing conditions and varies in the specimen cross-section [23]. Heat conduction along the length of the specimen, which is present in inhomogeneous temperature fields e.g. by necking, is neglected because of the low thermal conductivity of the polymers.

At the employed strain rate of $8.7 \cdot 10^{-3}$ s^{-1}, a typical test duration is about 10 s or longer, depending on the material and test temperature. Heat is transferred between the specimen and the environment mainly via the circulating air inside the temperature chamber. The heat transfer occurs at the specimen surface and the heat propagates through the specimen at a diffusion velocity that is determined by the material's thermal properties. Therefore, the specimen temperature is not homogeneous and the measured surface temperature is not equal to the temperature defined by the material's heat

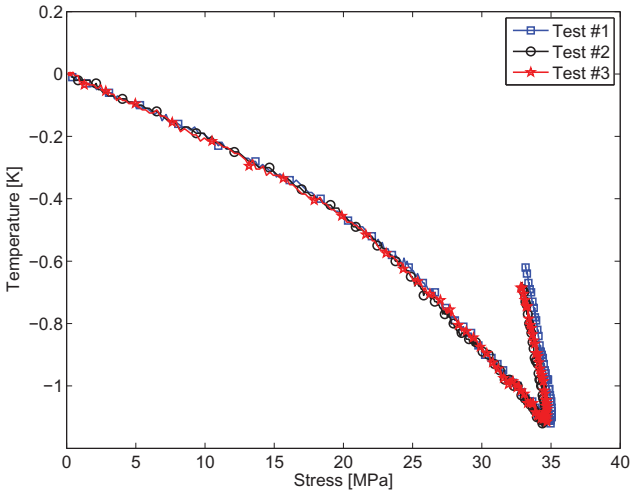

Figure 3: Temperature curves measured in three tests of PP(H) at 23°C. Note that for better visibility markers are only plotted for one out of ten data points. Thermal images were recorded at a rate of 50 frames per second.

sources, including the thermoelastic heat. Hence, the heat sources must be determined by solving equation (13).

The boundary $\mathfrak{B}$ of the cross-section is subject to the boundary conditions describing the convective heat transfer,

$$-\frac{\lambda}{h}\frac{\partial u(x,y,t)}{\partial n}\bigg|_{x,y\in\mathfrak{B}} = u_0 - u(x,y,t)\bigg|_{x,y\in\mathfrak{B}} \tag{14}$$

where n denotes the derivate in the direction normal to the boundary line. The heat transfer coefficient is estimated by

$$h = \mathrm{Nu}\frac{\lambda_{\mathrm{Air}}}{l} \tag{15}$$

where l is half the circumference of the specimen, which equals 14 mm. The Nusselt number is calculated using the Reynolds number and the Prandtl number by [24]

$$\mathrm{Nu} = 0.3 + \sqrt{0.440896\,\mathrm{RePr}^{2/3} + 0.001369\,\mathrm{Re}^{1.6}\mathrm{Pr}^2\left(1 + \frac{2.4443\,(\mathrm{Pr}^{2/3}-1)}{\mathrm{Re}^{0.1}}\right)^{-2}} \tag{16}$$

where Reynolds number is lv/ν. The average velocity of 1.05 m/s in the temperature chamber was measured using a propeller anemometer. Values for the remaining air

properties were taken from the literature [24]. These properties depend on temperature, thus making h temperature dependent, but as the temperature changes are small, it is assumed that the heat transfer coefficient and the specimens' physical properties are constant.

The ambient air temperature u_0 is also the initial temperature of the specimen, which gives the initial condition

$$u(x, y, 0) = u_0 \tag{17}$$

The system of differential equations (13),(14) and (17) is solved using the Crank-Nicolson finite differencing scheme [25, 26]. In finite differencing, the temperature field is solved on a spatial grid in discrete time steps, the derivatives being replaced by differences to adjacent grid points or consecutive time steps. Suppose the grid points are indexed by i and j in the x and y direction respectively, then the temperature at time step t_{n+1} at grid point (i, j), is determined using the value at the previous time step $u(x_i, y_j, t_n) \equiv u^n_{i,j}$ by

$$\begin{aligned} u^{n+1}_{i,j} = u^n_{i,j} \quad &+ \quad \frac{a\delta_t}{2\delta_x}\left(u^{n+1}_{i+1,j} - 2u^{n+1}_{i,j} + u^{n+1}_{i-1,j} + u^n_{i+1,j} - 2u^n_{i,j} + u^n_{i-1,j}\right) \\ &+ \quad \frac{a\delta_t}{2\delta_y}\left(u^{n+1}_{i,j+1} - 2u^{n+1}_{i,j} + u^{n+1}_{i,j-1} + u^n_{i,j+1} - 2u^n_{i,j} + u^n_{i,j-1}\right) \\ &+ \quad \delta_t q^n \end{aligned} \tag{18}$$

δ_x and δ_y is the grid spacing in x and y directions, and δ_t is the time step. Equation (18) is valid for inner points. Points on the boundary are subject to a discrete expression of equation (14), which is

$$u^{n+1}_{1,j} - u^{n+1}_{2,j} = \frac{h\delta_x}{\lambda}\left(u^{n+1}_{1,j} - u_0\right) \tag{19}$$

for the boundary at $x = 0$ or equivalently $i = 1$. Analogous equations hold for the other boundaries. Equations (18) and (19) constitute a system of linear equations for the grid values at each time step. The solution of this system provides the temperature field as function of the source term $q(t)$. Thus, the inverse problem of determining the source when a part of the solution, namely the temperature field on the surface, is known must be solved. This is done by minimizing the quadratic error between the measured surface temperature and the computed surface temperature on the grid as a function of the source term. When the source term is modelled by a m-term polynomial, the optimal polynomial coefficients $\boldsymbol{a} = (a_0, a_1, \ldots, a_{m-1})$ are defined by

$$\boldsymbol{a} = \min_{\boldsymbol{x}\in\mathbb{R}_m} \sum_{n=1}^{N} \left(T_{\text{surface}}(t_n) - u^n_{1,-}(\boldsymbol{x})\right)^2 \tag{20}$$

Here it was assumed that the boundary $i = 1$ corresponds to the 10 mm side of the specimen, on which the temperature T_{surface} has been measured in the experiments. The

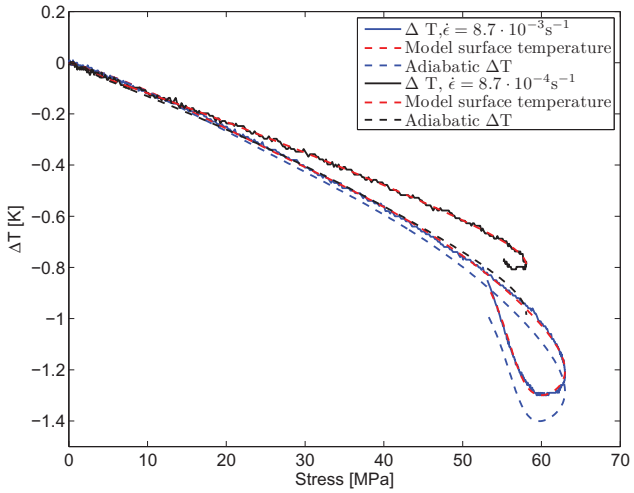

Figure 4: Temperature change of PBT at strain rates of $8.7 \cdot 10^{-3}$ s^{-1} and $8.7 \cdot 10^{-4}$ s^{-1} and adiabatic temperature.

dash in place of the j index indicates that averaging of the computed surface temperature over the inner third of the specimen is performed to match the procedure applied to the measured surface temperature. Under adiabatic conditions, the thus determined heat sources fully describe the heat released or absorbed during a mechanical tests. As the heat exchanged with the surroundings is small in the conducted tests, the data is treated as adiabatic and the thermodynamic equation (6) is used to account for the reversible contribution to the heat.

According to the results of Volodin and Slutsker [12], the temperature change in the thermoelastic regime (low stresses) does not depend on strain rate for the strain rates investigated. This observation thus provides an opportunity to test the solutions of equation (20). From the heat sources determined by equation (20), the surface temperature during a hypothetical adiabatic test can be calculated. Then, assuming no substantial change in the dominating deformation mechanisms, the temperatures calculated for two different strain rates should coincide at low stresses. Using PBT specimens, tests were conducted using strain rates of $8.7 \cdot 10^{-3}$ s^{-1} and $8.7 \cdot 10^{-4}$ s^{-1} and the heat sources were determined from each test. The measured surface temperatures, the calculated adiabatic temperatures and the model surface temperature for both strain rates are shown in figure 4. Contrary to the measured surface temperatures, which differ due to the heat transfer, the adiabatic curves agree up to a stress of 20 MPa. It was attempted to infer the heat transfer coefficient by minimizing the difference between the adiabatic curves from both strain rates. With the optimized heat transfer coefficient, the curves match closely up to 50 MPa, but the calculation gave an unrealistically high air velocity of 2.4 m/s, which is more than twice the measured average value. Additionally, trial computations also showed that the obtained value depends on the stress range that is used for fitting. To avoid the resulting ambiguity, the heat transfer coefficient as calculated from equations (15) and (16) was used.

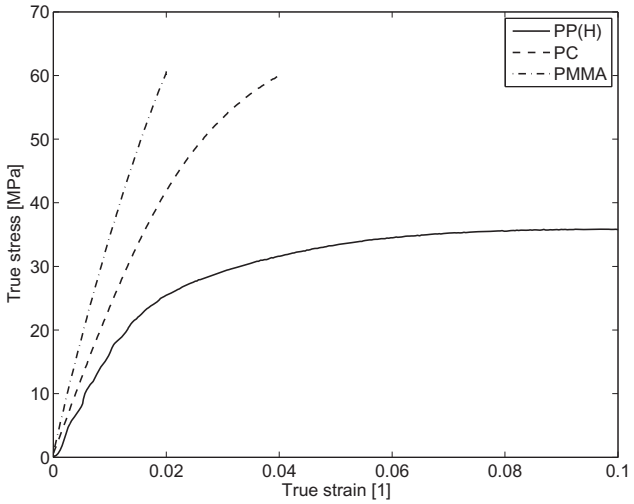

Figure 5: True stress-true strain curves from tensile tests of PP(H), PC and PMMA at 23°C and a strain rate of $8.7 \cdot 10^{-3}$ s^{-1}.

5. Results and discussion

Table 2: Material parameters.

	E [MPa]	dE/dT [MPa K^{-1}]	ρ [kg m^{-3}]	c_p [J kg^{-1} K^{-1}]	α [K^{-1}]	λ [W m^{-1}K^{-1}]	μ [1]
PP(H)	1820	−45	902	1570	$81 \cdot 10^{-6}$	0.14	0.41
PC	2510	−5	1190	1170	$65 \cdot 10^{-6}$	0.24	0.36
PMMA	3750	−30	1190	1360	$62 \cdot 10^{-6}$	0.21	0.34

A collection of the true stress-strain curves of the three materials for tension and compression is shown in figures 5 and 6, respectively. The pneumatic grips used in the tensile tests have a maximum load of 2.5 kN, which imposes a limit on the accessible strain range in the case of PC and PMMA.

From the tensile tests at several temperatures (figure 7), the change of the modulus with temperature, dE/dT, was calculated. The remaining material properties needed for evaluating equation (6) were measured as described above. All results are summarized in table 2. With the data given in table 2, the thermoelastic temperature change can be calculated according to equation (6). In uniaxial tension, the stress is positive. Hence, for a hypothetical elastic material with a positive CLTE, both terms on the right-hand side of equation (6) are negative, implying that the temperature decreases in tension. Figure 8 gives an example of this behavior for PMMA. The difference between the measured surface temperature and *adiabatic temperature* as derived from the solution of (20) shows that the error made by neglecting convection is small in this case, but may be larger in other cases (cf. figure 9). It is seen that the linear thermoelastic curve (2) matches the experimental data well up to 30 MPa and predicts higher temperatures at larger stress values. The area between the thermoelastic curve and the adiabatic temperature curve

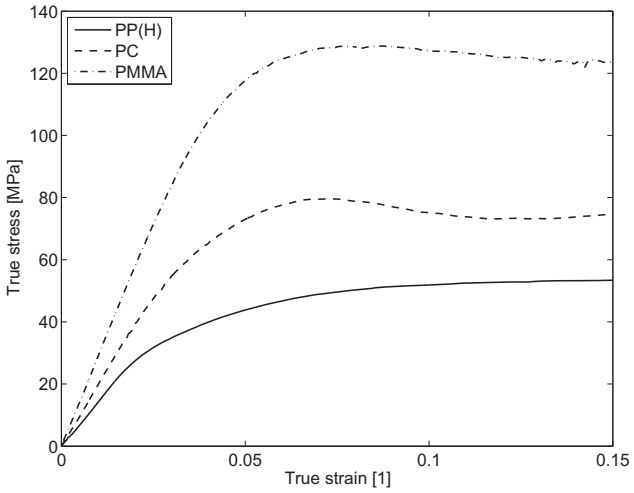

Figure 6: True stress-true strain curves from compression tests of PP(H), PC and PMMA at 23°C and a strain rate of $8.7 \cdot 10^{-3}$ s^{-1}.

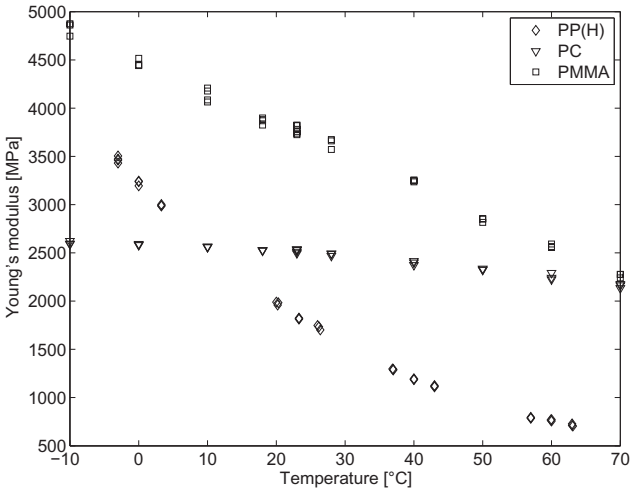

Figure 7: Young's modulus of PP(H), PC and PMMA at various temperatures ranging from −10°C to 70°C.

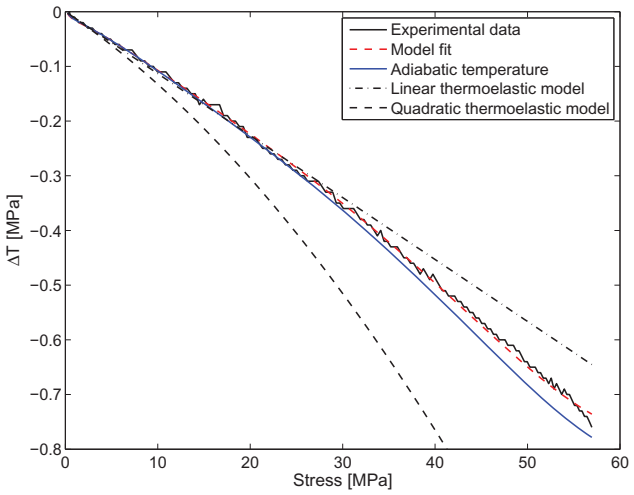

Figure 8: Experimental temperature data from a uniaxial tensile test, calculated adiabatic temperature and thermoelastic curves for PMMA.

relates to the dissipated heat. In terms of heat, this implies that no heat is dissipated up to 30 MPa, and that heat is absorbed at stresses above this level. This finding shows the importance of considering the material's temperature dependence. The quadratic thermoelastic curve (equation (6)) predicts smaller temperatures, consistent with the release of heat by viscoelastic and viscoplastic mechanisms during loading. Similar results were obtained in the tensile testing of PP(H) and PC (figure 9) and in the compression testing of PP(H), PMMA and PC (figures 10-12). In compression loading, the negative stress leads to a non-monotonic thermoelastic curve, giving positive temperature at the lowest stresses before the negative quadratic term dominates. Due to the proximity to the glass transition temperature, dE/dT of PP(H) is very large and the quadratic term is very pronounced. Similar to PMMA, it is strong enough to give rise to a temperature decrease significantly stronger than the classical linear equation.

By the first law of thermodynamics (equation (1)), the internal energy stored can be calculated when the heat and deformation work are known. To determine the viscoelastic and viscoplastic contribution, the elastic parts are substracted [1]. The elastic deformation work per unit volume is

$$w_{el} = \frac{\sigma^2}{2E} \tag{21}$$

and the total deformation work per unit volume is given by

$$w = \int \sigma d\epsilon \tag{22}$$

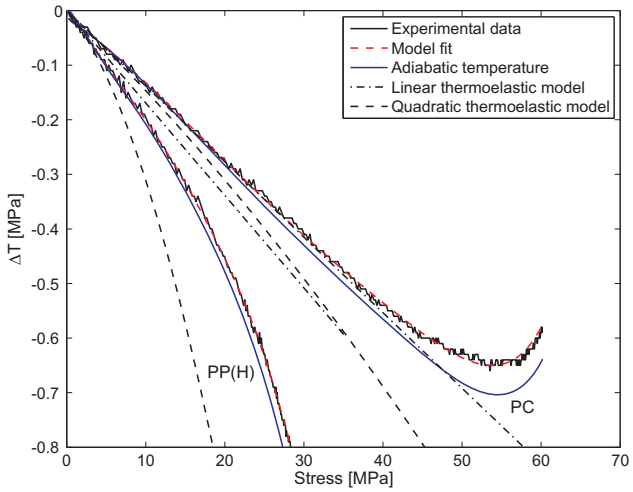

Figure 9: Experimental temperature data from uniaxial tensile tests, calculated adiabatic temperature and thermoelastic curves for PC and PP(H).

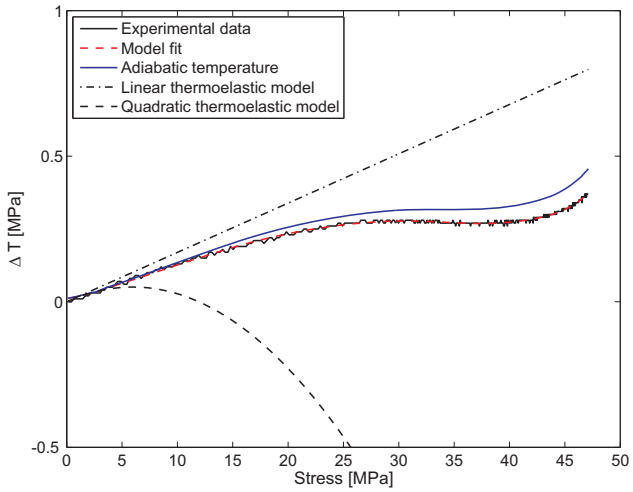

Figure 10: Experimental temperature data from a uniaxial compression, calculated adiabatic temperature and thermoelastic curves for PP(H).

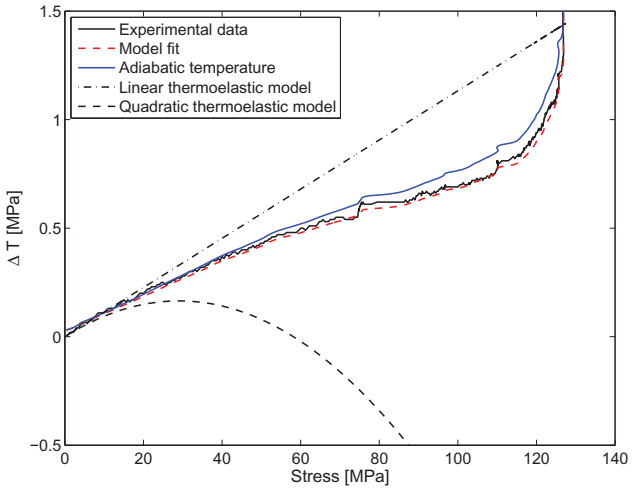

Figure 11: Experimental temperature data from a uniaxial compression, calculated adiabatic temperature and thermoelastic curves for PMMA.

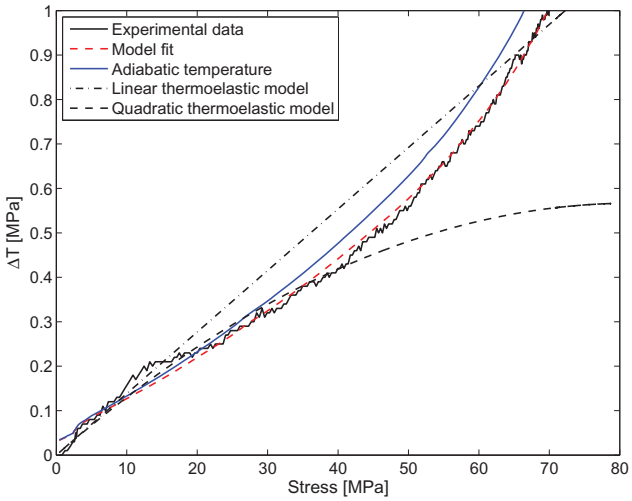

Figure 12: Experimental temperature data from a uniaxial compression, calculated adiabatic temperature and thermoelastic curves for PC.

The heat per unit volume is calculated from the heat source (equation (13)) by

$$q_v = \rho \int_0^t \dot{q}(t')dt' \tag{23}$$

The elastic contribution to the heat is determined by equation (6). Due to the strong effect of the quadratic term, there is already a distinct difference between the overall heat and the thermoelastic heat at low stresses in all conducted tests. However, the stress-strain curve does not notably deviate from its elastic component, which implies that the non-elastic work done at this stage is very small. An example of this observation on PC in tension is shown in figure 13. The non-elastic heat exceeds the non-elastic deformation work, whereas it is expected to be equal or smaller for conservation of energy. A part of this apparent inconsistency could arise from the viscoelastic contribution to the Young's modulus determined at a strain rate of $8.7 \cdot 10^{-3}$ s^{-1}. The modulus testing requires a strain-rate dependent amount of time. During this time, viscoelastic relaxation processes occur in the material, which reduce the observed modulus value. Hence, Young's modulus increases with strain rate. The higher modulus values obtained at high strain rates or frequencies reduce the magnitude of the quadratic thermoelastic term and could thus account at least in part for the discrepancy between the calculated non-elastic heat and deformation work. Additionally, the physical properties used in the thermoelastic model, such as density or CLTE, depend on the microstructure, which changes during deformation. The CLTE depends on the orientation of the polymer chains, which leads to e.g. a higher CLTE in the transverse direction than in the longitudinal direction of an injection-molded specimen. During tensile testing, further orientation is introduced, which may in turn reduce the CLTE and thus effectively change the elastic response of

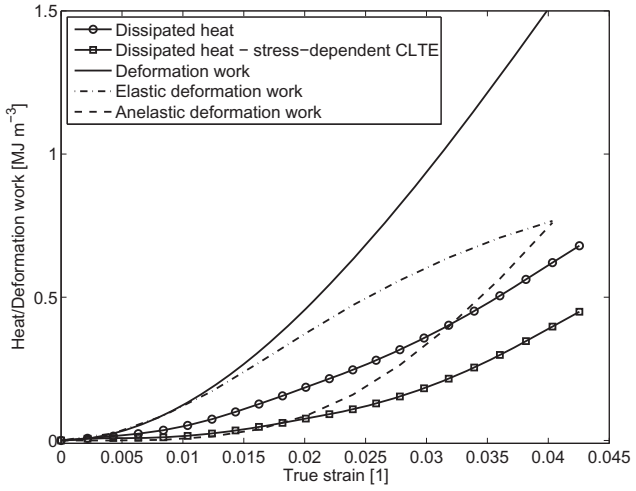

Figure 13: Dissipated heat and total, elastic and anelastic deformation work of PC in uniaxial tension. One heat curve (square markers) was calculated assuming an arbitrarily stress-dependent CLTE.

the material. A sample calculation was performed assuming a stress-dependent CLTE, which varies linearly with stress from the zero-stress value to a decrease of 20% at the maximum stress. This is completely arbitrary, but the result (figure 13, square markers) shows that changes in the percent range have a large impact on the result of the heat calculation.

6. Conclusion

An analysis of the contribution of the thermoelastic effect to the heat evolution during uniaxial tension and compression of PP, PC and PMMA was presented. It was shown that a carefully designed experimental setup with a differential measurement between a loaded and a non-loaded specimen allows for high precision temperature measurements. The heat conduction in the specimen cross-section and convection on the surface were considered and it followed that some error is introduced when the adiabatic assumption is made at the investigated strain rate of $8.7 \cdot 10^{-3}$ s^{-1}.

The results showed that the quadratic contribution to the thermoelastic effect, which arises from the temperature-dependence of the materials' mechanical properties, must be considered to obtain meaningful heat dissipation data. However, the calculated thermoelastic effect appears to be too pronounced when compared to the deformation work. It was found that with the present thermoelastic theory, the dissipated heat exceeds the deformation work. The cause of this observation is not yet clear, but an influence of viscoelasticity in the determination of elastic constants and the effect of microstructural changes during deformation may play a role.

Acknowledgements

The research work of this paper was performed at the Polymer Competence Center Leoben GmbH (PCCL, Austria) within the framework of the Kplus- and COMET-programs of the Austrian Ministry of Traffic, Innovation and Technology with contributions by the University of Leoben and Borealis Polyolefine GmbH. The PCCL is funded by the Austrian Government and the State Governments of Styria and Upper Austria.

References

[1] S. V. Shenogin, G. W. H. Höhne, E. F. Oleinik, Thermodynamics of the pre-yield deformation behavior of glassy polymers: measurements with new deformation calorimeter, Thermochim. Acta 391 (1-2) (2002) 13 – 23.

[2] A. Tregub, V. Privalko, Thermal calorimetry of polymer simple shear deformation and its applications, Thermochim. Acta 247 (1) (1994) 35–51.

[3] B. A. Schrauwen, R. P. Janssen, L. E. Govaert, H. E. Meijer, Intrinsic deformation behavior of semicrystalline polymers, Macromolecules 37 (2004) 6069–6078.

[4] A. Galeski, Strength and toughness of crystalline polymer systems, Prog. Polym. Sci. 28 (2003) 1643–1699.

[5] K. Friedrich, Crazes and shear bands in semi-crystalline thermoplastics, Adv. Polym. Sci. 52-53 (1983) 225–274.

[6] I. Narisawa, M. Ishikawa, Crazing in semi-crystalline thermoplastics, Adv. Polym. Sci. 91-92 (1990) 353–391.

[7] M. Jerabek, Z. Major, K. Renner, J. Móczó, B. Pukánszky, R. W. Lang, Filler/matrix-debonding and micro-mechanisms of deformation in particulate filled pp composites under tension, Polymer 51 (9) (2010) 2040–2048.

[8] C. Marano, M. Rink, Shear yielding threshold and viscoelasticity in an amorphous glassy polymer: a study on a styrene-acrylonitrile polymer, Polymer 42 (2001) 2113–2119.
[9] L. A. Fasce, V. Pettarin, C. Marano, M. Rink, P. M. Frontini, Biaxial yielding of polypropylene/elastomeric polyolefin blends: Effect of elastomer content and thermal annealing, Polym. Eng. Sci. 48 (7) (2009) 1414–1423.
[10] D. Tscharnuter, M. Jerabek, Z. Major, G. Pinter, Irreversible deformation of isotactic polypropylene in the pre-yield regime, submitted to Polymer.
[11] E. Oleinik, O. Salamatina, S. Rudnev, S. Shenogin, A new approach to treating plastic strain in glassy polymers, Polym. Sci. 35 (11) (1993) 1532–1558.
[12] V. Volodin, A. Slutsker, Specific features of the thermoelastic effect in polymers, Thermochim. Acta 247 (1994) 121–128.
[13] G. Pitarresi, E. Patterson, A review of the general theory of thermoelastic stress analysis, J. Strain Anal. 38 (5) (2003) 405–417.
[14] A. Wong, R. Jones, J. Sparrow, Thermoelastic constant or thermoelastic parameter?, J. Phys. Chem. Solids 48 (8) (1987) 749–753.
[15] A. Wong, J. Sparrow, S. Dunn, On the revised theory of the thermoelastic effect, J. Phys. Chem. Solids 49 (4) (1988) 395–400.
[16] A. Tregub, V. Privalko, H. Kilian, G. Marom, The thermoelastic behaviour of semicrystalline and of glassy poly(ether-ether-ketone), Appl. Compos. Mater. 1 (2) (1994) 167–176.
[17] S. Moreau, A. Chrysochoos, J.-M. Muracciole, B. Wattrisse, Analysis of thermoelastic effects accompanying the deformation of pmma and pc polymers, Comptes Rendus - Mecanique 333 (8) (2005) 648–653.
[18] A. Machin, J. Sparrow, M. Stimson, Mean stress dependence of the thermoelastic constant, Strain 23 (1987) 27–30.
[19] M. Jerabek, Z. Major, R. W. Lang, Uniaxial compression testing of polymeric materials, Polym. Test. 29 (3) (2010) 302–309.
[20] M. Cook, E. Larke, Resistance of copper and copper alloys to homogeneous deformation in compression, J. Inst. Metals 71 (1945) 371–390.
[21] C. Dudescu, J. Naumann, M. Stockmann, S. Nebel, Characterisation of thermal expansion coefficient of anisotropic materials by electronic speckle pattern interferometry, Strain 42 (2006) 197–205.
[22] S. Baker, I. Matthews, Lucas-kanade 20 years on: A unifying framework, Int. J. Comput. Vision 56 (3) (2004) 221–255.
[23] J.-W. Housmans, M. Gahleitner, G. W. Peters, H. E. Meijer, Structure-property relations in molded, nucleated isotactic polypropylene, Polymer 50 (2009) 2304–2319.
[24] VDI-Gesellschaft Verfahrenstechnik und Chemieingenieurwesen (Hrsg.), VDI-Wärmeatlas, 10th Edition, Springer, 2006.
[25] J. Crank, P. Nicolson, A practical method for numerical evaluation of solutions of partial differential equations of the heat-conduction type, Adv. Comput. Math. 6 (1996) 207–226.
[26] W. H. Press, S. A. Teukolsky, W. T. Vetterling, B. P. Flannery, Numerical Recipes The Art of Scientific Computing, 3rd Edition, Cambridge University Press, 2007.

Irreversible Deformation of Isotactic Polypropylene in the Pre-Yield Regime

D. Tscharnuter[a,*], M. Jerabek[b], Z. Major[c], G. Pinter[d]

[a]*Polymer Competence Center Leoben GmbH, Roseggerstrasse 12, 8700 Leoben, Austria*
[b]*Borealis Polyolefine GmbH, St. Peter Strasse 25, 4021 Linz, Austria*
[c]*Institute of Polymer Product Engineering, Johannes Kepler University Linz, Altenbergerstrasse 69, 4021 Linz, Austria*
[d]*Institute of Materials Science and Testing of Plastics, Otto-Glöckel-Strasse 2, 8700 Leoben, Austria*

Abstract

In the modeling of the mechanical response of a polymer over a large strain range, the nonlinear viscoelastic and viscoplastic behavior must be considered. For many polymers, nonlinear behavior is observed at low loads, e.g. by a stress-dependence of the creep compliance for stresses above 2 MPa in case of the polypropylene used in this study. Additionally, plastic deformation has been observed at strains below the yield point for several polymers. In this study, the irreversible deformation by cavitation and shear yielding of polypropylene are characterized in the pre-yield regime in uniaxial tensile tests using digital image correlation. The recovery of strain after unloading at a prescribed strain level is measured and used to identify the evolution of the plastic strain during uniaxial tension. An experimental technique for simultaneous determination of the true stress-true strain curve and the degree of stress whitening, which relates to the amount of cavitation, is introduced and the initiation of cavitation is compared to the plastic deformation detected in strain recovery at various temperatures.

Keywords: strain recovery, viscoplasticity, stress whitening, polypropylene

1. Introduction

The deformation mechanisms of polypropylene were investigated in several studies [1–5]. A sequence of deformation events leads to different forms of plastic deformation, which are not only of scientific interest, but also of engineering relevance. The initial stages of tensile deformation are governed by the straining of molecular chains of the interlamellar amorphous phase, interlamellar shear, rotation of lamellae stacks and lamellae separation [2]. The plastic deformation at later stages is a competition between plastic deformation of the interlamellar amorphous phase and the crystalline phase. This competition is influenced by experimental conditions such as strain rate [6] or temperature [7]. Above T_g, the initial deformation is located in the amorphous regions because of their low modulus. The tensile deformation of a spherulite is inhomogeneous because the amorphous regions and the radially oriented lamellae have different angles to the direction of the tensile force, depending on their location in either polar, diagonal or equatorial regions of the spherulite. The main mode of plastic deformation of the amorphous components is believed to be interlamellar sliding, or lamellae separation in the equatorial regions, where the lamellae are orientied perpendicularly to the drawing direction. The amorphous phase between lamellae is linked to the lamellae by tie molecules and chain entanglements. The mobility of these amorphous chains may vary locally and is different from the mobility of the amorphous bulk material, which is manifested e.g. by physical aging above T_g [8]. The constraints imposed by the lamellae imply that only a limited amount of deformation can be accomodated by the interlamellar amorphous phase [9]. When this limit is reached, further deformation can proceed either by cavitation of the amorphous phase or by plastic deformation of crystals. In the latter case, stretched tie chains can pull crystalline material from the lamellae [7] or cause crystal slips. Cavitation is apparent by stress whitening: Sufficiently large voids act as scattering sites for incident light, which makes the initially transparent material opaque. The degree of opacity is linked to the density of voids, hence it increases with tension. Which of the two mechanisms occurs is influenced by temperature [10]. Polypropylene shows a transition in the temperature region around 80°C, which is associated with mobility in the crystalline phase. When drawing is performed at elevated temperatures approaching this transition region, a change of the dominating deformation from cavitation towards shear yielding can be expected.

These irreversible deformations begin at strains below the yield strain. Knowledge of the irreversible deformation modes and load limits for reservible behavior is therefore essential for proper modeling of mechanical behavior and for optimizing polymer component designs. In this paper, two methods are applied to study the irreversible deformation of polypropylene in the pre-yield regime. The recovery

*Corresponding author
Email address: tscharnuter@pccl.at (D. Tscharnuter)

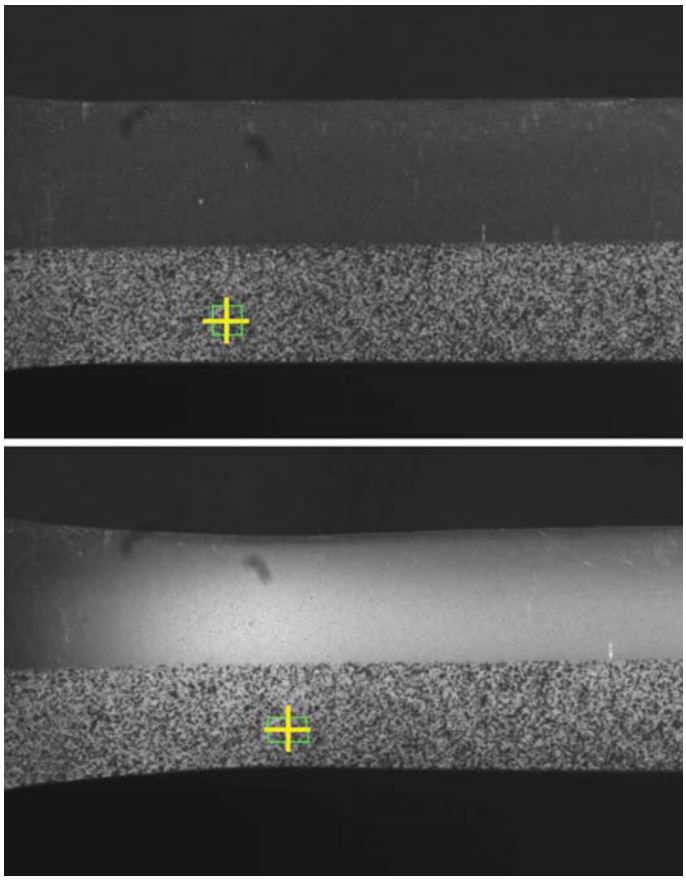

Figure 1: Semi-sprayed tensile specimen in unstrained (top) and strained (bottom) state. Pictures were taken at true strains of 0 and 0.305 during a test performed at 23°C.

of the reversible elastic and viscoelastic strain components after loading is measured to find the amount of plastic deformation. The strain measurements are performed using a digital image correlation system, which allows for a quite precise determination of the plastic strain. To analyze the deformation mode, specimens were prepared for a simultaneous measurement of the stress whitening and the 2D strain field, also using the digital image correlation system. Due to the viscoelastic nature of the polymer, the deformation depends not only on the applied stress, but on the entire stress history [11, 12] and the loading mode [12]. Therefore, strain recovery tests and stress whitening measurements were performed under the same experimental conditions to enable a comparison of the results.

2. Experimental

2.1. Material

The investigated material is a development grade polypropylene homopolymer from Borealis Polyolefine GmbH. Injection molded specimens according to ISO 3176 type B were manufactured by Borealis Polyolefine GmbH (Linz, A). This material was previously investigated in monotonic tension [13], long-term compressive [14] and tensile relaxation [15, 16].

2.2. Tensile strain recovery tests

The strain recovery tests were performed on a screw-driven electro-mechanical universal test system (type Zwick Z250; Zwick-Roell, Ulm, Germany) in uniaxial tension with a constant engineering strain rate of $8.7 \cdot 10^{-3}$ s^{-1}. The system is equipped with a temperature chamber to maintain the desired test temperature within ±0.2°C. A waiting period of 30 minutes after insertion of the specimen into the specimen grips was chosen for the temperature chamber to stabilize after the disturbance of opening the door and for the specimen to achieve a uniform temperature.

Full-field strain was measured using a digital image correlation (DIC) system (ARAMIS; GOM mbH, Germany). This system is discussed elsewhere [17]. For this study, the strain measurement was performed in 2D mode and the inherent scatter in the strain with this set-up was about 0.02% as determined by the standard deviation of a series of images taken of an unstrained specimen.

To measure the strain recovery from various strain levels, specimens were held at zero force for 100s before loading to a prescribed engineering strain, which is subsequently maintained in a stress relaxation mode for one or two seconds, which is the time it takes for the operator to unload the specimen by releasing a pneumatic grip. Thereby only the moving grip is released to ensure that the specimen remains in its initial position also during the strain recovery, which can then be measured with DIC to benefit from the high strain resolution also during the recovery phase. Note that for homogeneous deformations, averaging of the engineering strain of all subsets of the DIC is performed to improve accuracy. The recovery of the elastic and viscoelastic strain component after unloading is measured and the plastic strain component is identified as the strain in the steady state.

True longitudinal strain $\epsilon_{t,l}$ and transverse strain $\epsilon_{t,t}$ are calculated from the engineering strains by

$$\epsilon_{t,l} = \ln(\epsilon_{n,l} + 1) \tag{1}$$

and

$$\epsilon_{t,t} = \ln(\epsilon_{n,t} + 1) \tag{2}$$

The true stress is defined as

$$\sigma_t = \frac{F}{A_0} \frac{1}{(1 + \epsilon_{n,t})^2} \tag{3}$$

where F is the force and A_0 the cross-sectional area of the unstrained specimens.

The strain recovery is measured for up to 24 hours at a controlled test temperature. For amorphous polymers, it was found that the recovery can by accelerated by raising the temperature [18]. To avoid an alteration of the recovery from loading at room temperature due to possible changes of the crystalline structure [19], an accelerated recovery at higher temperatures was not attempted in this work. The tests performed at 40°C, 60°C and 80°C showed that the recovery is faster than at room temperature, but physical aging was observed. The origin of this aging was not investigated, but the temperature range where it occured suggests that it relates to changes in the lamellar structure.

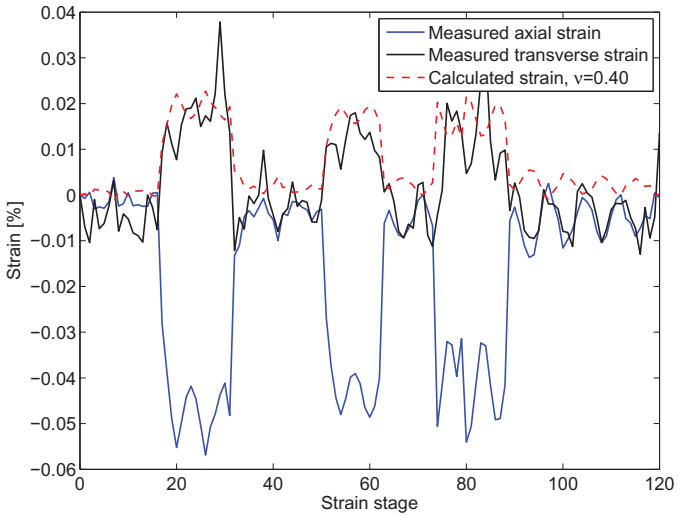

Figure 2: Measured transverse and axial strain and calculated transverse strain during closing and opening of the upper pneumatic grip.

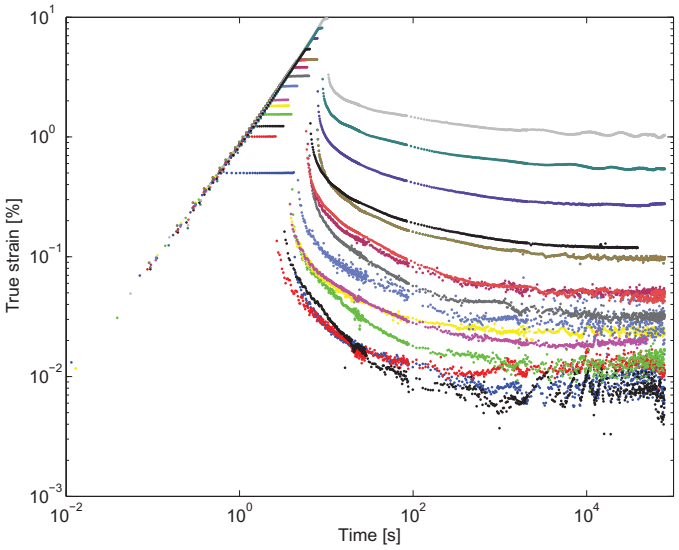

Figure 3: Strain recovery of polypropylene at room temperature from nominal strains between 0.5% and 8%.

2.3. Quantitative determination of stress whitening

Using the same tensile test setup described above, the stress whitening was measured during stretching of the specimen. A board sprayed with graphite spray was placed behind the specimen to serve as a non-specular dark background. Only one half of each specimen was coated with the random pattern for DIC to enable a simultaneous monitoring of the strain field and the degree of whitening. Exemplary pictures of an unstrained and strained specimen are shown in figure 1. Due to limitations on the illumination angle imposed by the rather narrow window of the temperature chamber, it was not possible to achieve a uniform level of illumination over the entire specimen. The specimens were placed in the grips with the less oriented end at the bottom grip to ensure that the necking zone is always in the same position. The lights were then adjusted to provide a uniform illumination of this zone of maximum deformation, which is used for the calculation of the true strain and the degree of whitening. Care must be taken to ensure sufficient illumination for the DIC while avoiding specular reflections on the uncoated part of the specimen.

The whitening is quantified by the digital data of the DIC images as an integer number for the gray level ranging from 0 to 255. The gray level value is taken as the average value of a typically 30x30 pixels section in the zone of maximum deformation, which is indicated by the crosshairs in figure 1. The crosshairs are placed in the images by the DIC software and are subsequently tracked by a motion tracking algorithm [20] for automated gray level evaluation of each image. For further evaluation, gray levels are referenced to the value at zero strain.

SAXS measurements were performed using a Bruker NanoStar (Bruker AXS, Karlsruhe, Germany). This system was equipped with a two-dimensional X-ray detector. The distance between the sample and the detector was 64 cm. A wavelength of 0.154 nm (Cu Kα) was used. The samples were measured in transmission and under vacuum with angles between 0.2° and 5°.

3. Results

3.1. Strain recovery

In 2D mode, the strain measurement is very sensitive to out-of-plane motion, hence a precise alignment of the specimen grips is needed. The alignment of the grips and the influence of the compressive stress applied upon closing were investigated by measuring the transverse and axial strain during a sequence of three times closing and opening of the upper grip. The transverse strain was also calculated from the axial strain using a Poisson's ratio value of 0.40, which is the value found in stress relaxation at short times [16]. Given the small strains, the agreement between the measured and calculated transverse strain (figure 2) is good enough to conclude that opening or closing the grip does not introduce an error in the 2D strain measurement. The lateral contraction itself is an out-of-plane

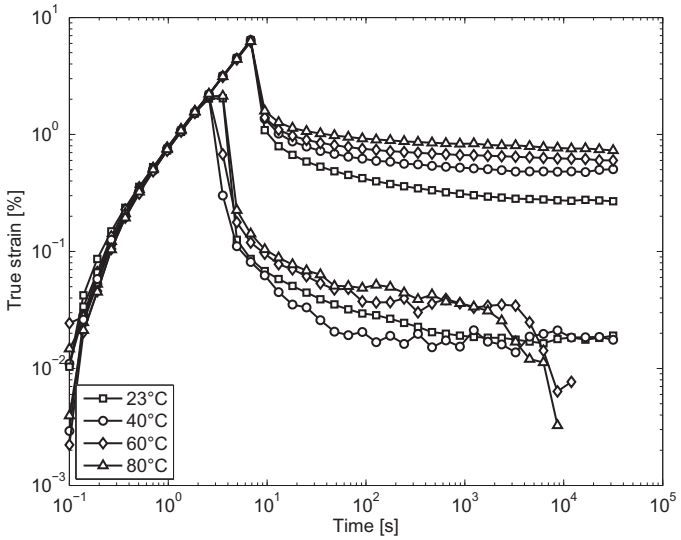

Figure 4: Strain recovery of polypropylene at 23°C, 40°C, 60°C and 80°C from nominal strains of 2% and 6%.

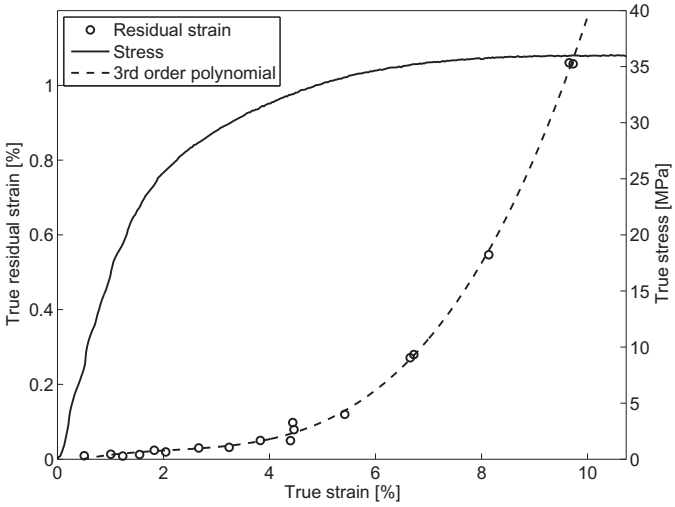

Figure 5: Residual strain and true stress-true strain curve for tests at 23°C.

displacement that leads to a systematic error [21], but the displacement along the 4mm thickness is very small compared to the roughly 500mm distance between specimen and camera.

Recovery tests were carried out from nominal strains between 0.5% and 8% at 23°C, 40°C, 60°C and 80°C. Due to the excessive need of liquid nitrogen for cooling, no tests were conducted below room temperature. The strain recovery at room temperature is shown in figure 3 and a comparison of the results at all temperatures for two selected strains is given in figure 4. It is seen that the major part of the strain recovery at room temperature is completed in the first three decades of recovery time. Only minor to no recovery occurs in the fourth decade, after roughly 3 hours. The strain measured during this decade is averaged to define the residual plastic strain. In figure 5, this residual strain is depicted over the peak true strain together with the true stress-true strain curve. Residual strain is already detected below 4% strain, which is less than half the yield strain (engineering strain at maximum engineering stress).

Repeated recovery tests were performed from 4%, 6% and 8% nominal strain to illustrate the effect of the irreversible deformation. In these tests, a specimen was subjected to a second recovery test after completing the first test. Each specimen had acquired a residual strain during the first test (figure 6). If no further change of the strain distribution on the specimen occurs during the second loading, the repeated deformation as prescribed by the crosshead displacement leads to a final strain that is equal to the sum of the final strain from the first loading and the thereby acquired residual strain. For the testing with 8% nominal strain, the maximum strain measured on the inhomogeneously deformed specimen was 9.7% and the residual strain was 1%, but the observed maximum strain during the second loading was 11.1%. The difference of 0.4% shows that the localization of the deformation increased. The increase in residual strain was approximately 0.8%. A comparison of the stress-strain curves of first and second loading (figure 7) shows softening of the material in all cases. Note that in figure 7, the residual strain from the first test was subtracted from the strain measured during the second loading. The decrease in stress at a given strain in the test at 4% peak nominal strain is small but nevertheless indicates irreversible deformation during the first loading. At the higher strains of 6% and 8%, a more pronounced weakening of the material is observed.

The effect of temperature on the viscoplasticity and strain recovery has been studied by testing at temperatures above room temperature. The drawing and recovery

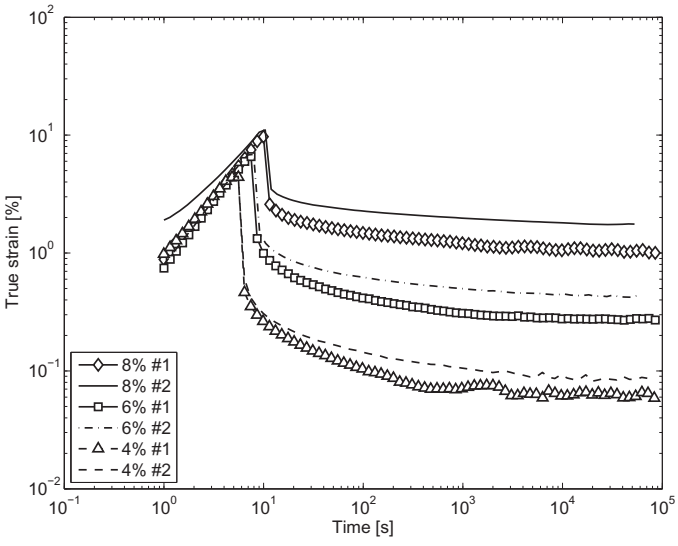

Figure 6: Strain recovery for repeated recovery tests at 4%, 6% and 8% nominal strain.

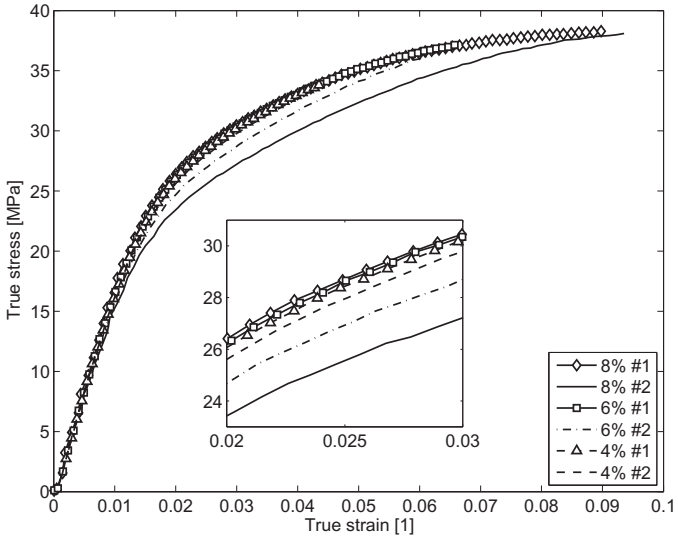

Figure 7: True stress-true strain curves for repeated recovery tests at 4%, 6% and 8% nominal strain. The small subfigure shows a magnified portion of the data for visibility of the 4% curve. The residual strain after the first loading has been subtracted from the strain measured during the second loading for this plot.

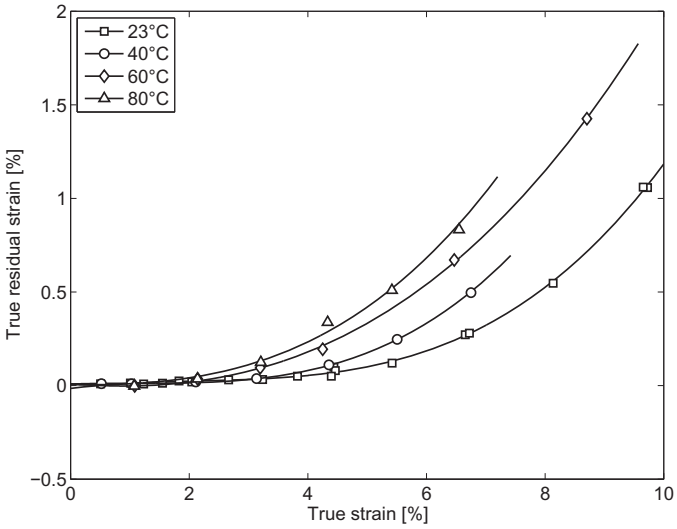

Figure 8: Residual strain for test temperatures of 23°C, 40°C, 60°C and 80°C.

were performed and measured at the same temperature. A physical aging effect was observed while testing at 60°C and 80°C. After a certain recovery time, shrinkage of the specimen occured. The effect is most distinct during recovery from lower strains, see figure 4. During recovery from higher strains, a slight change of curvature in the recovery curve is observed, which likely indicates the same shrinkage that is clearly visible in the lower strains. The shrinkage sets in before a fully steady recovery state is achieved. A detailed investigation of the aging effects in this context is beyond the scope of this paper, so for the present work, the residual strain is approximated by the strain achieved before the appearance of aging in the recovery curves. This approximation implies only a small error because the major part of the recovery occurs prior to the shrinking and only little recovery takes place in the time range where the aging effect is observed. The thus defined residual strains are shown in figure 8. Polynomials were fitted to the data to determine the onset of plastic deformation as the strain at which the plastic strain exceeds the arbitrarily chosen value of 0.05%. Based on this criterion, the limit of reversible loading under the present experimental conditions is 3.9% at 23°C and decreases to 2.2% at 80°C.

3.2. Stress whitening

Several tests were conducted at temperatures ranging from −20°C to 80°C as previously described and true stress and true strain were determined according to equations (3) and (1). The true stress and true strain curves are shown in figure 9. Tests were conducted until fracture (−20°C) or beyond the maximum engineering stress.

The gray level in the zone of maximum deformation was determined for each test. Figure 10 shows the true stress-true strain curve and the gray level vs. true strain from a test conducted at room temperature and at a strain rate of $8.7 \cdot 10^{-3}$ s^{-1}. The gray level is nearly constant for true strains up to 5%. At higher strains, the gray level strongly increases. As is evident from the cross-section pictures taken from specimens pulled to various strain levels (figure 11), the whitening zone starts at the core of the specimen and expands towards the skin layer with progressing strain. This localization of the stress whitening is due to the inhomogeneous morphology of the injection molded specimens [22], in which a spherulitic crystall structure prone to cavitation is present in the core. With progressing deformation, the inner zone becomes whiter with strain, which suggests an increase in void density. Both effects contribute to the gray level increase at intermediate strains. Note that the pictures presented in figure 11 were taken from unloaded specimens and hence only show a lower bound for the size of the cavitation zone because smaller voids may close due to the surface tension when the stress is removed. The decrease in slope of the gray level curve at the highest strains may be due to increased fibrillation of the material between the voids and growth of existing voids, with only little additional voids being created.

The definition of the onset from the gray level curve is somewhat arbitrary. Possible definitions include the intersection point of linear fits to distinct regions or the crossing of threshold levels. Yamaguchi and Nitta [23] conducted an analysis based on the light transmittance and used the point of maximum change of transmitted intensity as characteristic whitening point. This definition does not directly relate to the onset of whitening. In the present case, the onset of cavitation is assigned to the strain at which the gray level curve departs from its initial straight line.

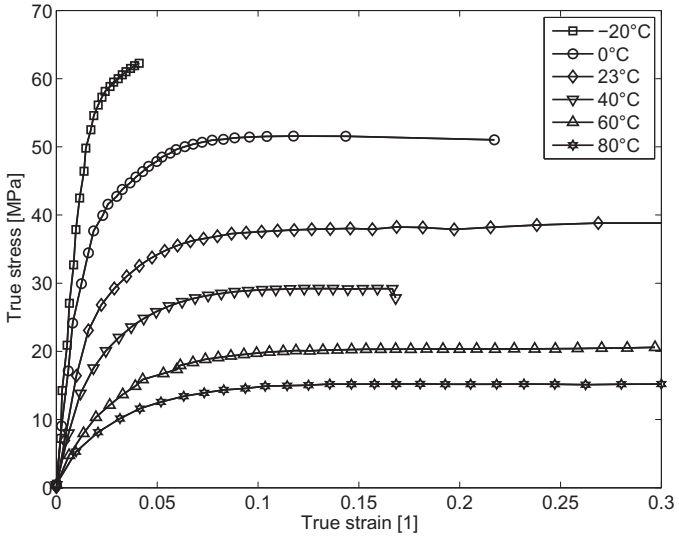

Figure 9: True stress and true strain curves for temperatures above and below T_g. For clarity of the plots markers are only shown for a subset of the data of each test.

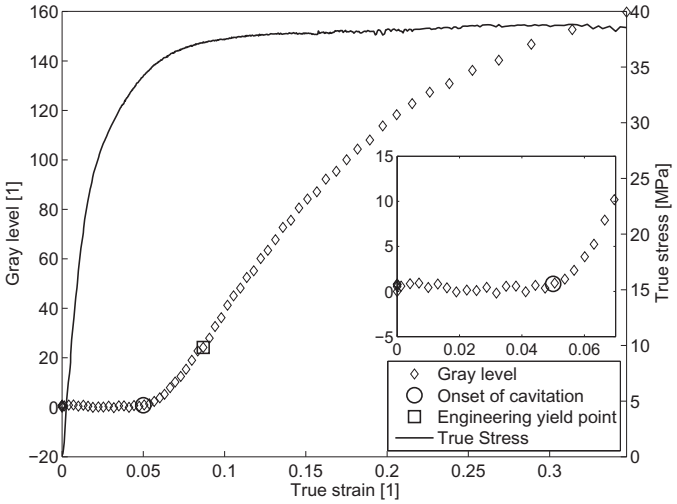

Figure 10: True stress-true strain curve and the gray level vs. true strain at room temperature and a strain rate of $8.7 \cdot 10^{-3}$. The strain at the onset of cavitation (circle) and the engineering yield strain (square) are indicated. For clarity of the plots markers are only shown for a subset of the data of each test. The detail figure shows the pre-yield regime with the sharp increase of gray level.

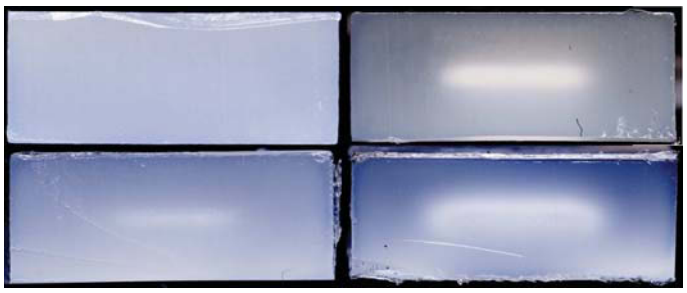

Figure 11: Cross-section pictures of specimens drawn to various nominal strains. Top-left: 0%, bottom-left: 4%, top-right: 6%, bottom-right: 8%.

For the room temperature test, the corresponding strain is around 5% and is indicated by the circular marker in figure 10. The yield strain is 8.7% (square marker). Thus, cavitation occurs well before the yield point. The achievable sensitivity of this technique is believed to depend on the transparency of the unstrained material and could possibly be improved by ways of illumination other than the frontal illumination used for the simultaneous DIC measurement. Furthermore, it must be considered that the strain at cavitation may be somewhat lower than indicated by the degree of stress whitening, because cavities must reach a proper size to cause the intense light scattering. SAXS measurements are sensitive to nano-size cavities and were therefore performed on specimens tested at 23°C and 60°C and selected strains ex-situ after three months of recovery at room temperature (figure 12). The SAXS results of specimens drawn to 3% at 23°C were quasi identical to the results on an untested specimen, showing no cavities. For a detailed discussion of SAXS patterns at various strains the reader is referred to reference [2]. The cross-section of the specimen elongated to 4% strain (figure 11) reveals a small zone that already shows weak whitening. This stress whitening is below the sensitivity of the gray level analysis, which detected whitening at 5% strain. An initial slow increase of transparency was observed at 60°C and 80°C. At 60°C, the transparency started to increase at a strain of 7%. The SAXS pattern showed spherical cavities after drawing to 8% at 60°C, but none after drawing to 6%. Hence, bearing in mind an overestimation of the onset of cavitation by roughly 1%, presumably depending on the initial transparency, the stress whitening measurement is a useful technique that can be easily applied in-situ using standard digital cameras. In a recent work [24], it was reported that no cavitation was observed above 70°C in the drawing of 1mm thick polypropylene films. The differing observations could result from the different specimen geometry and strain rate used, or differences in molecular parameters, such as entanglement density or number of tie molecules, and morphological differences, which have an effect on the deformation [7].

At all investigated temperatures, the strain recovery data showed that irreversible deformation occurs close to or prior to cavitation by a varying amount of strain, which increases with temperature. The strain at cavitation is temperature dependent, as is the yield strain. Figure 13 shows the strain at yield, onset of cavitation and beginning of irreversible deformation for various temperatures. For the test at −20°C, the fracture strain was used for reference because fracture occured before a yield point appeared. It was found that the cavitational strain increases stronger with temperature than the classical yield strain. Below the glass transition temperature, crazes appear and grow with little regard to the local crystalline structure [4]. Above T_g, craze-like features can form on spherulite boundaries [2] and cavitation can occur in the

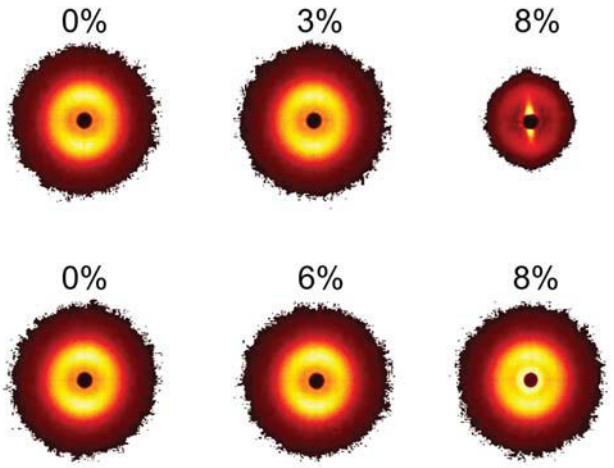

Figure 12: SAXS patterns of specimens drawn to strain up to 8% nominal strain at 23°C and 60°C. The reference specimen for 60°C was subjected to the same thermal history as the tested specimens to account for effects of physical aging. The drawing direction is vertical in the pictures.

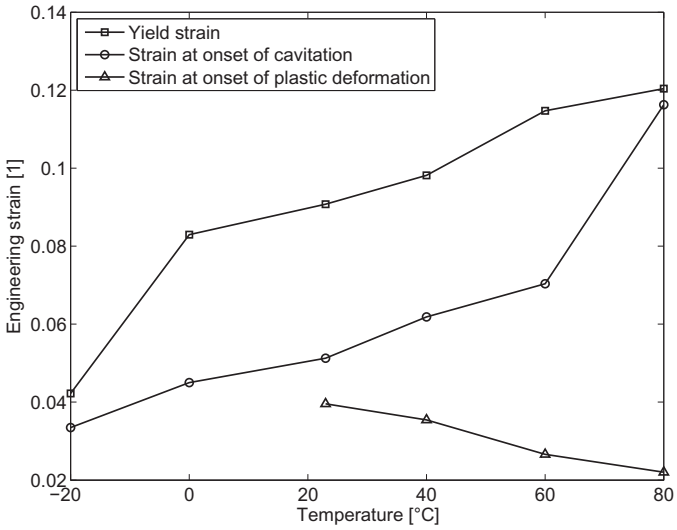

Figure 13: Yield strain and strain at the onset of cavitation and irreversible deformation at various temperatures. For comparability with the engineering yield strain, the latter strains have been converted to engineering strains for this figure.

interlamellar amorphous phase. As already described, the latter depends on a competition between the deformation of the interlamellar amorphous phase and the crystal lamellae. As the test temperature is increased, the cavitational deformation is reduced and stress whitening occurs weaker and at higher strains, e.g. close to the yield strain at 80°C. In contrast, the limit of reversible deformation decreases with temperature. It has been observed that the amount of recoverable strain saturates above a certain strain level due to substantial stretching and orientation of the amorphous chains, leading to major deformation of the crystalline phase. This strain level is of the order of 25% for HDPE [25] and of similar magnitude for PP [2]. In the pre-yield regime, the amount of recoverable strain is much larger than the plastic strain and increases with the applied strain, implying that most of the deformation occurs in the amorphous zones. Thus, the observed initiation of plasticity between 2% and 4%, depending on temperature, may indicate that at these strain levels, a notable fraction of the tie molecules becomes taut and transfers stress on the lamellae. Deformation may then proceed either by cavitation at sufficiently low temperatures, or by slip processes in the lamellae at higher temperatures, which allows further stretching of the remaining interlamellar chains. Due to the length distribution of tie molecules, this is a gradual process leading to a gradually increasing amount of plastic deformation.

4. Conclusion

A tensile test setup with strain field measurement by 2D digital image correlation was used to characterize plastic deformation of polypropylene in uniaxial tension. Two methods, strain recovery and stress whitening analysis, were used to determine reversibility limits and to detect cavitation.

Strain recovery after loading to various strain levels showed that plastic deformation occurs well before the yield point at all investigated temperatures between 23°C and 80°C. The reversible limit was found at about 4% strain at room temperature, which is less then half the yield strain. The strain limit decreases with increasing temperature, becoming only 2.2% at 80°C.

The degree of stress whitening was quantified by the gray levels taken from the images recorded by the digital image correlation system. This allows for a simultaneous measurement of the strain field and the stress whitening. The stress whitening is due to cavitation of the amorphous phase of the polymer. The initiation of cavitation was determined from the gray level vs. true strain curves. Cavitation was detected at all investigated temperatures before the yield strain was reached. With increasing temperature, the strain for cavitation increases due to the softening of the crystalline phase. On the other hand, it was found that the residual strain after drawing to a certain strain level increases with temperature. It was thus concluded that the plastic deformation of the crystal lamellae contributes to the deformation at the elevated temperatures.

Acknowledgements

The authors are indebted to Michael Feuchter, who performed the SAXS measurements of the specimens after recovery testing. The research work of this paper was performed at the Polymer Competence Center Leoben GmbH (PCCL, Austria) within the framework of the Kplus- and COMET-programs of the Austrian Ministry of Traffic, Innovation and Technology with contributions by the Uni-

versity of Leoben and Borealis Polyolefine GmbH. The PCCL is funded by the Austrian Government and the State Governments of Styria and Upper Austria.

References

[1] A. Galeski, Strength and toughness of crystalline polymer systems, Prog. Polym. Sci. 28 (2003) 1643–1699.
[2] A. Pawlak, A. Galeski, Cavitation during tensile deformation of polypropylene, Macromolecules 41 (8) (2008) 2839–2851.
[3] A. Pawlak, A. Galeski, Plastic deformation of crystalline polymers: The role of cavitation and crystal plasticity, Macromolecules 38 (23) (2005) 9688–9697.
[4] K. Friedrich, Crazes and shear bands in semi-crystalline thermoplastics, Adv. Polym. Sci. 52-53 (1983) 225–274.
[5] I. Narisawa, M. Ishikawa, Crazing in semi-crystalline thermoplastics, Adv. Polym. Sci. 91-92 (1990) 353–391.
[6] R. Gensler, C. Plummer, C. Grein, H.-H. Kausch, Influence of the loading rate on the fracture resistance of ipp and impact modified ipp, Polymer 41 (2000) 3809–3819.
[7] H.-H. Kausch, R. Gensler, C. Grein, C. Plummer, P. Scaramuzzino, Crazing in semicrystalline thermoplastics, J. Macromol. Sci., Part B: Phys. 38 (1999) 803–815.
[8] L. Struik, The mechanical and physical aging of semicrystalline polymers, Polymer 28 (1987) 1521–1533.
[9] Z. Bartczak, A. Galeski, A. Argon, R. Cohen, One the plastic deformation of the amorphous component in semicrystalline polymers, Polymer 37 (11) (1996) 2113–2123.
[10] E. Oleinik, Plasticity of semicrystalline flexible-chain polymers at the microscopic and mesoscopic levels, Polym. Sci. - Ser. C 45 (1) (2003) 17–117.
[11] C. Marano, M. Rink, Shear yielding threshold and viscoelasticity in an amorphous glassy polymer: a study on a styrene-acrylonitrile polymer, Polymer 42 (2001) 2113–2119.
[12] L. A. Fasce, V. Pettarin, C. Marano, M. Rink, P. M. Frontini, Biaxial yielding of polypropylene/elastomeric polyolefin blends: Effect of elastomer content and thermal annealing, Polym. Eng. Sci. 48 (7) (2009) 1414–1423.
[13] M. Jerabek, Z. Major, K. Renner, J. Móczó, B. Pukánszky, R. W. Lang, Filler/matrix-debonding and micro-mechanisms of deformation in particulate filled pp composites under tension, Polymer 51 (9) (2010) 2040–2048.
[14] M. Jerabek, D. Tscharnuter, Z. Major, K. Ravi-Chandar, R. W. Lang, Relaxation behavior of neat and particulate filled polypropylene in uniaxial and multiaxial compression, Mech. Time-Depend. Mater. 14 (1) (2010) 47–68.
[15] D. Tscharnuter, M. Jerabek, Z. Major, R. W. Lang, On the determination of the relaxation modulus of pp compounds from arbitrary strain histories, Mech. Time-Depend. Mater. (2010) 1–14.
[16] D. Tscharnuter, M. Jerabek, Z. Major, R. W. Lang, Time-dependent poisson's ratio of polypropylene compounds for various strain histories, Mech. Time-Depend. Mater. (in press).
[17] M. Jerabek, Z. Major, R. W. Lang, Strain determination of polymeric materials using digital image correlation, Polym. Test. 29 (3) (2010) 407–416.
[18] R. Quinson, J. Perez, M. Rink, A. Pavan, Components of non-elastic deformation in amorphous glassy polymers, J. Mater. Sci. 31 (1996) 4387–4394.
[19] M. Gahleitner, J. Fiebig, J. Wolfschwenger, G. Dreiling, C. Paulik, Post-crystallization and physical aging of polypropylene: materials and processing effects, J. Macromol. Sci., Part B: Phys. B41 (4-6) (2002) 833–849.
[20] S. Baker, I. Matthews, Lucas-kanade 20 years on: A unifying framework, Int. J. Comput. Vision 56 (3) (2004) 221–255.
[21] E. Parsons, M. Boyce, D. Parks, An experimental investigation of the large-strain tensile behavior of neat and rubber-toughened polycarbonate, Polymer 45 (2004) 2665–2684.
[22] J.-W. Housmans, M. Gahleitner, G. W. Peters, H. E. Meijer, Structure-property relations in molded, nucleated isotactic polypropylene, Polymer 50 (2009) 2304–2319.
[23] M. Yamaguchi, K.-H. Nitta, Optical and acoustical investigation for plastic deformation of isotactic polypropylene/ethylene-1-hexene copolymer blends, Polym. Eng. Sci. 39 (5) (1999) 833–840.
[24] A. Pawlak, A. Galeski, Cavitation and morphological changes in polypropylene deformed at elevated temperatures, J. Polym. Sci., Part B: Polym. Phys. 48 (2010) 1271–1280.
[25] L. Lin, A. Argon, Structure and plastic deformation of polyethylene, J. Mater. Sci. 29 (1994) 294–323.

Uniaxial nonlinear viscoelastic viscoplastic modeling of polypropylene

Daniel Tscharnuter · Michael Jerabek · Zoltan Major · Gerald Pinter

Abstract This paper presents the application of a Schapery-type nonlinear viscoelastic viscoplastic model to strain recovery data of polypropylene. In a previous study, the recovery of strain after monotonic uniaxial tensile loading was measured to gather information on the viscoelasticity and viscoplasticity. The viscoplastic part of the tensile deformation is used to determine parameters of a viscoplastic model. The nonlinear viscoelastic part is determined using an iterative procedure to solve the one-dimensional Schapery model equation without assuming a specific load history. The model parameters are identified from the strain recovery data and also applied to stress relaxation data.

Keywords nonlinear viscoelasticity, viscoplasticity, Schapery model

1 Introduction

The mechanical behavior of polymers depends on time, stress state and other influences such as temperature or moisture. In mechanical testing, nonlinear behavior can be observed at strains below 1%, which limits the applicability of the theory of linear viscoelasticity. In addition to the nonlinear viscoelastic deformation, load histories can activate irreversible deformation mechanisms. As these deformations depend not only on the applied stress or strain levels, but on the entire load history, they are referred to as viscoplasticity.

Several approaches to the modeling of nonlinear viscoelasticity for a variety of problems exist in the literature. A popular type of model is the Schapery nonlinear viscoelastic model (Schapery, 1969). This model can be built to ensure that it exhibits linear viscoelastic behavior at low stresses and its integral formulation is similar in structure to the Boltzmann integral of linear viscoelasticity. It has been applied to several materials, often to model creep behavior, e.g. by Lai & Bakker (1995a); Nordin & Varna (2006). The assumption of instantaneous loading is frequently used because it allows for a rather uncomplicated determination of the material functions. However, significant error can be introduced by this simplification (Sorvari *et al.*, 2006). With the computational power that is available to present day scientists, it is no longer necessary to use the step loading assumption. Methods to solve the Schapery equation were developed e.g. for FE implementation by Henriksen (1984); Lai & Bakker (1996); Muliana & Haj-Ali (2004) and Crochon *et al.* (2010). These methods are not restricted to a specific load history.

D. Tscharnuter
Polymer Competence Center Leoben GmbH, Roseggerstrasse 12, 8700 Leoben, Austria
E-mail: tscharnuter@pccl.at

M. Jerabek
Borealis Polyolefine GmbH, St. Peter Strasse 25, 4021 Linz, Austria

Z. Major
Institute of Polymer Product Engineering, Johannes Kepler University Linz, Altenbergerstrasse 69, 4021 Linz, Austria

G. Pinter
Institute of Materials Science and Testing of Plastics, Otto-Glöckel-Strasse 2, 8700 Leoben, Austria

In a previous work by the authors, the strain recovery of polypropylene from uniaxial monotonic tensile loading was investigated and the viscoplastic strains were determined. The aim of this paper is to discuss the aspects of using these data to define a Schapery nonlinear viscoelastic viscoplastic model. The iterative scheme introduced by Muliana & Haj-Ali (2004) is used to calculate the strain response of the strain recovery load history and optimization is used to find the model parameters.

2 Experimental

The investigated material is a development grade polypropylene homopolymer. Injection molded specimens according to ISO 3176 type B were manufactured by Borealis Polyolefine GmbH (Linz, A). This material was previously investigated in monotonic compression (Jerabek *et al.*, 2010b) and tension (Jerabek *et al.*, 2010a), long-term compressive (Jerabek *et al.*, 2010c) and tensile relaxation (Tscharnuter *et al.*, 2010b,c). The strain recovery data used for the modeling in this work is presented in detail elsewhere (Tscharnuter *et al.*, 2010a).

The tests were performed on a screw-driven electro-mechanical universal test system (type Zwick Z250; Zwick-Roell, Ulm, Germany) in uniaxial tension with a constant engineering strain rate of $8.7 \cdot 10^{-3}$ s^{-1}. The system is equipped with a temperature chamber to maintain the desired test temperature of 23°C within ±0.2°C. A waiting period of 30 minutes after insertion of the specimen into the specimen grips was chosen for the temperature chamber to stabilize after the disturbance of opening the door and for the specimen to achieve a uniform temperature.

Full-field strain was measured using the digital image correlation (DIC) system ARAMIS (GoM mbH, Braunschweig, Germany). This system is discussed by Jerabek *et al.* (2010d). For this study, the strain measurement was performed in 2D mode and the inherent scatter in the strain with this set-up was about 0.02% as determined by the standard deviation of a series of images taken of an unstrained specimen.

In the strain recovery tests, specimens are stretched to a certain engineering strain and then unloaded by releasing a specimen grip. The subsequent recovery of the elastic and viscoelastic strain component is measured and the plastic strain component is calculated. Prior to starting the test, the specimen was held at zero force for 100s before loading to the desired engineering strain, which is subsequently maintained in a stress relaxation mode for one or two seconds, which is the time it takes for the operator to unload the specimen by releasing a pneumatic grip.

True longitudinal strain $\epsilon_{t,l}$ and transverse strain $\epsilon_{t,t}$ are calculated from the engineering strains by

$$\epsilon_{t,l} = \ln(\epsilon_{n,l} + 1) \tag{1}$$

and

$$\epsilon_{t,t} = \ln(\epsilon_{n,t} + 1) \tag{2}$$

The true stress is defined as

$$\sigma_t = \frac{F}{A_0} \frac{1}{(1 + \epsilon_{n,t})^2} \tag{3}$$

where F is the force and A_0 the cross-sectional area of the unstrained specimens. The strain recovery was measured over approximately 24 hours.

3 Determination of model parameters

The strain recovery data provides a good basis for modeling for several reasons. First, for a stress-based model, the loading at constant strain rate is a complex load history which includes nonlinear behavior. Second, the stress-controlled recovery phase provides data on the time-dependence. Third, the determination of residual strain yields information on the evolution of plastic strain during the constant strain rate loading. To describe these observations, a uniaxial stress-based Schapery-type nonlinear viscoelastic viscoplastic model is used. The model equation for the axial strain is

$$\epsilon(t) = D_0 g_0 \sigma(t) + g_1 \int_0^t \Delta D(\psi(t) - \psi(\tau)) \frac{\partial}{\partial \tau} \left(g_2 \sigma(\tau)\right) d\tau + \epsilon_{\mathrm{vp}}(t) \tag{4}$$

In this equation, D_0 is the initial and ΔS the transient creep compliance and g_i are the nonlinearizing functions of the stress implemented as polynomials. The shifted time ψ is defined by

$$\psi(t) = \int_0^t \frac{1}{a_\sigma(\sigma(\tau))} d\tau \tag{5}$$

with the time-shift function a_σ. The functional form(Pasricha *et al.*, 1996; Zapas & Crissman, 1984)

$$\epsilon_{\mathrm{vp}} = C \left(\int_0^t \sigma(\tau)^M d\tau \right)^m \tag{6}$$

is assumed for the viscoplastic strain ϵ_{vp}. This form was e.g. used by Nordin & Varna (2006) to model the viscoplastic strain formed during creep. Here it is used to account for the plastic strain created during the constant strain rate loading prior to the recovery. Due to the viscoelastic nature of the polymer, the plastic strain depends not only on the applied stress, but on the entire stress history (Marano & Rink, 2001; Fasce *et al.*, 2009) and the loading mode (Fasce *et al.*, 2009). Therefore, a simple viscoplastic law as given in equation (6) is limited to a certain type of loading and a more complex law, e.g. as proposed by Lai & Bakker (1995b), is needed for a general description. Specifically for the tests of this study, the parameters are determined from the plastic strain that is created during monotonic uniaxial tension. At any given strain, the predicted plastic strain is related to the area under the time-stress curve (equation (6)). Before the recovery phase is started by releasing a specimen grip, the specimen is held at constant strain for one or two seconds. Marano & Rink (2001) studied the residual strain of styrene-acrylonitrile after stress relaxation for different relaxation periods and strain levels. They showed that the residual strain increases with the duration of the stress relaxation, but generation of residual strain was not observed until after 50 minutes of stress relaxation at 7%. For PC, Marano & Rink (2006) reported even larger times. A similar investigation of the influence of the relaxation duration could not be conducted in this work and it is therefore assumed that a few seconds of stress relaxation have no effect on the residual strain. In contrast, the plastic strain predicted during the short relaxation phase according to the above equation is of the order of the loading ramp contribution after only a few seconds. Hence, the applicability of this viscoplastic model is limited to the loading ramp and is thus only evaluated up to the maximum stress for each test. To determine the viscoplastic parameters C, M and m, equation (6) is solved by numerical integration up to each strain level and fit to the corresponding residual strains.

With the viscoplastic model determined, the remaining nonlinear viscoelastic parameters can be obtained. The nonlinearizing functions g_0, g_1, g_2 and $1/a_\sigma$ are chosen as polynomial functions of the stress and a Prony series is assumed for the compliance. The choice of the Prony series allows for an iterative solution of equation (4) (Henriksen, 1984). Different approaches in defining the iterative procedure are found in the literature (Crochon *et al.*, 2010). In this study, the equation is solved by the scheme derived by Muliana & Haj-Ali (2004). For the brief description of the method, the compact notation used by Muliana & Haj-Ali (2004) with independent variables written as superscripts is useful. The Prony series is expressed with inverse retardation times $\lambda_j = 1/\tau_j$ as

$$\Delta D^{\psi^t} = \sum_{j=1}^{N} D_n (1 - \exp(-\lambda_j \psi^t)) \tag{7}$$

and the Schapery equation is

$$\epsilon^{t_{n+1}} = g_0^{t_{n+1}} D_0 \sigma^{t_{n+1}} + g_1^{t_{n+1}} g_2^{t_{n+1}} \sum_{j=1}^{N} D_j - g_1^{t_{n+1}} \sum_{j=1}^{N} D_j q_j^{t_{n+1}} \tag{8}$$

where

$$q_j^{t_{n+1}} = \int_0^{t_{n+1}} \exp(-\lambda_j(\psi^{t_{n+1}} - \psi^\tau))\frac{\partial g_2^\tau \sigma^\tau}{\partial \tau} d\tau \tag{9}$$

The above integral is decomposed into the integral up to time step t_n and in the integral from t_n to t_{n+1} to derive the iterative formula

$$q_j^{t_{n+1}} = q_j^{t_n} \exp(-\lambda_j \Delta\psi^{n+1}) + (g_2^{t_{n+1}}\sigma^{t_{n+1}} - g_2^{t_n}\sigma^{t_n})\frac{1 - \exp(-\lambda_j \Delta\psi^{n+1})}{\lambda_j \Delta\psi^{n+1}} \tag{10}$$

Thereby, the incremental reduced time is

$$\Delta\psi^{n+1} \equiv \psi^{t_{n+1}} - \psi^{t_n} = \frac{\Delta t_n}{a_\sigma^{n+1}} \tag{11}$$

4 Results and Discussion

4.1 Determination of viscoplastic parameters

Figures 1 and 2 show the strain recovery data and the residual strain along with the stress-strain curve, respectively. The parameters for the viscoplastic model were obtained as described previously and are compared to the strain recovery data in figure 3. The agreement is good at higher strains, but poor at intermediate strains, although the absolute error is tolerable. At the lowest strains, the accuracy of the strain measurement is reached and it is not practical to consider the prediction of plastic strain.

4.2 Determination of viscoelastic parameters

For each of the recovery tests, the Schapery-model strain was computed using the iterative scheme. The model parameters were determined by least-squares fitting to the strain data of all tests. The measured strain ϵ at time t_j in test i is expressed as ϵ_{ij}. Analogously, the model strain is written as $\hat{\epsilon}_{ij}$. The parameters are thus determined as the set of parameters that minimizes

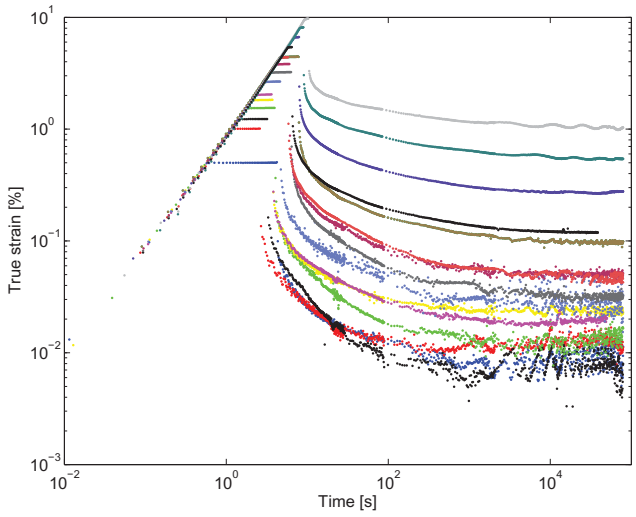

Fig. 1 Strain recovery of polypropylene at room temperature from nominal strains between 0.5% and 8% (true strains between 0.5% and 9.7%.

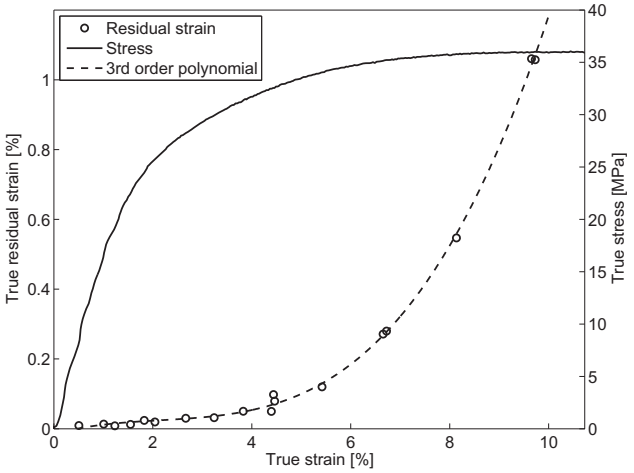

Fig. 2 True stress-true strain curve of polypropylene at room temperature and residual strain determined from recovery of true strains between 0.5% and 9.7%.

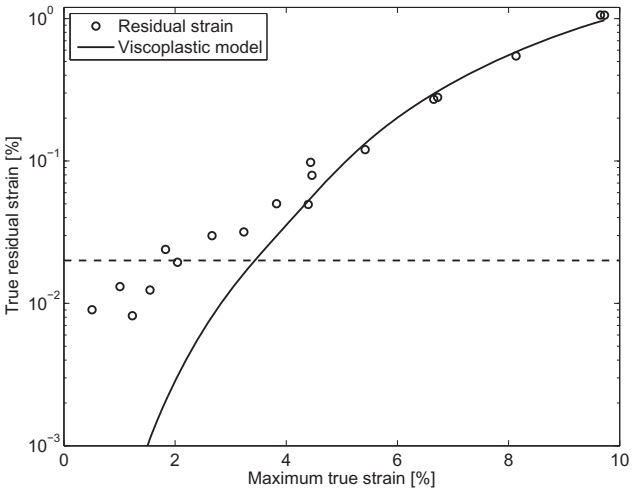

Fig. 3 Residual strain data and fit of the viscoplastic law. The dashed line shows the level of reliable strain measurements.

$$E = \sum_{i,j} \left(w_{ij} \frac{\epsilon_{ij} - \hat{\epsilon}_{ij}}{\epsilon_{ij}} \right)^2 \tag{12}$$

w_{ij} are weights that are individual to each test. These weights were introduced to address an experimental issue specific to the present tests. Recording of images for the strain measurements is performed at constant frame rates. The frame rates are changed in steps over the testing time, but nevertheless the recording at constant rate implies an uneven spacing of data on the logarithmic time scale. Hence, there are comparatively few data points in the loading phase compared to later decades of testing time. To counter this effect, higher weight is assigned to the data up to unloading.

In this optimization problem, constraints are imposed due to physical requirements (Lévesque *et al.*, 2008). First, all polynomial coefficients of the nonlinearizing functions are positive to enforce monotonic behavior, ensuring that the material becomes more compliant with increasing stress. The constant term of the polynomials is equal to 1 as required by the limit of linear viscoelastic behavior. Second, the Prony series coefficients and retardation times are positive. Some trial calculations showed that with the optimization algorithm used by the authors (*lsqnonlin*, MATLAB) it is advantageous to use a fixed set of logarithmically spaced retardation times. In view of computational speed in e.g. FE simulations, it is desirable to use an optimized set of retardation times with the smallest possible number of terms, but no investigations in this regard were carried out for this study.

The result of the fitting process is shown for representative tests in figure 4. The parameters are given in tables 1-3. Good agreement was achieved in the loading ramp and in the initial recovery, but it is also apparent that the agreement during the recovery at larger times is limited by the accuracy of the viscoplastic term, see figure 3. When the viscoplastic strain in the model is too small (strain below 4%), a very large term in the Prony series is obtained in the least-squares optimization to account for the difference between the viscoplastic prediction and the measured residual strain (table 2, n= 9). As this term is thus an artifact of the fitting procedure, it is

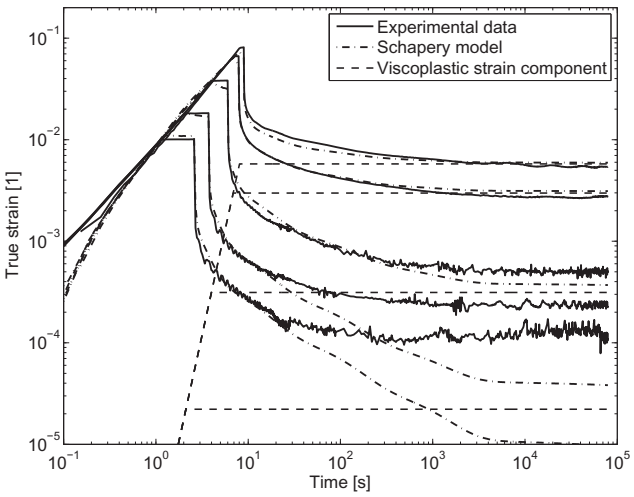

Fig. 4 Strain recovery data and Schapery model result for recovery tests conducted with peak true strains of 8.1%, 6.7%, 3.8%, 1.8% and 1.0%.

omitted in the calculations. The emergence of this large term however shows that an accurate modeling of the viscoplastic strain is important for the determination of the viscoelastic parameters.

There is some deviation between model and data in the short relaxation portion before the unloading. Application of the model to stress relaxation data[1] (figure 5) at 2% showed a reasonable overall agreement, but also waviness, resulting in the deviation in the short relaxation periods. Lévesque *et al.* (2008) demonstrated that a model determined from one type of load history does not necessarily give good results on a different one and concluded that verification against various load histories is needed. Trial computations with different choices of the nonlinearizing function parameters where conducted and it was found that parameter sets yielding similarly good descriptions of the strain recovery can show significant differences when applied to stress relaxation. Hence, these results suggest that a variety of load histories must be used in the identification of proper model parameters, in the present case also including viscoplasticity. Furthermore, the optimization algorithm that was used for the parameter identification is gradient based. Such algorithms find a solution in the vicinity of the initial guess that is made for the parameters. The initial guess may or may not lead to a useful solution, and often some trial and error is needed to find a suitable initial guess. The application of stochastic optimization methods, for which the result does not depend on the initial guess, should be explored in future work. For the linear viscoelastic model, stochastic optimization has been successfully applied by the authors (Tscharnuter *et al.*, 2010b).

The experimental effort to find sufficient data to determine the viscoplastic and viscoelastic behavior for several load histories is considerable even when only limited to uniaxial loadings. It is well known that the mechanical behavior of polymers depends on the hydrostatic stress. Further experimental work for parameter

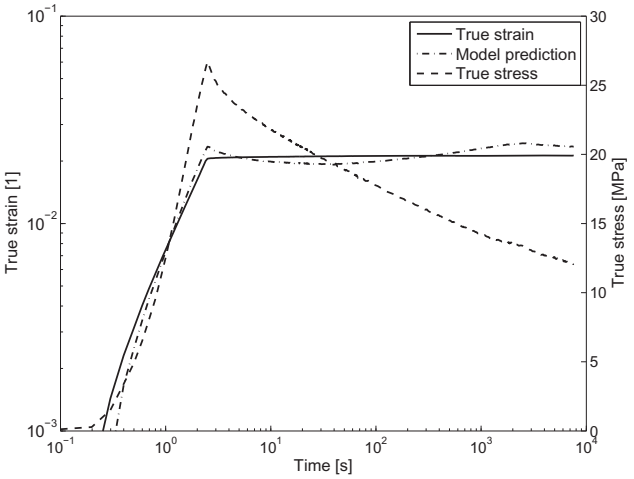

Fig. 5 Stress relaxation data and Schapery model result for stress relaxation at 2%.

[1] Viscoplasticity during stress relaxation was not considered.

Table 1 Polynomial coefficients

degree	4	3	2	1	0
g_0		2.60e−6	2.82e−4	6.15e−3	1
g_1		2.37e−6	2.61e−5	2.63e−3	1
g_2	9.28e−7	2.54e−6	2.68e−4	2.82e−4	1
$1/a_\sigma$			3.50e−4	5.19e−4	1

Table 2 Prony series parameters

n	τ [s]	D [MPa^{-1}]
1	10^{-2}	6.60e−5
2	10^{-1}	6.54e−5
3	1	6.31e−5
4	10^{1}	7.88e−5
5	10^{2}	2.15e−4
6	10^{3}	6.65e−4
7	10^{4}	1.95e−4
8	10^{5}	9.47e−4
9	10^{6}	1.73e−1

Table 3 Viscoplastic parameters

C	M	m
1.76e−5	4.3e−14	4.16e+0

identification should therefore also include multiaxial and compression testing to clarify the proper dependence of the nonlinearizing functions on the stress state.

5 Conclusion

Strain recovery data from a previous paper of the authors were used to identify the parameters of a Schapery-type nonlinear viscoelastic viscoplastic model. The parameters describing the viscoplasticity were determined by fitting the viscoplastic model to the residual strains observed in strain recovery. The viscoelastic part of the model was solved using an iterative scheme and nonlinear optimization was used to determine the nonlinearizing functions and the Prony series compliance parameters from the collection of strain recovery tests. Good agreement was obtained for the loading ramp and the initial recovery, but it was also shown that the accuracy of the viscoplastic component has a strong influence on the identification of the viscoelastic parameters. Some error was found in the application of the determined model to stress relaxation data and it was found that different models that give equally good representations of the strain recovery data can show very different behaviors in stress relaxation. It was thus concluded that a variety of different load histories needs to be used in the parameter identification.

Acknowledgements

The research work of this paper was performed at the Polymer Competence Center Leoben GmbH (PCCL, Austria) within the framework of the Kplus- and COMET-programs of the Austrian Ministry of Traffic, Innovation and Technology with contributions by the University of Leoben and Borealis Polyolefine GmbH. The PCCL is funded by the Austrian Government and the State Governments of Styria and Upper Austria.

References

Crochon, T., Schönherr, T., Li, C., & Lévesque, M. 2010. On finite-element implementation strategies of Schapery-type constitutive theories. *Mechanics of Time-Dependent Materials*, 1–29.

Fasce, Laura A., Pettarin, Valeria, Marano, Claudia, Rink, Marta, & Frontini, Patricia M. 2009. Biaxial Yielding of Polypropylene/Elastomeric Polyolefin Blends: Effect of Elastomer Content and Thermal Annealing. *Polymer Engineering and Science*, **48**(7), 1414–1423.

Henriksen, Mogens. 1984. Nonlinear Viscoelastic Stress Analysis - A Finite Element Approach. *Computers & Structures*, **18**(1), 133–139.

Jerabek, Michael, Major, Zoltan, Renner, Károly, Móczó, János, Pukánszky, Béla, & Lang, Reinhold W. 2010a. Filler/Matrix-debonding and micro-mechanisms of deformation in particulate filled PP composites under tension. *Polymer*, **51**(9), 2040–2048.

Jerabek, Michael, Major, Zoltan, Pukánszky, Béla, & Lang, Reinhold W. 2010b. Mechanics and modeling of the tensile yield behavior of particulate filled PP composites. *submitted to Composite Science and Technology*.

Jerabek, Michael, Tscharnuter, Daniel, Major, Zoltan, Ravi-Chandar, Krishnaswamy, & Lang, Reinhold W. 2010c. Relaxation behavior of neat and particulate filled polypropylene in uniaxial and multiaxial compression. *Mechanics of Time-Dependent Materials*, **14**(1), 47–68.

Jerabek, Michael, Major, Zoltan, & Lang, Reinhold W. 2010d. Strain determination of polymeric materials using digital image correlation. *Polymer Testing*, **29**(3), 407–416.

Lai, J., & Bakker, A. 1995a. Analysis of the non-linear creep of high-density polyethylene. *Polymer*, **36**(1), 93–99.

Lai, J., & Bakker, A. 1995b. An Integral Constitutive Equation for Nonlinear Plasto-Viscoelastic Behavior of High-Density Polyethylene. *Polymer*, **35**(17), 1339–1347.

Lai, J., & Bakker, A. 1996. 3D schapery representation for non-linear viscoelasticitiy and finite element implementation. *Computational Mechanics*, **18**, 182–191.

Lévesque, M., Derrien, K., Baptiste, D., & Gilchrist, M.D. 2008. On the development and parameter identification of Schapery-type constitutive theories. *Mechanics of Time-Dependent Materials*, **12**(2), 95–127.

Marano, Claudia, & Rink, Marta. 2001. Shear yielding threshold and viscoelasticity in an amorphous glassy polymer: a study on a styrene-acrylonitrile polymer. *Polymer*, **42**, 2113–2119.

Marano, Claudia, & Rink, Marta. 2006. Viscoelasticity and shear yielding onset in amorphous glassy polymers. *Mechanics of Time-Dependent Materials*, **10**(3), 173–184.

Muliana, Anastasia H., & Haj-Ali, Rami M. 2004. Numerical finite element formulation of the Schapery non-linear viscoelastic material model. *International Journal for Numerical Methods in Engineering*, **59**(1), 25–45.

Nordin, Lars-Olof, & Varna, Janis. 2006. Nonlinear viscoplastic and nonlinear viscoelastic material model for paper fiber composites in compression. *Composites: Part A*, **37**, 344–355.

Pasricha, A., Tuttle, M.E., & Emery, A.F. 1996. Time-dependent response of IM7/5260 composites subjected to cyclic thermo-mechanical loading. *Composites Science and Technology*, **56**(1), 55–62.

Schapery, R.A. 1969. On the Characterization of Nonlinear Viscoelastic Materials. *Polymer Engineering and Science*, **9**(4), 295–310.

Sorvari, Joonas, Malinen, Matti, & Hämäläinen, Jari. 2006. Finite ramp time correction method for nonlinear viscoelastic material model. *International Journal of Non-Linear Mechanics*, **41**, 1050–1056.

Tscharnuter, Daniel, Jerabek, Michael, Major, Zoltan, & Pinter, Gerald. 2010a. Irreversible Deformation of Isotactic Polypropylene in the Pre-Yield Regime. *submitted to Polymer*.

Tscharnuter, Daniel, Jerabek, Michael, Major, Zoltan, & Lang, Reinhold W. 2010b. On the determination of the relaxation modulus of PP compounds from arbitrary strain histories. *Mechanics of Time-Dependent Materials*, 1–14.

Tscharnuter, Daniel, Jerabek, Michael, Major, Zoltan, & Lang, Reinhold W. 2010c. Time-Dependent Poisson's Ratio of Polypropylene Compounds for various Strain Histories. *submitted to Mechanics of Time-Dependent Materials*.

Zapas, L.J., & Crissman, J.M. 1984. Creep and recovery behaviour of ultra-high molecular weight polyethylene in the region of small uniaxial deformations. *Polymer*, **25**(1), 57 – 62.